Title
Structural Influences of Noncovalent Interactions in the Gas Phase

Author
Chang, Terrence

Publication Date
2014

Peer reviewed|Thesis/dissertation

Structural Influences of Noncovalent Interactions in the Gas Phase

by

Terrence Chang

A dissertation submitted in partial satisfaction of the requirements for the degree of

Doctor of Philosophy

in

Chemistry

in the

Graduate Division

of the

University of California, Berkeley

Committee in charge:

Professor Evan R. Williams, Chair
Professor Kristie A. Boering
Professor Robert M. Glaeser

Spring 2014

Abstract

Structural Influences of Noncovalent Interactions in the Gas Phase

by

Terrence Chang

Doctor of Philosophy in Chemistry

University of California, Berkeley

Professor Evan R. Williams, Chair

The physical properties of molecules in solution, such as basicity and structure, depend on the cooperation and competition of noncovalent intra- and intermolecular interactions. Studying these interactions in the condensed phase is made difficult by the presence of competing influences from counterions and impurities. In the gas phase, however, specific ions, ion complexes and hydration states can be isolated and studied by Fourier transform mass spectrometry coupled with infrared (IR) laser spectroscopy. Using these two techniques, it is possible to isolate specific ions before inducing dissociation via absorption of IR photons. The extent of absorption at a given wavelength correlates to the relative abundance of product ions produced via dissociation, which can be measured using mass spectrometry. The absorption of IR photons only occurs at specific wavelengths depending on which functional groups are present and how their vibrational modes are influenced by interactions such as hydrogen bonding. Structural information is obtained from these spectra by interpreting the presence of certain bands and their frequencies. In addition, information can also be obtained by comparing the spectra from ions of interest to the spectra of reference ions, with known structures, or the simulated spectra of computed geometries. These types of studies provide valuable insight into how noncovalent interactions govern the structure of biomolecules and hydrogen-bonded networks. This dissertation reports experiments utilizing IR spectroscopy to study how water-ion interactions can affect both the structure of an ion solvated by an aqueous nanodrop as well as the hydrogen-bonding network of the nanodrop itself. In addition, the structural effects of ion-peptide interactions, which are relevant to understanding how ions influence biological processes, are also investigated.

In order to study the ability of water to stabilize protonation sites on larger molecules, I investigated the influence of sequential hydration on the structure of protonated *p*-aminobenzoic acid ($PABAH^+$), which has different preferred aqueous solution and gas-phase protonation sites. The preferred protonation site of PABA is the amine in aqueous solution, but the preferred protonation site is the carbonyl O atom of the carboxylic acid in the gas phase. The spectrum of $PABAH^+•(H_2O)_1$ contains an absorption band at a particular photon energy indicating that protonation occurs at the carboxylic acid, i.e. there is a spectroscopic signature for the O-protonated structure. This absorption band persists for $PABAH^+•(H_2O)_{2–6}$, indicating that these

ions have a population of O-protonated isomers as well. Spectra for $PABAH^+•(H_2O)_6$ are also consistent with presence of a second isomer, in which the amine is protonated. These results indicate that $PABAH^+$ exists in the preferred gas-phase structure for $PABAH^+•(H_2O)_{1–6}$, but there is a transition to the preferred solution-phase structure when the ion is solvated by six or more water molecules. In isolation, the excess charge associated with protonation at the carbonyl O atom of the carboxylic acid can be resonantly stabilized and delocalized into the phenyl ring and amine. When six or more water molecules are attached, however, a more favorable hydrogen-bonding network can be formed at the protonated amine than at the carboxylic acid.

In contrast to $PABAH^+$, protonation for *m*-aminobenzoic acid (MABA) occurs at the amine site even when solvated by only one water molecule due to orientation of the amine and carboxylic acid group. This orientation prevents the positive charge from being delocalized into the amine. Thus, $MABAH^+$ serves as an ideal model for the solvation of the N- and C-termini of a protonated amino acid, for which the N- and C-termini typically interact with each other. The measured spectra for $MABAH^+•(H_2O)_{1,2}$ are consistent with the attachment of water to a H atom of the protonated amine. For $MABAH^+•(H_2O)_3$, the measured spectrum indicates that the dominant isomer has a hydrogen-bonded water bridge between the amine and carbonyl O atom of the carboxylic acid. This result indicates that the formation of this water bridge is more energetically favorable than the formation of a third ionic hydrogen bond to the amine group. The spectra for $MABAH^+•(H_2O)_n$ also indicate that water molecules attach to the carboxylic acid H atom, i.e. the ion is fully hydrogen-bonded when there are ≥6 water molecules attached.

Ion spectroscopy can also be used to study how ion-water interactions influence hydration structures. Certain positive ions are known to induce cage-like clathrate structures when hydrated by 20 water molecules. The hydration of NH_4^+ as well as selected, protonated primary, secondary and tertiary amines solvated by 19 – 21 water molecules was investigated in order to elucidate details about how amines can stabilize clathrate structures. The spectra of NH_4^+ as well as monomethyl-, n-heptyl-, and tert-butylammonium$^+$ with 20 water molecules attached are consistent with the nearly exclusive presence of clathrate structures, whereas nonclathrate structures are present for the more highly substituted amines. By comparison, nonclathrate structures are observed for all ions when 19 or 21 water molecules are attached. Spectroscopic evidence for clathrate structures for $NH_4^+•(H_2O)_{20}$ has been previously reported, but the location of the ion, whether at the surface or the interior, was difficult to determine based on the IR spectrum of this ion alone. Thus, the spectra of NH_4^+, monomethyl- and n-heptylammonium$^+$ solvated by 20 water molecules were compared to those for Rb^+ and tert-butylammonium$^+$, which serve as references for clathrate structures with the ion located in the interior or at the surface, respectively. These comparisons indicate that NH_4^+ goes to the interior, whereas protonated primary amines are located at the surface, irrespective of the size of the alkyl group.

In addition to ion-water interactions, ion-biomolecule interactions can also be probed by ion spectroscopy. Although there are several studies that have used ion spectroscopy to investigate cations coordinated to amino acids and peptides, there are fewer studies focused on these same biomolecules complexed with anion adducts. The ions $Gly_3•X^–$, $Ala_3•X^–$ and $Leu_3•X^–$ (X = Cl, Br and I) were studied in order to investigate how the size of anion adducts and alkyl side chains influence the coordination of halide anions to aliphatic peptides. The spectra of

$Gly_3•Cl^-$, $Ala_3•Cl^-$ and $Leu_3•Cl^-$ suggest that all three complexes adopt similar structures, where Cl^- coordinates to the peptides by accepting three or four hydrogen bonds from the amides as well as the N- and C-termini. These results indicate that the size of the alkyl chain does not have a significant influence on the coordination geometry of these complexes. These structures are "inverted" in comparison to previously reported structures for $Gly_3•Na^+$ and $Ala_3•Na^+$, where the Na^+ coordinates to lone pair electrons of the N atom of the N-terminus, or the carbonyl O atoms of the amides and C-terminus. The spectra of $Gly_3•X^-$, $Ala_3•X^-$ and $Leu_3•X^-$ each appear similar to each other within each peptide, indicating that the size of the anion does not significantly affect the coordination geometry.

In memory of those who saw me start this journey but are not here to see me finish.

Table of Contents

Chapter 1. Introduction

1.1. Overview

Intra- and intermolecular interactions play an important role in governing the structure of molecules and hydrogen-bonded networks in solution. Understanding how these interactions compete and cooperate with each other is crucial to elucidating the details of how they influence larger scale phenomena, such as protein structure and functionality. In the gas phase, it is possible to isolate and study specific ion complexes without interfering effects from counter ions in solution. It is also possible to isolate specific hydration states of ions, thus the interactions associated with specific solute or solvent molecules can be determined. Gas-phase infrared (IR) ion spectroscopy is a powerful structural probe that can provide valuable insight into the influences of noncovalent interactions from solvent molecules or ion adducts. Spectroscopic data, from which structural isomers present in an ion population can be identified, can also be supplemented by laser induced dissociation kinetics studies. These kinetics experiments can provide the relative populations for each structural isomer.

In this dissertation, results from gas-phase IR ion spectroscopy and laser induced dissociation kinetics studies are reported. These experiments were performed in order to gain a better understanding of how noncovalent interactions affect the structure of bare ions and ion complexes as well as hydrogen-bonded water networks in the gas phase. In Chapter 1, I provide motivations for these studies as well as an overview of the instrumentation used for these types of experiments. The following chapters discuss the structural effects of water-ion interactions for solvated ions and how they can affect the structure of the ion (Chapter 2) or how the ion can influence the hydrogen-bonding network (Chapters 3 and 4). The coordination of aliphatic tripeptides to halide anions, and how the size of the anion or alkyl chain influences coordination patterns is investigated in Chapter 5.

1.2. Motivation

Ions play an essential role in biological processes, such as pH regulation,[1,2] uptake of amino acids by bacteria[3] and neuron signaling.[4] Ions can also influence protein structure, a phenomena that was discovered by F. Hofmeister in 1888 when he observed that different ions could affect protein solubility.[5] The resulting "Hofmeister series" of ions is an ordering of cations or anions based on the extent of their abilities to influence solubilities, and it is thought that this effect is due to either direct ion-protein interactions or changes in the hydrogen-bonding network of water induced by the presence of the ions in solution.[6-10] Ion-water interactions have been extensively studied in order to elucidate the details of the Hofmeister effect as well those of other properties and phenomena such as surface activity,[11-13] molecular folding[14,15] and the influence ions have on hydration structure.[16-25] These studies have elucidated some of the details of how intra- and intermolecular interactions compete and cooperate with each other in solution.

Ion-biomolecule and ion-water interactions can also be studied in the gas-phase, where complexes and hydrated clusters can be mass selected by various types of mass spectrometers.

In comparison to condensed phased studies, gas-phase experiments can provide more detailed information about the relative contributions from intra- or intermolecular interactions of specific water molecules or ions, including sequential hydration energies[26-35] and the structural influence of ion adducts.[36-42] Gas-phase IR ion spectroscopy is a powerful tool for investigating the structures of ions and ion complexes and has been used to study the stability of the zwitterionic forms of amino acids and peptides in the gas phase. Amino acids are zwitterions in solution, and can form salt bridges between nearby charged functional groups. In contrast, amino acids exist in the gas phase in their canonical form, where the amine at the N- and the carboxylic acid of the C-termini are formally neutral. It has been shown that the attachment of cation and anion adducts, can induce the formation of zwitterions.[43-49] Similarly, the attachment of ion adducts can induce zwitterionic structures in peptides.[50] In addition, the composition of peptides[51] and the order of amino acids have an effect as well.[52] The majority of these experiments have focused on the structure of amino acids and peptides bound to cations, but the structure of anions complexed to peptides has not been investigated using IR spectroscopy.

Hydrated ions have also been probed by ion spectroscopy in order to elucidate the details of how water-ion interactions influence the structure of hydrogen-bonded water networks. Some ions, such as tetramethyl ammonium, bind to water clusters but have no significant influence on the hydrogen-bonding water network.[20] In contrast, sulfate dianion has been shown to affect water structure up to the third solvation shell.[16] Several aspects of ion hydration have been investigated with ion spectroscopy, such as coordination number,[17,18] the ability to induce cage-like clathrate structures,[21-24] and even the relative binding affinities for different hydration sites of protonated amino acids.[53,54] These types of studies have provided insight into the extent to which ions can influence hydrogen-bonding networks. Despite the advances in understanding from previous studies, certain details how ion-water interactions can stabilize a protonation site or influence the propensity of an ion to be located at the surface of a nanodrop remain to be elucidated.

1.3. Gas-Phase Infrared Ion Spectroscopy

Before discussing the experiments contained in this dissertation, it is beneficial to briefly review the processes and instrumentation involved. IR spectra of ions are typically measured via action spectroscopy, in which the extent of photodissociation is measured. Ions or ion complexes can absorb IR photons that are in resonance with vibrational modes. The absorption of photons increases the internal energy of the ions, eventually leading to dissociation. Figure 1.1 illustrates the process of acquiring data at a single photon energy of an action spectrum. When studying hydrated ions, a distribution of multiple cluster sizes is generated. From this distribution, a single cluster (or an ensemble) of interest can be isolated with a mass filter. After mass selection, ions can be trapped and irradiated by tunable radiation from either a pulsed free electron laser (FEL) or an optical parametric oscillator/amplifier (OPO/OPA) laser, which provide IR photons in the ~100 – 2500 cm^{-1} and ~600 – 4100 cm^{-1} ranges, respectively. The range from ~800 to ~1900 cm^{-1} corresponds to N–H and O–H bends as well as carbonyl C=O stretches whereas the range from ~2600 – 3900 cm^{-1} is associated with hydrogen-bonded and free N–H and O–H stretches.

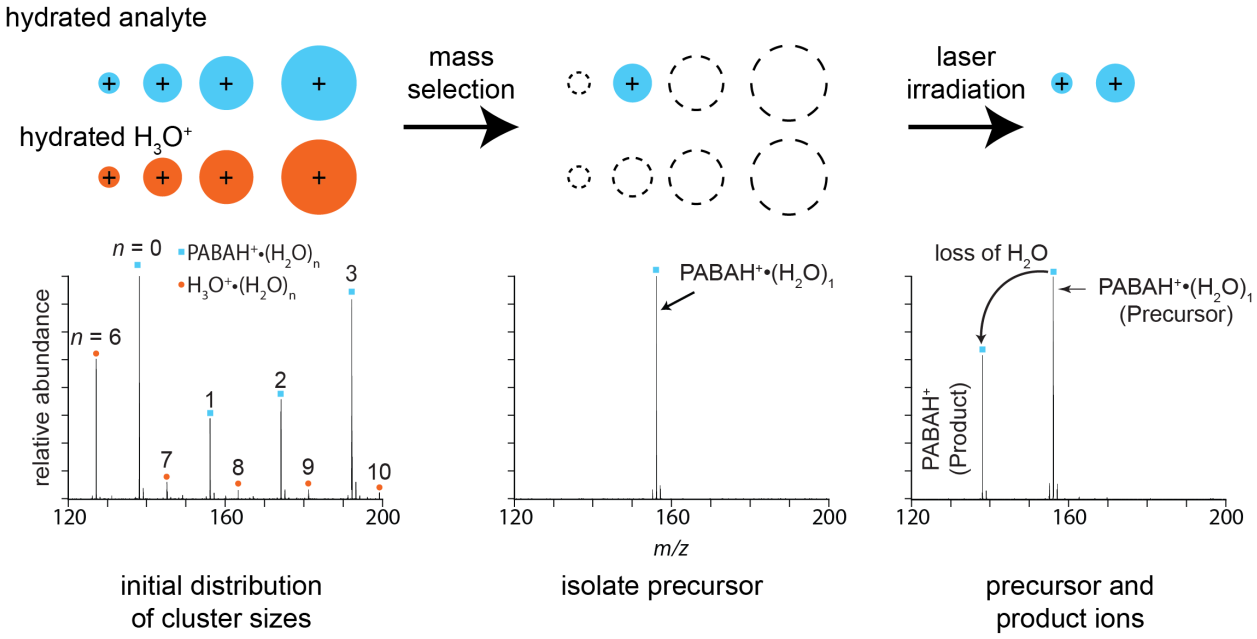

Figure 1.1. Illustrative diagram depicting the process of inducing the laser dissociation of protonated *p*-aminobenzoic acid ($PABAH^+$) with one water molecule attached. After generating an initial distribution of hydration states (left), the precursor of interest, $PABAH^+•(H_2O)_1$, is then isolated (middle). The precursor is then irradiated with infrared photons of a single wavelength, producing product ions (right). The relative abundances of the product and precursor ions can then be used to calculate a dissociation rate constant.

The absorption of photons results in an increase in internal energy of an ion or ion complex, which can lead to dissociation via bond cleavages or, in the case of hydrated clusters, loss of water molecules. The fragmentation of bare molecular ions[55-60] as well as tightly bound complexes[43,44,47-52,61-75] requires absorption of several photons per laser pulse in order to heat the ions and raise their internal energy above the dissociation limit. This process, infrared multiple photon dissociation (IRMPD), can be induced with the relatively high fluences generated by FELs, such as FELIX[76] and CLIO.[77] In contrast, infrared photodissociation (IRPD) spectra are measured for ions that have sufficient internal energy to undergo dissociation even without irradiation from laser photons (i.e. they also dissociate via blackbody infrared radiative dissociation, BIRD, which is not the case for ions that undergo IRMPD), such as hydrated clusters.[15-25,53,54,78-93] For these ions, the absorption of a single laser photon can result in an increase in the dissociation rates for these ions above that for BIRD. Because IRPD requires the absorption of only a single photon, they do not require high photon fluences and can be measured using OPO/OPA laser systems, which produce lower photon fluences than FELs but do not require specialize facilities.

Absorption band intensities for both IRMPD and IRPD spectra are related to the extent of laser induced dissociation, but IRPD spectra must also be corrected for the inherent BIRD rate constant (i.e. IRPD intensities correspond *only* to laser induced dissociation and *not* the combination of IRPD and BIRD).[83] Both types of spectra are generated by plotting the laser induced dissociation rate constants, which are calculated from the precursor and product ion abundances and corrected for black body infrared dissociation. In order to measure IR(M)PD

spectra, tunable IR sources are typically coupled to mass spectrometers, which are capable of isolating a precursor of interest and measuring precursor and product ion abundances after irradiations. Several instrumental setups are used, including triple-quadrupole,[94,95] time-of-flight,[96-100] and Fourier-transform ion cyclotron resonance (FT/ICR) mass spectrometers.[45,58,74,101] The spectra contained in this dissertation were acquired using FT/ICR mass spectrometers, which are capable of simultaneously measuring the abundances of product ions and any remaining precursor ions after irradiation. Time-of-flight mass spectrometers can also measure multiple ion abundances, but quadrupolar mass analyzers can only measure the abundance of a single ion at a given time.

Structural information is obtained from these spectra by interpreting the presence of spectral bands and their frequencies. Bands corresponding to N–H and O–H stretch and bending motions are sensitive to their hydrogen-bonding environment. The frequencies of these vibrational modes are influenced by the Stark and charge transfer effects. A Stark shift is induced by the alignment of the dipole of a bond with the electric field of a cation or an anion, which cause the vibrational frequencies of the bond to red or blue shift depending on whether the alignment is favorable or unfavorable, respectively.[72,82,84] The withdrawal or donation of electron density by cation and anion adducts, respectively, result in charge transfer effects, which can also affect vibrational frequencies.[102,103] Analyzing these shifts provides structural information because they depend on hydrogen-bonding geometries and ion coordination. The free O–H stretches are a particularly sensitive structural probe of the surface of a hydrated ion. In some cases, the presence or absence of diagnostic features can be indicative of certain structures. For example, zwitterionic and nonzwitterionic forms of amino acids and peptides with ion adducts can be readily identified by the appearance of the carboxylate asymmetric stretch or carboxylic acid carbonyl C=O stretch, respectively.[51,52,71,72]

The interpretation of IR(M)PD spectra can be aided by the use of reference ions, which have known structures, as well as by computational chemistry. Using reference ions, it is possible to obtain spectral data corresponding to known structures. Similarly, computational chemistry can be used to generate possible candidate structures and their simulated spectra. By comparing the measured spectra of reference ions or the simulated spectra of calculated structures to that of an ion of interest, structural information can be obtained by analyzing the similarities and differences.

For some ions or ion complexes, more than one structural isomer may exist. In order to help spectroscopically distinguish between isomers, ions can also be cooled prior to irradiation through a variety of techniques.[95,104-109] Cooling can simplify the bands present in a spectrum such that contributions from individual conformers can be readily identified. Although the spectrum of the entire ion packet is the result of the superposition of the individual spectra for each conformer present, determining the relative contributions from each conformation can be difficult. Dissociation pathways that require multiple photons or differences in fragmentation barriers between conformers can influence the relative intensities of spectral bands such that the relative population of a conformer and the relative intensity of a conformer-specific absorption are not linearly related.[17,52,110] Thus, another technique must be used to measure the relative abundances of isomers, which is described below.

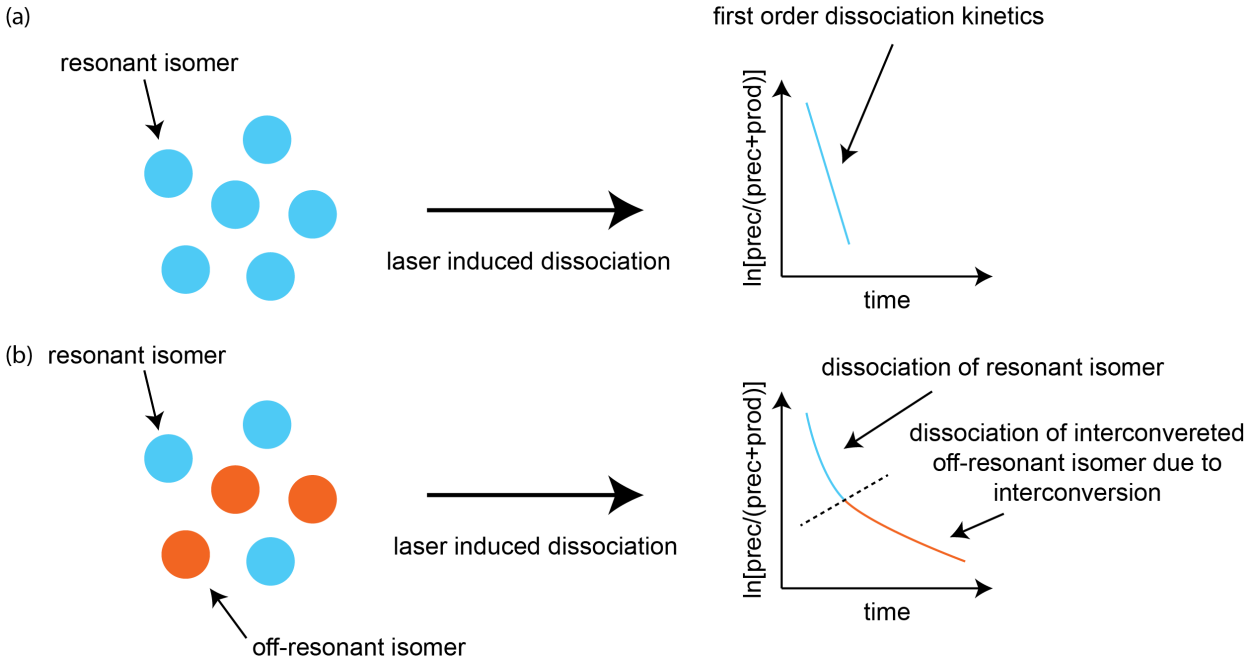

Figure 1.2. (a) Laser induced dissociation kinetics of an ion population containing only a resonant isomer results in first order kinetics whereas (b) the kinetics of an ion population with multiple isomers that slowly interconvert are biexponential. The kinetic data are derived from the precursor and product abundances (prec and prod, respectively) as a function of time.

1.4. Laser Induced Dissociation Kinetics

Dissociation kinetics experiments can be used to probe the relative isomer abundances in an ion population, from which accurate relative Gibbs free energies can be derived. In these experiments, dissociation can be induced via absorption of blackbody[111] or, more recently, laser photons.[53,54,58,112,113] It is possible to differentiate between isomers if they do not interconvert rapidly. Laser induced dissociation experiments allow for the direct excitation of specific isomers. Ions are irradiated at a single excitation frequency for varying durations. The resulting dissociation kinetics depend on whether the ion populations consists of a single isomer or multiple isomers. If only a single isomer is present, the kinetic data should be first order (Figure 1.2a). The presence of two or more rapidly interconverting isomers can also result in first order kinetics. However, if the isomers interconvert slowly, the resulting dissociation kinetics can be biexponential (Figure 1.2b), where the fast rate constant corresponds to the dissociation of the resonant isomer. It is possible to observe the presence of multiple isomers even in cases where the IR(M)PD spectra suggest the presence of only a single isomer.[58,112,113] Biexponential kinetics can also result from poor overlap between the laser beam and the ion cloud such that only a fraction of the ion population is irradiated. Thus, when conducting laser induced dissociation experiments, it is important to measure the extent of overlap between the laser beam and the ion population by irradiating an ion with linear dissociation kinetics.

The relative isomer abundances can be used to determine the relative Gibbs free energies of structural isomers assuming that the ions have a Boltzmann distribution of energies (equation 1.1).

$$\frac{N_a}{N_b} = \exp\left(\frac{\Delta G_b - \Delta G_a}{kT}\right) \qquad (1.1)$$

These relative energies provide detailed information such as the relative stabilities of solution-phase structures of amino acid complexes in the gas phase[112,113] and the binding affinities of individual hydration sites of protonated amino acids.[53,54] For example, although the protonated amine is the preferred hydration site for protonated phenylalanine with one water molecule attached, hydration of the carboxylic acid was measured to be higher in energy by only ~1 kJ mol^{-1}.[53] The information about relative energetics obtained by these types studies provide valuable insight into the relationship between structure and relative energies, and they establish stringent benchmarks for computational studies investigating the structures of gas-phase ions.

1.5. Systems Studied

Both gas-phase IR ion spectroscopy and laser induced dissociation kinetics were used to investigate the structures of hydrated ions (Chapters 2 – 4) and ion-peptide complexes (Chapter 5) with the aid of computational chemistry. These studies elucidate the details of how water-ion and ion-peptide interactions influence the structures of molecules and hydrogen-bonded water networks.

1.5.1. Hydrated ions

In solution, the functional groups of a molecule can interact with nearby solvent molecules, and these interactions can influence physical properties such as molecular structure[15,34,57,58,114,115] and basicity.[116-120] By using a gas-phase technique, it is possible to study mass-selected analytes, including isolating ions with a certain number of water molecules attached. Previous studies of sequentially hydrated ions have led to a better understanding of how water-biomolecule interactions influence structure and functionality of proteins and protein complexes, including stabilizing excess charge due to protonation or deprotonation of functional groups. For example, arginine adopts a nonzwitterionic structure for Arg•Li^+,[45,71] but the attachment of a single water molecule to this complex can stabilize a zwitterionic form or arginine, where the side chain is protonated and the C-terminus is deprotonated.[114] Experimental studies on *p*-aminobenzoic acid have shown that the amine is the preferred protonation site in aqueous solution,[121] but that the preferred gas-phase protonation site is the carboxylic acid.[58,122] In chapter 2, I investigate the intermediate hydration states, elucidating new details about how the sequential addition of water molecules can eventually stabilize protonation of the amine N atom over the carbonyl O atom. Although the carboxylic acid has a higher proton affinity than the amine, the protonated amine allows for a more optimized hydrogen-bonded water network at higher hydration states. The water molecules, which go to the charged functional group, stabilize the N-protonated structure by forming stronger hydrogen bonds compared to those of a water network solvating a protonated carboxylic acid.

Although water molecules preferentially interact with positively charged ammonium group for protonated *p*-aminobenzoic acid, this is not the case for protonated amino acids. There is experimental evidence that the hydration of the H atom of a neutral carboxylic acid can be competitive with and even favorable to hydration of the protonated amine for protonated amino acids.[33,53,54] For these ions, however, the H atoms of the protonated amine can interact with the carbonyl O atom of the C-terminus, or the phenyl ring side chain for phenylalanine. These interactions prevent water molecules from freely interacting with these H atoms and potentially influence the relative binding affinities of these hydration sites. It is unclear to what extent that these interactions affect the intrinsic solvation of both a protonated amine and a neutral carboxylic acid. Unlike *p*-aminobenzoic acid, *m*-aminobenzoic acid is protonated at the amine both in isolation and in aqueous solution. In addition, the amine and carboxylic acid functional groups are oriented such that they cannot form a hydrogen bond with each other. Thus, the hydration of *m*-aminobenzoic acid, discussed in Chapter 3, can be studied in order to elucidate how water molecules interact with both of these functional groups in the absence of intramolecular hydrogen bonds. Spectroscopy results indicate that water molecules do not bind to the carboxylic acid H atom until the protonated amine group is fully hydrogen-bonded. These results, when compared to those for hydrated, protonated amino acids, suggest that intramolecular hydrogen bonds between the protonated amine and neutral carboxylic acid groups influence the relative water binding affinities to these sites.

The ability for a functional group to form hydrogen bonds to surrounding water molecules, along with other factors, can affect the structure of the solvating water network. It has been shown that some ions, such as tetramethylammonium, do not significantly affect the structure of a water droplet in the gas-phase[20] whereas other ions, such as sulfate dianion, have a significant effect.[16] Certain cations, such as H_3O^+,[21,22] NH_4^+,[23] and the larger metal alkali ions,[24] can induce the formation of cage-like clathrate structures when hydrated by 20 water molecules in the gas phase, whereas other positive ions do not. Although the IR spectra of these ions are consistent with the presence of clathrate structures, information about whether the ion is located at the surface or in the interior can more difficult to determine. The spectra contained in Chapter 4 of NH_4^+ and other selected, protonated amines with 20 water molecules attached reveal slight differences in the region of the IR spectrum that corresponds to hydrogen-bonded O–H stretches. In order to obtain structural information from this region and determine the location of the ion, spectra of reference ions are used in comparisons with the spectra of the ions of interest in order to provide the first experimental evidence determining which amines are located at the surface or in the interior of a clathrate.

1.5.2. Anion-peptide Complexes

In addition to ion-water interactions, it is also important to understand the structural influences of ion-molecule interactions. Ions are involved in several biological processes.[1-4,123-125] Thus, elucidation of details on how ions affect protein structure and functionality is crucial to establishing a better understanding of the role ions play in these processes. The use of the FEL coupled with electrospray ionization has made it possible to study the structure of amino acids and peptides when protonated, deprotonated, and complexed with other ions. Amino acids and peptides complexed with metal cations have been the subject of several studies. In contrast there are fewer studies on amino acids with anions, and no previous reports for anion-peptide complexes. The structures of halide anions bound to aliphatic peptides are investigated in

chapter 5 in order to study the influence of anion and alkyl side chain size on the coordination geometry of these complexes. This chapter provides new insight into how anions interact with biomolecules, and is the first study to investigate the structure of anion-peptide complexes with IR spectroscopy.

1.6. Summary

IR Ion spectroscopy is a powerful structural probe that can elucidate the details of how intra-and intermolecular interactions cooperate in the gas phase. The interpretation of spectra can be aided by comparisons with the measured spectra of reference ions and simulated spectra of calculated structures. Laser induced dissociation kinetics can provide complementary data about the relative energetics of the isomers identified in an ion population. The results from the studies contained in this dissertation provide insight into how hydrogen-bonding interactions can influence the relative stability of protonation sites, the formation of ionic vs. neutral hydrogen bonds, the incorporation of guest ions into clathrate structures, and peptide coordination geometries. The stabilities of these structures depend not only on the number of the hydrogen bonds formed but also their quality. This includes the competition between ionic and neutral hydrogen bonds. These results provide insight into how noncovalent interactions influence the structure of molecules in solution and serve as stringent benchmarks for computational studies investigating ion solvation and ion-peptide interactions.

1.7. References

1. Chesler, M. *Physiol. Rev.* **2003**, *83*, 1183-1221.
2. Russell, J. M.; Boron, W. F. *Nature* **1976**, *264*, 73-74.
3. Dashper, S. G.; Brownfield, L.; Slakeski, N.; Zilm, P. S.; Rogers, A. H.; Reynolds, E. C. *J. Bacteriology* **2001**, *183*, 4142-4148.
4. Frings, S.; Reuter, D.; Kleene, S. J. *Prog. Neurobiol.* **2000**, *60*, 247-289.
5. Hofmeister, F. *Arch. Exp. Pathol. Pharmacol.* **1888**, *24*, 247–260.
6. Uejio, J. S.; Schwartz, C. P.; Duffin, A. M.; Drisdell, W. S.; Cohen, R. C.; Saykally, R. J. *Proc. Nat. Acad. Sci. U. S. A.* **2008**, *105*, 6809-6812.
7. Freire, M. G.; Neves, C. M. S. S.; Silva, A. M. S.; Santos, L. M. N. B. F.; Marrucho, I. M.; Rebelo, L. P. N.; Shah, J. K.; Maginn, E. J.; Coutinho, J. A. P. *J. Phys. Chem. B* **2010**, *114*, 2004-2014.
8. Smith, J. D.; Saykally, R. J.; Geissler, P. L. *J. Am. Chem. Soc.* **2007**, *129*, 13847-13856.
9. Pegram, L. M.; Record, M. T., Jr. *J. Phys. Chem. B* **2007**, *111*, 5411-5417.
10. Chen, X.; Sagle, L. B.; Cremer, P. S. *J. Am. Chem. Soc.* **2007**, *129*, 15104-15105.
11. Jungwirth, P.; Tobias, D. J. *Chem. Rev.* **2006**, *106*, 1259-1281.
12. Ishiyama, T.; Morita, A. *J. Phys. Chem. C* **2007**, *111*, 721-737.
13. Onorato, R. M.; Otten, D. E.; Saykally, R. J. *J. Phys. Chem. C* **2010**, *114*, 13746-13751.
14. Wende, T.; Wanko, M.; Jiang, L.; Meijer, G.; Asmis, K. R.; Rubio, A. *Angew. Chem. Int. Ed.* **2011**, *50*, 3807-3810.
15. Demireva, M.; O'Brien, J. T.; Williams, E. R. *J. Am. Chem. Soc.* **2012**, *134*, 11216-11224.
16. O'Brien, J. T.; Prell, J. S.; Bush, M. F.; Williams, E. R. *J. Am. Chem. Soc.* **2010**, *132*, 8248-8249.
17. O'Brien, J. T.; Williams, E. R. *J. Phys. Chem. A* **2008**, *112*, 5893-5901.
18. O'Brien, J. T.; Williams, E. R. *J. Phys. Chem. A* **2011**, *115*, 14612-14619.
19. Miller, D. J.; Lisy, J. M. *J. Am. Chem. Soc.* **2008**, *130*, 15393-15404.
20. Prell, J. S.; Williams, E. R. *J. Am. Chem. Soc.* **2009**, *131*, 4110-4119.
21. Miyazaki, M.; Fujii, A.; Ebata, T.; Mikami, N. *Science* **2004**, *304*, 1134-1137.
22. Shin, J.-W.; Hammer, N. I.; Diken, E. G.; Johnson, M. A.; Walters, R. S.; Jaeger, T. D.; Duncan, M. A.; Christie, R. A.; Jordan, K. D. *Science* **2004**, *304*, 1137-1140.
23. Diken, E. G.; Hammer, N. I.; Johnson, M. A.; Christie, R. A.; Jordan, K. D. *J. Chem. Phys.* **2005**, *123*, 164309.
24. Cooper, R. J.; Chang, T. M.; Williams, E. R. *J. Phys. Chem. A* **2013**, *117*, 6571–6579.
25. Ke, H.; van der Linde, C.; Lisy, J. M. *J. Phys. Chem. A* **2014**, *118*, 1363-1373.
26. Ye, S. J.; Moision, R. M.; Armentrout, P. B. *Int. J. Mass Spectrom.* **2006**, *253*, 288-304.
27. Klassen, J. S.; Blades, A. T.; Kebarle, P. *J. Phys. Chem.* **1995**, *99*, 15509–15517.
28. Meot-Ner, M. **2005**, *105*, 213-284.
29. Wincel, H. *Chem. Phys. Lett.* **2007**, *439*, 157-161.
30. Lemoff, A. S.; Bush, M. F.; Wu, C. C.; Williams, E. R. *J. Am. Chem. Soc.* **2005**, *127*, 10276–10286.
31. Lemoff, A. S.; Wu, C. C.; Bush, M. F.; Williams, E. R. *J. Phys. Chem. A* **2006**, *110*, 3662–3669.

32. Jockusch, R. A.; Lemoff, A. S.; Williams, E. R. *J. chem. Phys. A.* **2001**, *105*, 10929–10942.
33. Gao, B.; Wyttenbach, T.; Bowers, M. T. *J. Am. Chem. Soc.* **2009**, *131*, 4695-4701.
34. Gao, B.; Wyttenbach, T.; Bowers, M. T. *J. Phys. Chem. B* **2009**, *113*, 9995-10000.
35. Wyttenbach, T.; Bowers, M. T. *Chem. Phys. Lett.* **2009**, *480*, 1–16.
36. Taraszka, J. A.; Li, J. W.; Clemmer, D. E. *J. Phys. Chem. B* **2000**, *104*, 4545-4551.
37. Wyttenbach, T.; Grabenauer, M.; Thalassinos, K.; Scrivens, J. H.; Bowers, M. T. *J. Phys. Chem. B* **2010**, *114*, 437-447.
38. Kohtani, M.; Jarrold, M. F.; Wee, S.; O'Hair, R. A. J. *J. Phys. Chem. B* **2004**, *108*, 6093-6097.
39. Seo, Y.; Schenauer, M. R.; Leary, J. A. *Int. J. Mass Spectrom.* **2011**, *303*, 191-198.
40. Lemoff, A. S.; Bush, M. F.; Williams, E. R. **2005**, *109*, 1903-1910.
41. Strittmatter, E. F.; Lemoff, A. S.; Williams, E. R. *J. Phys. Chem. A* **2000**, *104*, 9793-9796.
42. Flick, T. G.; Merenbloom, S. I.; Williams, E. R. *J. Am. Soc. Mass Spectrom.* **2013**, 1-9.
43. Bush, M. F.; Oomens, J.; Saykally, R. J.; Williams, E. R. *J. Am. Chem. Soc.* **2008**, *130*, 6463-6471.
44. Armentrout, P. B.; Rodgers, M. T.; Oomens, J.; Steill, J. D. *J. Phys. Chem. A.* **2008**, *112*, 2248-2257.
45. Bush, M. F.; O'Brien, J. T.; Prell, J. S.; Saykally, R. J.; Williams, E. R. *J. Am. Chem. Soc.* **2007**, *129*, 1612-1622.
46. Carl, D. R.; Cooper, T. E.; Oomens, J.; Steill, J. D.; Armentrout, P. B. *Phys. Chem. Chem. Phys.* **2010**, *12*, 3384-3398.
47. Dunbar, R. C.; Hopkinson, A. C.; Oomens, J.; Siu, C. K.; Siu, K. W. M.; Steill, J. D.; Verkerk, U. H.; Zhao, J. F. *J. Phys. Chem. B* **2009**, *113*, 10403-10408.
48. O'Brien, J. T.; Prell, J. S.; Steill, J. D.; Oomens, J.; Williams, E. R. *J. Phys. Chem. A.* **2008**, *112*, 10823-10830.
49. Dunbar, R. C.; Polfer, N. C.; Oomens, J. *J. Am. Chem. Soc.* **2007**, *129*, 14562-14563.
50. Prell, J. S.; Flick, T. G.; Oomens, J.; Berden, G.; Williams, E. R. *J. Phys. Chem. A* **2010**, *114*, 854-860.
51. Prell, J. S.; O'Brien, J. T.; Steill, J. D.; Oomens, J.; Williams, E. R. *J. Am. Chem. Soc.* **2009**, *131*, 11442-11449.
52. Prell, J. S.; Demireva, M.; Oomens, J.; Williams, E. R. *J. Am. Chem. Soc.* **2009**, *131*, 1232-1242.
53. Prell, J. S.; Chang, T. M.; O'Brien, J. T.; Williams, E. R. *J. Am. Chem. Soc.* **2010**, *132*, 7811-7819.
54. Prell, J. S.; Correra, T. C.; Chang, T. M.; Biles, J. A.; Williams, E. R. *J. Am. Chem. Soc.* **2010**, *132*, 14733-14735.
55. Oomens, J.; Steill, J. D. *J. Phys. Chem. A* **2008**, *112*, 3281-3283.
56. Oomens, J.; Steill, J. D.; Redlich, B. *J. Am. Chem. Soc.* **2009**, *131*, 4310-4319.
57. Steill, J. D.; Oomens, J. *J. Am. Chem. Soc.* **2009**, *131*, 13570-13571.
58. Schmidt, J.; Meyer, M. M.; Spector, I.; Kass, S. R. *J. Phys. Chem. A.* **2011**, *115*, 7625-7632.
59. Lorenz, U. J.; Lemaire, J.; Maitre, P.; Crestoni, M.-E.; Fornarini, S.; Dopfer, O. *Int. J. Mass Spectrom.* **2007**, *267*, 43-53.

60. Lorenz, U. J.; Solca, N.; Lemaire, J.; Maitre, P.; Dopfer, O. *Angew. Chem. Int. Ed.* **2007**, *46*, 6714-6716.
61. Balaj, O. P.; Kapota, C.; Lemaire, J.; Ohanessian, G. *Int. J. Mass Spectrom.* **2008**, *269*, 196-209.
62. Balaj, O. P.; Semrouni, D.; Steinmetz, V.; Nicol, E.; Clavaguera, C.; Ohanessian, G. *Chem. Eur. J.* **2012**, *18*, 4583-4592.
63. Bush, M. F.; Oomens, J.; Williams, E. R. *J. Phys. Chem. A* **2009**, *113*, 431-438.
64. Chen, X.; Yu, L.; Steill, J. D.; Oomens, J.; Polfer, N. C. **2009**, *131*, 18272-18282.
65. Citir, M.; Stennett, E. M. S.; Oomens, J.; Steill, J. D.; Rodgers, M. T.; Armentrout, P. B. *Int. J. Mass Spectrom.* **2010**, *297*, 9-17.
66. Drayss, M. K.; Blunk, D.; Oomens, J.; Gao, B.; Wyttenbach, T.; Bowers, M. T.; Schafer, M. **2009**, *113*, 9543-9550.
67. Drayss, M. K.; Blunk, D.; Oomens, J.; Polfer, N.; Schmuck, C.; Gao, B.; Wyttenbach, T.; Bowers, M. T.; Schafer, M. **2009**, *281*, 97-100.
68. Dunbar, R. C.; Oomens, J.; Berden, G.; Lau, J. K. C.; Verkerk, U. H.; Hopkinson, A. C.; Siu, K. W. M. *J. Phys. Chem. A* **2013**, *117*, 5335-5343.
69. Dunbar, R. C.; Polfer, N. C.; Berden, G.; Oomens, J. *Int. J. Mass Spectrom.* **2012**, *330*, 71-77.
70. Dunbar, R. C.; Steill, J. D.; Oomens, J. *Int. J. Mass Spectrom.* **2010**, *297*, 107-115.
71. Forbes, M. W.; Bush, M. F.; Polfer, N. C.; Oomens, J.; Dunbar, R. C.; Williams, E. R.; Jockusch, R. A. *J. Phys. Chem. A.* **2007**, *111*, 11759-11770.
72. O'Brien, J. T.; Prell, J. S.; Berden, G.; Oomens, J.; Williams, E. R. *Int. J. Mass Spectrom.* **2010**, *297*, 116-123.
73. O'Brien, J. T.; Prell, J. S.; Steill, J. D.; Oomens, J.; Williams, E. R. *J. Am. Chem. Soc.* **2009**, *131*, 3905-3912.
74. Polfer, N. C.; Oomens, J.; Moore, D. T.; von Helden, G.; Meijer, G.; Dunbar, R. C. *J. Am. Chem. Soc.* **2006**, *128*, 517-525.
75. Rodgers, M. T.; Armentrout, P. B.; Oomens, J.; Steill, J. D. *J. Phys. Chem. A* **2008**, *112*, 2258-2267.
76. Oepts, D.; Vandermeer, A. F. G.; Vanamersfoort, P. W. *Infrared Phys. Technol.* **1995**, *36*, 297-308.
77. Lemaire, J.; et al. *Phys. Rev. Lett.* **2002**, *89*.
78. Bush, M. F.; O'Brien, J. T.; Prell, J. S.; Wu, C. C.; Saylkally, R. J.; Williams, E. R. *J. Am. Chem. Soc.* **2009**, *131*, 13270-13277.
79. Bush, M. F.; Saykally, R. J.; Williams, E. R. *J. Am. Chem. Soc.* **2008**, *130*, 15482-15489.
80. Bush, M. F.; Saykally, R. J.; Williams, E. R. *J. Am. Chem. Soc.* **2008**, *130*, 9122-9128.
81. Cooper, T. E.; O'Brien, J. T.; Williams, E. R.; Armentrout, P. B. *J. Phys. Chem. A* **2010**, *114*, 12646-12655.
82. O'Brien, J. T.; Williams, E. R. *J. Am. Chem. Soc.* **2012**, *134*, 10228-10236.
83. Prell, J. S.; O'Brien, J. T.; Williams, E. R. *J. Am. Mass. Spectrom.* **2010**, *21*, 800-809.
84. Prell, J. S.; O'Brien, J. T.; Williams, E. R. *J. Am. Chem. Soc.* **2011**, *133*, 4810-4818.
85. Cheng, T. C.; Bandyopadhyay, B.; Mosley, J. D.; Duncan, M. A. *J. Am. Chem. Soc.* **2012**, *134*, 13046-13055.
86. Douberly, G. E.; Walters, R. S.; Cui, J.; Jordan, K. D.; Duncan, M. A. *J. Phys. Chem. A* **2010**, *114*, 4570-4579.
87. Walters, R. S.; Pillai, E. D.; Duncan, M. A. *J. Am. Chem. Soc.* **2005**, *127*, 16599-16610.

88. Ayotte, P.; Bailey, C. G.; Weddle, G. H.; Johnson, M. A. *J. Phys. Chem. A* **1998**, *102*, 3067-3071.
89. Headrick, J. M.; Bopp, J. C.; Johnson, M. A. *J. Chem. Phys.* **2004**, *121*, 11523-11526.
90. Robertson, W. H.; Diken, E. G.; Price, E. A.; Shin, J. W.; Johnson, M. A. *Science* **2003**, *299*, 1367-1372.
91. Ke, H.; van der Linde, C.; Lisy, J. M. *J. Phys. Chem. A* **2014**, *118*, 1363-1373.
92. Nicely, A. L.; Miller, D. J.; Lisy, J. M. *J. Mol. Spectrosc.* **2009**, *257*, 157-163.
93. Kamariotis, A.; Boyarkin, O. V.; Mercier, S. R.; Beck, R. D.; Bush, M. F.; Williams, E. R.; Rizzo, T. R. *J. Am. Chem. Soc.* **2006**, *128*, 905-916.
94. Rizzo, T. R.; Stearns, J. A.; Boyarkin, O. V. *Int. Rev. Phys. Chem.* **2009**, *28*, 481-515.
95. Miller, D. J.; Lisy, J. M. *J. Am. Chem. Soc.* **2008**, *130*, 15381-15392.
96. Duncan, M. A. *Int. Rev. Phys. Chem.* **2003**, *22*, 407-435.
97. Goebbert, D. J.; Garand, E.; Wende, T.; Bergmann, R.; Meijer, G.; Asmis, K. R.; Neumark, D. M. *J. Phys. Chem. A* **2009**, *113*, 7584-7592.
98. Heine, N.; Fagiani, M. R.; Rossi, M.; Wende, T.; Berden, G.; Blum, V.; Asmis, K. R. *J. Am. Chem. Soc.* **2013**, *135*, 8266-8273.
99. Lorenz, U. J.; Rizzo, T. R. *Anal. Chem.* **2011**, *83*, 7895-7901.
100. Johnson, M. A.; Lineberger, W. C. In *Techniques for the Study of Gas-Phase Ion Molecule Reactions*; Farrar, J. M., Saunders, W., Eds.; Wiley: New York, 1988; p 591.
101. Eyler, J. R. **2009**, *28*, 448-467.
102. Hobza, P.; Havlas, Z. *Theor. Chem. Acc.* **2002**, *108*, 325-334.
103. Wright, A. M.; Howard, A. A.; Howard, C.; Tschumper, G. S.; Hammer, N. I. *J. Phys. Chem. A* **2013**, *117*, 5435-5446.
104. Duncan, M. A. *Int. J. Mass Spectrom.* **2000**, *200*, 545-569.
105. Boyarkin, O. V.; Mercier, S. R.; Kamariotis, A.; Rizzo, T. R. **2006**, *128*, 2816-2817.
106. Vaden, T. D.; Lisy, J. M.; Carnegie, P. D.; Pillai, E. D.; Duncan, M. A. *Phys. Chem. Chem. Phys.* **2006**, *8*, 3078-3082.
107. Friedrich, B.; Doylei, J. M. *Chemphyschem* **2009**, *10*, 604-623.
108. Altinay, G.; Metz, R. B. *Int. J. Mass Spectrom.* **2010**, *297*, 41-45.
109. Jasik, J.; Zabka, J.; Roithova, J.; Gerlich, D. *Int. J. Mass Spectrom.* **2013**, *354*, 204-210.
110. Kupser, P.; Steill, J. D.; Oomens, J.; Meijer, G.; von Helden, G. *Phys. Chem. Chem. Phys.* **2008**, *10*, 6862-6866.
111. Schnier, P. D.; Williams, E. R. *Anal. Chem.* **1998**, *70*, 3033-3041.
112. Prell, J. S.; Chang, T. M.; Biles, J. A.; Berden, G.; Oomens, J.; Williams, E. R. *J. Phys. Chem. A* **2011**, *115*, 2745-2751.
113. Schmidt, J.; Kass, S. R. *J. Phys. Chem. A* **2013**, *117*, 4863-4869.
114. Bush, M. F.; Prell, J. S.; Saykally, R. J.; Williams, E. R. *J. Am. Chem. Soc.* **2007**, *129*, 13544-13553.
115. RodriguezCruz, S. E.; Klassen, J. S.; Williams, E. R. *J. Am. Soc. Mass Spectrom.* **1997**, *8*, 565-568.
116. Aue, D. H.; Webb, H. M.; Bowers, M. T. *J. Am. Chem. Soc.* **1976**, *98*, 311-317.
117. Brauman, J. I.; Riveros, J. M.; Blair, L. K. *J. Am. Chem. Soc.* **1971**, *93*, 3914-3918.
118. Brown, H. C. *Science* **1946**, *103*, 385-387.
119. Trotman-Dickenson, A. F. *J. Am. Chem. Soc.* **1949**, 1293-1297.
120. Hall, H. K. *J. Am. Chem. Soc.* **1957**, *79*, 5441-5444.
121. Kumler, W. D.; Strait, L. A. *J. Am. Chem. Soc.* **1943**, *65*, 2349-2354.

122. Tian, Z. X.; Kass, S. R. *Angew. Chem. Int. Ed.* **2009**, *48*, 1321-1323.

Chapter 2. Where's the Charge? Protonation Sites in Gaseous Ions Change with Hydration

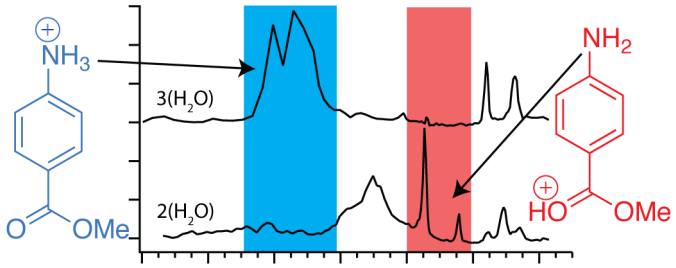

Originally published in the Journal of the American Chemical Society
http://dx.doi.org/10.1021/ja304929h

2.1. Abstract

The role of water in stabilizing sites of protonation in small gaseous ions is investigated using electrospray ionization (ESI) coupled with infrared photodissociation spectroscopy and computational chemistry. Protonation of *p*-aminobenzoic acid (PABA) and *p*-aminobenzoic acid methyl ester (PABAOMe) occurs at the carbonyl oxygen atom both in isolation and when one water molecule is attached. However, protonation occurs at the amine nitrogen atom, which is the most favorable site in aqueous solution, for PABAOMeH$^+$•$(H_2O)_3$ and for a significant fraction of PABAH$^+$•$(H_2O)_6$. Fewer water molecules are necessary to stabilize the solution-phase isomer of PABAOMeH$^+$ (3) than for PABAH$^+$ (≥6), indicating that the favorable hydrogen bonding in PABAH$^+$ is a more important factor than the higher gas-phase basicity of PABAOMeH$^+$ in stabilizing protonation at the carbonyl oxygen atom. Relative Gibbs free energies (133 K) calculated using B3LYP and MP2 with the 6-311++G** basis set were significantly different from each other, and both are in poor agreement with results from the experiments. ωB97X-D/6-311++G**, which includes empirical dispersion corrections, gave results that were most consistent with the experimental data. The relative stabilities of protonating at the carbonyl oxygen atom for PABAH$^+$•$(H_2O)_{0–6}$ and PABAOMeH$^+$•$(H_2O)_{0–2}$ can be rationalized by resonance delocalization. These findings provide valuable insights into the solvent interactions that stabilize the location of a charge site and the structural transitions that can occur during the ESI desolvation process.

2.2. Introduction

The structure of a molecule in solution depends on the intrinsic properties of the molecule itself as well as the interactions between the molecule and its surrounding solvent environment. Solvents with high dielectric constants are especially effective at stabilizing charges on molecules. For example, amino acids adopt zwitterionic structures in aqueous solutions within a wide range of pH, but in the gas phase, the most stable form of the naturally occurring amino acids is nonzwitterionic.[1-3] The zwitterionic forms can be stabilized by the presence of adjacent charges,[4-11] and salt bridges can occur even in small protonated dipeptides[12] as well as larger peptides[13,14] and proteins.[15,16] Solvent also affects the relative ordering of the acid-base properties of molecules. The gas-phase basicity (GB) of methylamines follows the order $NH_3 < MeNH_2 < Me_2NH < Me_3N$, increasing monotonically with an increasing number of methyl groups attached to the nitrogen atom.[17,18] In contrast, the pK_a values in water follow the order $NH_3 < Me_3N < MeNH_2 \approx Me_2NH$.[19-21] Additional methyl groups can stabilize charge due to their polarizability,[17] but less sterically hindered charge sites can be more favorably solvated.[19] These two effects result in the different ordering of the gas- and solution-phase basicities of these molecules.

Electrospray ionization (ESI) can gently transfer intact molecules from solution into the gas phase, and this method has been widely used to produce gaseous ions ranging in size from individual atomic species[22] up to analytes with molecular weights in excess of a MDa.[23,24] Ions are typically desolvated completely prior to mass analysis or characterization by other structural methods, but extensively hydrated ions can also be formed and investigated.[25-30] Structural changes to analytes can occur during the ion desolvation process that takes place in ESI and in the gas phase. Many studies have shown that protein ions can retain a "memory" of their solution structures,[31-37] indicating that large gaseous ions can be kinetically trapped in higher-energy structures during the desolvation process. This kinetic trapping makes it possible in some cases to deduce information about solution-phase structures from gas-phase experiments.

Recent results show that the solvent used in ESI can also affect the structures of small gaseous ions.[38-41] Deprotonated *p*-hydroxybenzoic acid ($[PHBA–H]^-$) was found to predominantly adopt a phenoxide structure when sprayed from CH_3OH/H_2O solutions, whereas the carboxylate was predominantly produced from CH_3CN containing solutions.[38] In contrast, the opposite behavior was observed when the structure of deprotonated PHBA was investigated with different methods and apparatus.[38,39] These results suggest that the form of the ion that is produced by ESI can depend on both the solvent used and the experimental conditions.

Related studies on protonated *p*-aminobenzoic acid ($PABAH^+$, Figure 2.1) show that the ESI solvent can also affect the structure of the gaseous protonated ions. In aqueous solution, the amine group of PABA is the most basic site for protonation to occur,[42] but both calculations[43] and results from recent experiments[40,41] show that protonation of the carbonyl oxygen atom is more favorable in the gas phase. The lowest-energy gas-phase isomer was formed exclusively from a CH_3OH/H_2O solution, but a population of ions adopting the lowest energy aqueous-solution structure was reported to be formed from a solution containing CH_3CN.[40,41]

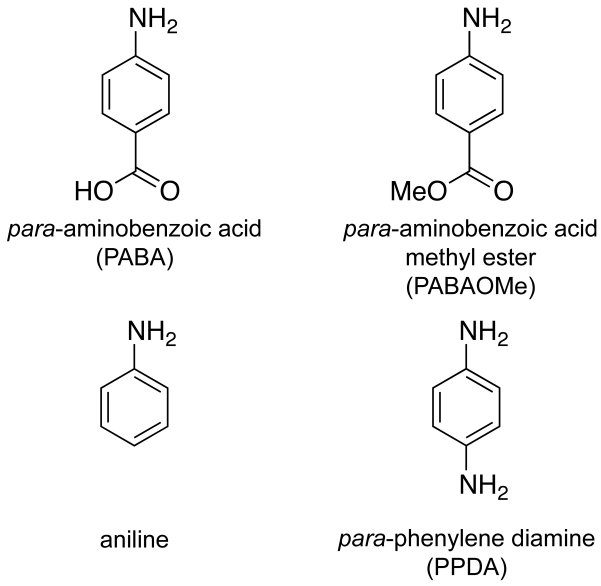

Figure 2.1. Structure and abbreviations for *p*-aminobenzoic acid and related molecules.

Here, the structures of $PABAH^+$ and structurally related molecules are investigated using infrared photodissociation (IRPD) spectroscopy and theory to determine how water stabilizes protonation of these molecules and to determine what structural changes occur during the desolvation process. Unlike previous studies that used mixed solvent systems, the results presented here are from aqueous solutions so that the solvent environment is unaffected by preferential evaporation of a more volatile component. These results indicate that protonated PABA and *p*-aminobenzoic acid methyl ester ($PABAOMeH^+$) are in the lowest-energy gas-phase form when one water molecule is attached, but the more stable solution-phase form is observed when just a few more water molecules are bound. Calculations using B3LYP, ωB97X-D, and MP2 and the 6-311++G** basis set gave widely contrasting results, with ωB97X-D being mostly closely consistent with the experimental data.

2.3. Experimental Section

2.3.1. IRPD Spectroscopy

A 2.75 T Fourier-transform ion cyclotron resonance (FT/ICR) mass spectrometer was used to measure the IRPD spectra of hydrated, protonated PABA as well as structurally related molecules: PABAOMe, aniline, and *p*-phenylene diamine (PPDA), (Figure 2.1). A description of the experimental apparatus is reported elsewhere.[5] All samples were obtained from Sigma-Aldrich (St. Louis, MO) and were electrosprayed from water, purified by a Milli-Q purification system (Millipore, Billerica, MA), at a concentration of 4 – 5 mM using borosilicate capillaries pulled to an inner tip diameter of ~2 μm. A platinum wire in contact with the solution in the capillary is held at a potential between ~700 and ~1000 V relative to a heated metal capillary of the nanoelectrospray interface. Electrostatic lenses guide the ions through five stages of differential pumping and into the ion cell of the mass spectrometer. The ion cell temperature is controlled by a copper jacket that is cooled to 133 K with a regulated flow of liquid nitrogen.[44] A pulse of dry nitrogen gas is introduced into the vacuum chamber at a pressure of $\sim 10^{-6}$ Torr for

~5 s to improve ion trapping and thermalization and is followed by a ~7 s pumpdown to reduce the pressure inside the cell to $<10^{-8}$ Torr. A stored waveform inverse Fourier transform is subsequently used to mass select precursor clusters prior to photodissociation.

The 1064 nm fundamental of a Nd:YAG laser (Continuum Surelight I-10, Santa Clara, CA) is pulsed at a 10 Hz repetition rate to pump the OPO/OPA (LaserVision, Bellevue, WA) used to photodissociate mass-selected clusters. Irradiation times from 5 – 60 s are used to induce substantial but not complete photodissociation of the precursor. First-order photodissociation rate constants are obtained from the precursor and product ion abundances after irradiation as a function of laser frequency.[45] These rate constants are then corrected for frequency-dependent variations in laser power as well as BIRD, which occurs as a result of absorption of blackbody photons from the 133 K ion cell and cell jacket.

2.3.2. Computational Chemistry

A Monte Carlo conformational search for $PABAH^+$ with up to six water molecules attached was performed by using Macromodel 9.1 (Schrödinger, Inc., Portland, OR) to generate at least 300 geometries for the amino-protonated and for the carbonyl-protonated isomers. Separate conformational searches were carried out for $PABAOMeH^+$ and $anilinium^+$ with up to three water molecules, and $PPDAH^+$ with three water molecules. A selection of the low-energy conformers as well as structures obtained from chemical intuition were used to create isomer geometries that represent different hydrogen bonding patterns. Q-Chem 3.1[46] (Q-Chem, Inc., Pittsburgh, PA) was then used to perform a geometry optimization at the B3LYP/6-31+G** level of theory prior to vibrational frequency and intensity calculations at the same level of theory. For calculated spectra, vibrational frequencies were scaled by 0.955 and convolved with a 100 and 15 cm^{-1} fwhm Lorentzian for the 2900 – 3100 cm^{-1} and 3100 – 3900 cm^{-1} regions, respectively. Zero-point energies, enthalpy, and entropy corrections at 133 K were calculated for these structures using unscaled B3LYP/6-31+G** harmonic oscillator vibrational frequencies. Additional optimizations were performed for $PABAOMeH^+•(H_2O)_{2,3}$ and $PABAH^+•(H_2O)_6$ using the B3LYP, MP2, and ωB97X-D methods and the 6-311++G** basis set. Zero-point energy, enthalpy and entropy corrections for these structures were calculated using frequencies obtained at the B3LYP/6-311++G** level of theory.

2.4. Results

2.4.1. Hydration of $PABAH^+$

Protonation of isolated PABA occurs at the carbonyl oxygen atom of the carboxylic acid,[40,41] but protonation of the amine group is most favorable in aqueous solution.[42] To investigate how water solvates the protonated molecule in the gas phase and to determine how many water molecules are required to make protonation at the amine site favorable, IRPD spectra of $PABAH^+•(H_2O)_{1–6}$ were measured in the spectral region between 2600 and 3900 cm^{-1} (Figure 2.2). The bands in the spectrum of $PABAH^+•(H_2O)_1$ at 3443 and 3553 cm^{-1} correspond to the free N–H symmetric stretch (s.s.) and asymmetric stretch (a.s.), respectively, of the neutral amine group. These same two bands persist in the spectrum of $PABAH^+$ with up to six water molecules attached. The presence of these bands indicates that there is a population of ions that

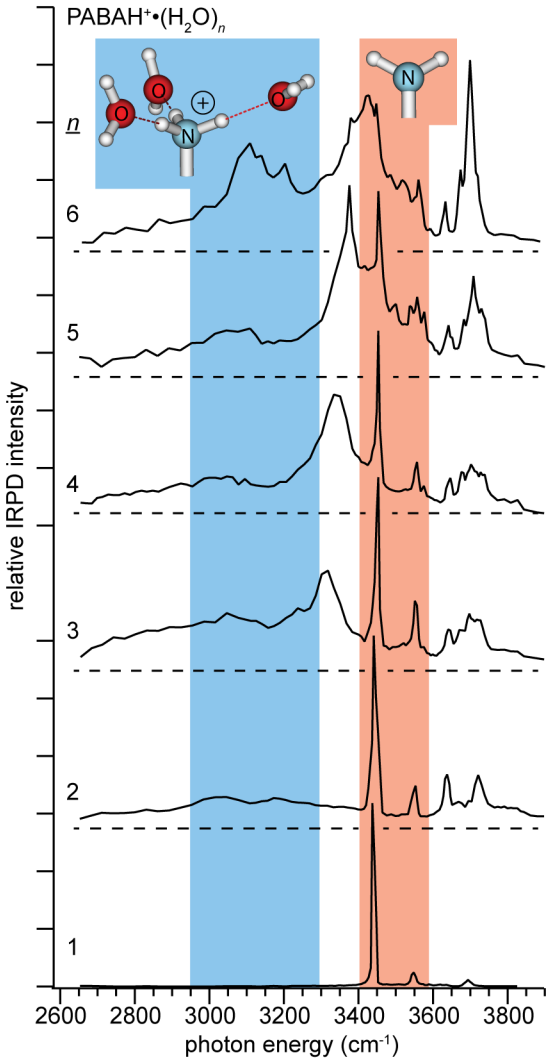

Figure 2.2. IRPD spectra of $PABAH^+•(H_2O)_{1–6}$ at 133 K. Bands associated with a fully hydrated protonated amine or unhydrated neutral amine group are designated by the blue and red regions, respectively.

is not protonated at the amine group, and therefore this population must be protonated at the carbonyl oxygen atom. The assignment of these bands as free N–H stretches of a protonated amine can be ruled out based on the spectra of structurally related ions (see below).

The spectrum of $PABAH^+•(H_2O)_6$ has a broad and intense band near 3100 cm^{-1} corresponding to a hydrogen bonded (HB) N–H stretch of a protonated amine. In comparison, this feature appears in the spectra of hydrated, protonated Val,[47] Phe,[48] and Pro[49] between 2900 and 3200 cm^{-1}. These results indicate that a significant fraction of the ion population is protonated and hydrated at the amine group for $PABAH^+•(H_2O)_6$. Dissociation below 3200 cm^{-1} is also observed for $PABAH^+•(H_2O)_{2–5}$, but this feature is much weaker and broader than the HB N–H stretches that appear in the spectrum of $PABAH^+•(H_2O)_6$. The difference in the width of these two features suggests that they originate from two different vibrational modes. In addition, the absence of a free N–H band of a protonated amine from the spectrum of $PABAH^+•(H_2O)_2$ (which is shown below to occur between 3250 and 3350 cm^{-1}) is further evidence that this

feature does not correspond to the N–H stretch of a protonated amine. Therefore the broad dissociation observed for $PABAH^+•(H_2O)_{2–5}$ is attributed to the HB O–H stretches of the protonated carboxylic acid. Because this feature overlaps with the HB N–H stretches associated with a protonated amine group, it is difficult to unambiguously conclude whether a small population of the solution-phase isomer contributes to the signal below 3200 cm^{-1} for $PABAH^+•(H_2O)_{3–5}$.

In addition to the free N–H features, there are several bands in the spectra of $PABAH^+•(H_2O)_{2–4}$ between 3300 and 3900 cm^{-1} that indicate protonation and hydration occurs predominantly at the carboxylic acid. The bands near 3650 and 3730 cm^{-1} in each of these spectra correspond to a single-acceptor (SA) water s.s. and a.s. New bands appear in the spectra of $PABAH^+•(H_2O)_{3,4}$ at 3340 and 3705 cm^{-1} corresponding to the HB O–H and free O–H stretch of an acceptor-donor (AD) water molecule. The appearance of bands associated with an AD water molecule indicates that the number of solvating water molecules exceeds the number of acidic H-atoms at the charge site to which water can bind. The absence of these bands for doubly hydrated $PABAH^+$, but not for triply hydrated $PABAH^+$, suggests that the charge site has two H-atoms where water can bind, consistent with a protonated carboxylic acid. In contrast, a protonated amine group has three H-atoms to which water can directly coordinate, and these sites are more favorable for water to bind to than the formation of a second hydration shell with the third water molecule. The appearance of an outer solvation shell has been reported for $NH_4^+•(H_2O)_4$, where the number of water molecules equals the number of hydration sites, but such isomers are higher in energy.[50] A second solvation shell has also been reported for $ValH^+•(H_2O)_4$, where one water molecule hydrogen bonds to the carboxylic acid and two water molecules hydrogen bond to the protonated nitrogen atom. The fourth water molecule forms a second solvation shell to the amine and is stabilized by forming a HB to the carbonyl oxygen atom of the C-terminus, an interaction that is not possible for hydrated $PABAH^+$.[47]

The spectrum of $PABAH^+•(H_2O)_1$ has just one band in the free O–H region at 3697 cm^{-1}, which is too low in energy to be a SA water a.s. Therefore, this band is assigned to a double-acceptor (DA) water a.s. The DA water s.s. is not observed, but this may be due to weak absorption typical of this mode.[51,52] The presence of a DA water molecule indicates that the water molecule forms HBs to both H-atoms of the protonated carboxylic acid. These results indicate that with up to five water molecules, $PABAH^+$ is predominantly protonated and hydrated at the carboxylic acid site, but a transition to the more favorable protonation site in aqueous solution occurs when this ion is hydrated by six or more water molecules.

2.4.2. Hydration of $PABAOMeH^+$

The IRPD spectra of $PABAOMeH^+•(H_2O)_{1–3}$ are shown in Figure 2.3. The spectra of $PABAOMeH^+•(H_2O)_{1,2}$ have bands near 3450 and 3555 cm^{-1}, corresponding to the free N–H s.s. and a.s., respectively, of a neutral amine group, consistent with protonation and hydration at the carbonyl oxygen of the ester group. The signature of a DA and a SA water molecule in the spectra of the single hydrates of $PABAH^+$ and $PABAOMeH^+$, respectively, is consistent with the inability of a water molecule to form two HB in the latter ion. The free N–H stretches are largely absent in the spectrum of $PABAOMeH^+•(H_2O)_3$, and two bands appear between 2930 and 3200 cm^{-1}, consistent with the HB N–H stretches of a protonated amine, indicating that protonation and hydration occurs at the amine. These results suggest that $PABAOMeH^+$ is protonated at the

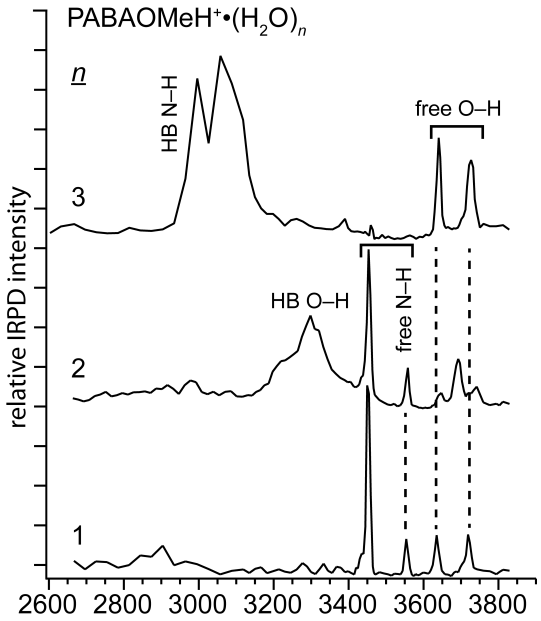

Figure 2.3. IRPD spectra of $PABAOMeH^+•(H_2O)_{1–3}$ at 133 K.

carbonyl oxygen atom when singly and doubly hydrated, but protonation occurs at the amine group when three water molecules are attached.

The appearance of a significant population of the solution-phase isomer occurs at a lower hydration state for $PABAOMeH^+$ (3 water molecules) than it does for $PABAH^+$ (6 water molecules). Although there is evidence for both isomers in the spectrum of $PABAH^+•(H_2O)_6$, the IRPD spectrum for triply hydrated $PABAOMeH^+$ indicates that the vast majority of the ion population is the amino-protonated isomer. The origin for the different behavior these two molecules is discussed below.

2.4.3. Confirmation of Band Assignments

Here, we confirm the assignments of all the bands in the spectra of hydrated $PABAH^+$ and $PABAOMeH^+$ from comparisons to the IRPD spectra of structurally related compounds, shown in Figure 2.1, and by comparisons to calculated spectra. Hydrated $anilinium^+$ is a model for protonation and hydration at the amine, and hydrated $PPDAH^+$ is a reference for the N–H stretches of an unprotonated amine. The spectra of these hydrated ions are discussed below.

2.4.4. Hydration of $Anilinium^+$

The spectra of $anilinium^+•(H_2O)_{1–3}$ (Figure 2.4a) can be readily interpreted based on previous results for other ions as well as from a comparison to calculated spectra of lowest-energy structures (Figure 2.4b). The spectrum of singly hydrated $anilinium^+$ has a band at 2841 cm^{-1} that blue shifts to 3054 cm^{-1} and increases in intensity for $anilinium^+•(H_2O)_3$. This band is too low in energy to be an O–H or a free N–H stretch. It is therefore assigned to the HB N–H stretch of a protonated amine group. This assignment is supported by calculations, which remarkably predict frequencies for these bands to within 50 cm^{-1} of the observed frequencies despite the harmonic oscillator approximation and the single scaling factor used in these

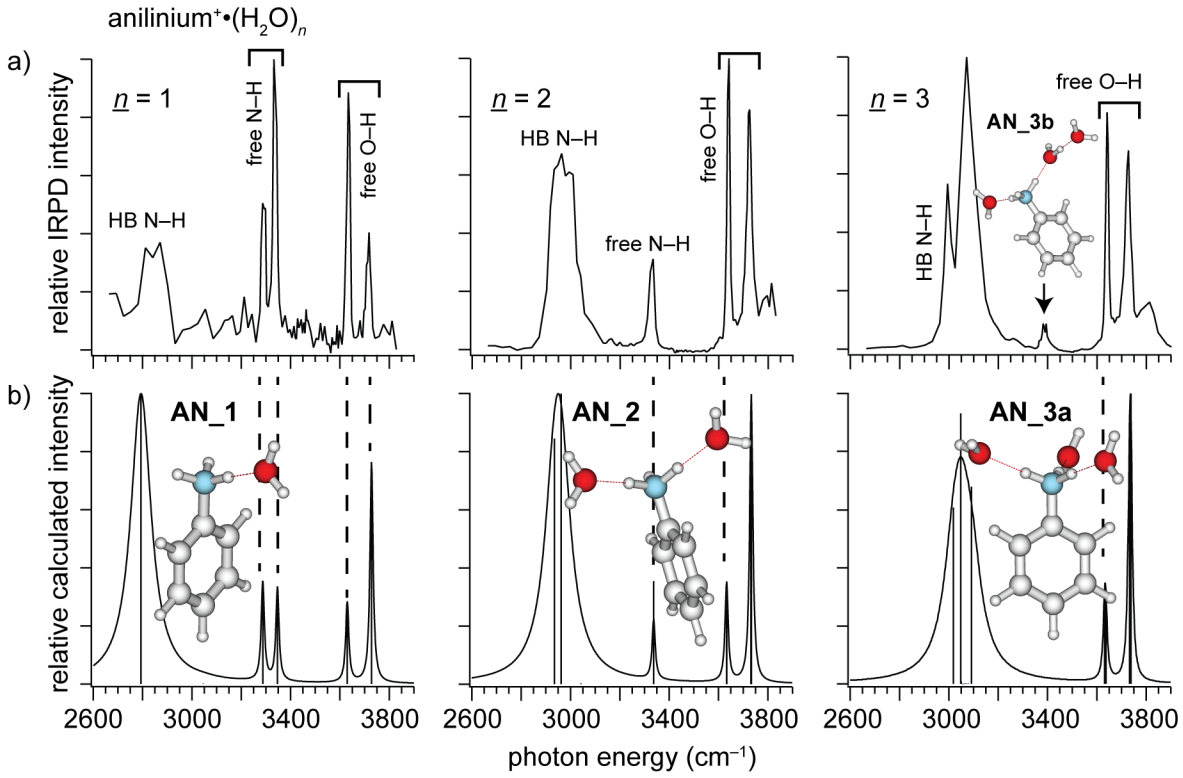

Figure 2.4. (a) IRPD spectra at 133 K and (b) calculated structures and spectra for lowest energy structures of anilinium$^+$•$(H_2O)_{1–3}$ at the B3LYP/6-31+G** level of theory.

calculations. This band also appears in the spectra of anilinium$^+$•$(H_2O)_{4–6}$ (Figure 2.5), although it is blue shifted to 3100 cm^{-1}. This HB N–H stretch band occurs in the same region as a similar band in the spectrum of PABAH$^+$•$(H_2O)_6$, confirming the presence a population of the amino-protonated isomer for these ions. This HB N–H stretch band in the spectrum of anilinium$^+$•$(H_2O)_3$ (Figure 2.4 top right) is nearly the same as the corresponding band in the spectrum of PABAOMeH$^+$•$(H_2O)_3$ (Figure 2.3 top), confirming that the amine in the latter ion is both protonated and hydrated.

The calculated spectra of the lowest-energy isomers of anilinium$^+$•$(H_2O)_{1–3}$ (Figure 2.4b) have two, one and no free N–H stretches, respectively, between 3250 and 3350 cm^{-1} that closely match in frequency with the corresponding bands in the measured spectra. The appearance of a comparatively low-intensity band in this region for anilinium$^+$•$(H_2O)_3$ indicates that there is also a small population of ions where water forms a second solvation shell, i.e., only two of the three water molecules HB to the protonated amine, as seen with structure **AN_3b**. The structure with all three water molecules coordinating to the protonated amine group (**AN_3a**) is calculated to be the lowest-energy structure, but **AN_3b** is only 4.9 kJ mol^{-1} higher in energy, consistent with the appearance of a minor population of this ion in the measured spectrum. The bands associated with the free N–H stretch of a protonated amine are absent from the spectrum of PABAH$^+$•$(H_2O)_2$, supporting the assignment of the dissociation below 3200 cm^{-1} to the HB O–H stretches of the carboxylic acid.

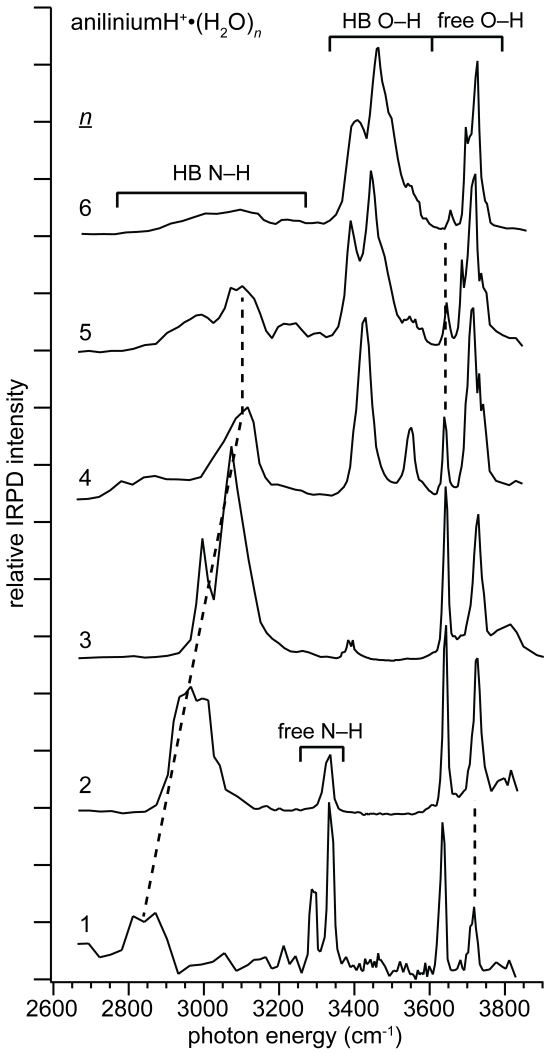

Figure 2.5. IRPD spectra of anilinium$^+$•$(H_2O)_{1–6}$ at 133 K.

The bands in the HB O–H and free O–H regions can be assigned based both on calculations and on previous results for hydrated ammonia.[50,53] The spectra of anilinium$^+$•$(H_2O)_{1–3}$ have bands near 3640 and 3720 cm^{-1} corresponding to a SA water s.s. and a.s., respectively, and these frequencies are also accurately predicted by theory to within 15 cm^{-1} (Figure 2.4). New bands appear in the spectra of anilinium$^+$•$(H_2O)_{4–6}$ (Figure 2.5) between 3340 and 3600 cm^{-1}, consistent with HB O–H stretches also observed for NH_4^+•$(H_2O)_{5–7}$.[50] Additionally, the band near 3717 cm^{-1} increases in intensity due to the appearance of an AD water free O–H stretch that overlaps with the SA water a.s. Interestingly, bands associated with the formation of a second solvation shell for anilinium$^+$•$(H_2O)_4$ occur at 3430 and 3552 cm^{-1}, potentially overlapping with the free N–H stretches of a neutral amine group. However, these bands can be distinguished by their widths. The neutral amine N–H stretch bands have a fwhm of less than 20 cm^{-1}, whereas the HB O–H stretch features have a fwhm of greater than 30 cm^{-1}. The greater widths of the HB O–H stretch bands can be attributed to the effects of anharmonicity and dynamics associated with HBs that are not present for the free N–H stretches.[54]

2.4.5. Hydration of $PPDAH^+$

$PPDAH^+$ has both a protonated and a neutral amine group. Thus, the spectrum of $PPDAH^+•(H_2O)_3$ provides information about where the N–H stretches of an uncharged amine in $PABAH^+$ and $PABAOMeH^+$ should occur, and the IRPD spectrum of this ion as well as that of $anilinium^+•(H_2O)_3$ are shown in Figure 2.6a. The bands for the HB N–H stretches of a

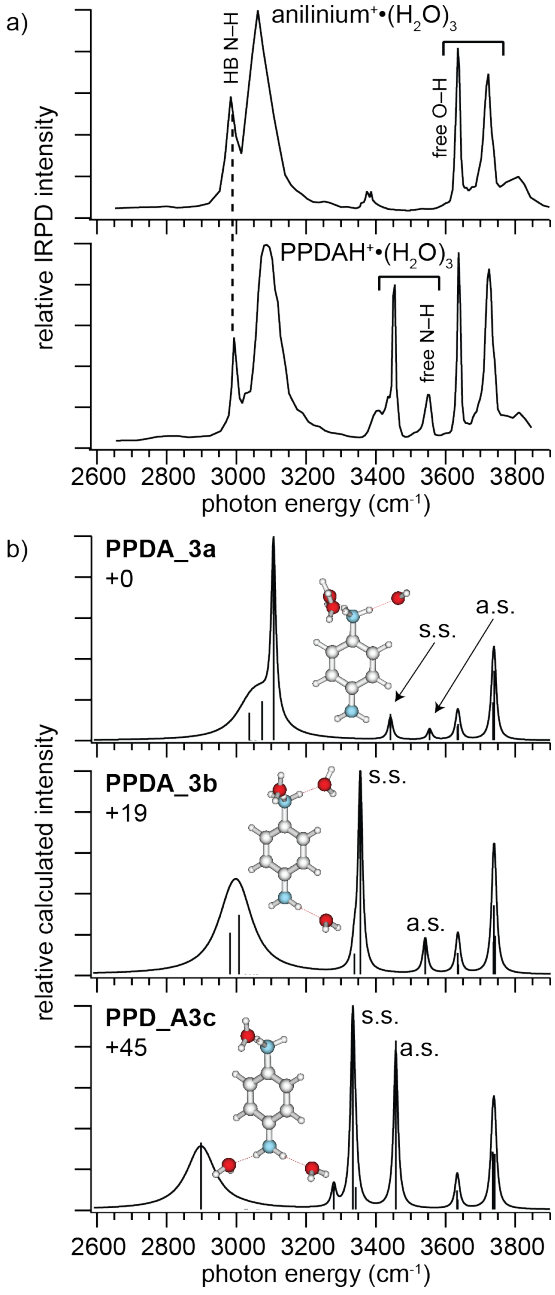

Figure 2.6. (a) IRPD spectra of $anilinium^+•(H_2O)_3$ and $PPDAH^+•(H_2O)_3$ at 133 K. (b) Calculated spectra and 133 K relative Gibbs free energies (in kJ mol^{-1}) of low-energy structures (the symmetric stretch (s.s.) and asymmetric stretch (a.s.) of the neutral N–H stretches are indicated on the spectra). Structures, spectra and relative Gibbs free energies are calculated at the B3LYP/6-31+G** level of theory.

protonated amine group and SA water O–H stretches appear in both spectra, indicating an ion structure where all of the water molecules solvate the protonated amine for $PPDAH^+•(H_2O)_3$. The band near 3400 cm^{-1} indicates that a small fraction of the population has a water molecule in the outer solvation shell. In addition to the bands observed for $anilinium^+•(H_2O)_3$, the spectrum of $PPDAH^+•(H_2O)_3$ also has bands at 3458 and 3557 cm^{-1}. These bands can be confidently assigned to the free N–H stretches of an unhydrated neutral amine group and support the assignments for the corresponding peaks in the spectra of $PABAH^+•(H_2O)_{1–6}$, and $PABAOMeH^+•(H_2O)_{1,2}$.

Figure 2.6b shows calculated structures and spectra of low-energy conformers along with calculated relative 133 K Gibbs free energies. The lowest-energy structure, **PPDA_3a**, has a fully solvated, protonated amine group and an unsolvated, neutral amine group. The calculated spectrum for **PPDA_3a** is a close frequency match to the IRPD spectrum, supporting the above assignments for these bands. The structure that has two water molecules solvating the protonated amine and one water molecule solvating the neutral amine, **PPDA_3b**, is a poor frequency match with the experimental spectrum and is 19 kJ mol^{-1} higher in energy than **PPDA_3a**. Attaching a water molecule to the neutral amine group causes a red shift in the neutral amine s.s. to ~3350 cm^{-1}. The neutral amine a.s., however, remains relatively unperturbed. The addition of a second water molecule to the neutral amine group, shown in **PPDA_3c**, causes a red shift in the neutral amine a.s. to ~3450 cm^{-1}, while the frequency of the s.s. exhibits only a subtle red shift in comparison to the spectrum of **PPDA_3b**. **PPDA_3c** is a poor frequency match with the experimental spectrum, and is calculated to be 45 kJ mol^{-1} higher in energy. Thus, it is unlikely that the ion population contains a significant amount of this isomer. These results indicate that the ion population is predominantly **PPDA_3a**.

2.5. Discussion

2.5.1. Gas-phase Basicity vs. Hydrogen Bonding

In the absence of solvent, $PABAH^+$ is protonated at the carboxylic acid[40,41] whereas in aqueous solution, protonation of the amine is more favorable.[42] The GB of PABAOMe is 20.7 kJ mol^{-1} greater than that of PABA,[55] which should make protonation of the carbonyl oxygen of $PABAOMeH^+$ even more favorable. So why are fewer water molecules required for $PABAOMeH^+$ to adopt its solution-phase structure (3) than for $PABAH^+$ (≥6)? $PABAOMeH^+$ has one fewer H-atom at this site that can form a HB to water, making it somewhat less favorable to adduct water molecules to the ester. Evidently, protonation of a carbonyl oxygen atom is better stabilized by more favorable solvation of the protonated carboxylic acid of $PABAH^+$ than by the higher basicity of the methyl ester for $PABAOMeH^+$.

2.5.2. Stability of a Protonated Carboxylic Acid

The higher basicity of the carboxylic acid compared to the amine for isolated PABA can be attributed to resonance stabilization. The GB of aniline is 18.3 kJ mol^{-1} greater than that of PABA and 60.5 kJ mol^{-1} greater than that of benzoic acid.[55] Thus, the basicity at each group is significantly affected by the presence of the other group. A neutral amine can donate electron density into the conjugated π system to better stabilize the positive charge associated with the

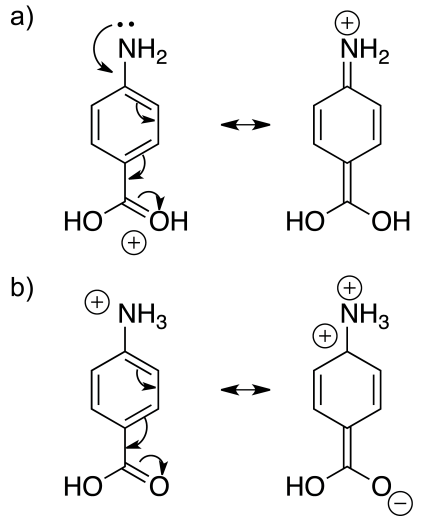

Figure 2.7. Resonance contributors for $PABAH^+$ protonated at the (a) carboxylic acid or at the (b) amine.

protonated carboxylic acid (Figure 2.7a). If the amine is protonated, the carboxylic acid withdraws electron density due to the electronegativity of the oxygen atom, which destabilizes the positive charge at the protonated amine group (Figure 2.7b). This conjugation between the two functional groups results in the carboxylic acid of a neutral PABA molecule being the most basic site in the gas phase. Similarly, the stability of the phenoxide form of deprotonated PHBA was attributed to resonance stabilization.[39] Based on the measured GB values, conjugation stabilizes protonation of the carboxylic acid by as much as ~42 kJ mol^{-1}, and the protonation of the amine is destabilized by more than ~18 kJ mol^{-1}.

2.5.3. Kinetic Trapping?

Kass and co-workers reported that the gaseous structures of $PABAH^+$ depend on the electrospray solvent used, indicating that kinetic trapping of high-energy structures occurrs.[40,41] In order to determine whether the structures observed in these experiments are the lowest-energy structures, or if they are higher-energy structures that are kinetically trapped by evaporation of water molecules from more extensively hydrated ions, the structures of these ions and their hydrates were investigated using computational chemistry. The relative Gibbs free energies for $PABAH^+•(H_2O)_{0–3,6}$ and $PABAOMeH^+•(H_2O)_{0–3}$ at 133 K were calculated at the B3LYP/6-31+G** level of theory. Protonation at the carbonyl oxygen atom is lower in energy than protonation at the amine nitrogen by 35 and 41 kJ mol^{-1} for isolated PABA and PABAOMe, respectively (structures in Figures S2.1 and S2.2, top). The value for isolated PABA is consistent with a previously reported 298 K enthalpy difference of 33 kJ mol^{-1} at this same level of theory.[40] An enthalpy difference of 17 kJ mol^{-1} was calculated with the G3 method, although the difference in enthalpy decreased to less than 12 kJ mol^{-1} if this value was corrected for deviations in computed and experimental proton affinities of aniline and benzoic acid.[41] Protonation at a carbon atom in the ring of PABA is at least 40 kJ mol^{-1} higher in energy (Figure S2.3), consistent with previous calculations.[40]

Protonation of the carbonyl oxygen atom is favored by 36 and 32 kJ mol^{-1} for $PABAH^+•(H_2O)_1$ and $PABAOMeH^+•(H_2O)_1$, respectively (low-energy structures are shown in Figure S2.1 and S2.2). Although the difference in energy decreases with increasing hydration

state, protonation of the carbonyl oxygen atom is still calculated to be lower in energy by 22 and 19 kJ mol^{-1} for PABAH$^+$•$(H_2O)_6$ and PABAOMeH$^+$•$(H_2O)_3$, respectively. Protonation at the carbon atom in the ring is even higher in energy when these ions are hydrated (Figure S2.3). These results indicate that the most stable structures for PABAH$^+$•$(H_2O)_{1–6}$ and PABAOMeH$^+$•$(H_2O)_{1–3}$ are protonated at the carbonyl oxygen atom, and that amino-protonated structures should not be observed in these experiments. In striking contrast, the experiments indicate that protonation at the amine occurs for the most extensively hydrated ions studied. To the extent that the energetic values obtained from these calculations are accurate, the solution-phase isomers that are observed in these experiments at higher hydration states must be formed by solvent evaporation and kinetic trapping from more extensively hydrated ions for which the solution-phase structure is most stable.

To evaluate the accuracy of these calculations, additional calculations were performed for PABAOMeH$^+$•$(H_2O)_{2,3}$ and PABAH$^+$•$(H_2O)_6$, and these results are summarized in Table 2.1 (structures shown in Figure 2.8). PABAOMeH$^+$•$(H_2O)_{2,3}$ is potentially an excellent benchmark for theory because of the distinct transition from a carbonyl-protonated structure for PABAOMeH$^+$•$(H_2O)_2$ to an amino-protonated structure for PABAOMeH$^+$•$(H_2O)_3$ indicated by the experimental data. For PABAOMeH$^+$ with two and three water moleculues, B3LYP/6-31+G** indicates that protonation of the carbonyl oxygen atom is 22 and 19 kJ mol^{-1} more favorable, respectively. With the 6-311++G** basis set, these differences are reduced slightly to 19 and 13 kJ mol^{-1}, respectively. In sharp contrast, MP2/6-311+G** indicates that amine protonation is favorable by 14 and 33 kJ mol^{-1} for this ion with two and three water molecules attached, respectively. With MP2, structure **PABAOMe_G_3a** (Figure 2.8) is not stable, and this structure underwent a proton transfer to form neutral PABAOMe and a hydronium ion (Figure S2.4). The relative B3LYP and MP2 energies calculated with the 6-311++G** basis set for O vs. N protonation for PABAOMeH$^+$ with two and three water molecules differ by 33 and 46 kJ mol^{-1}, respectively.

The ωB97X-D functional, which includes empirical atom-atom dispersion corrections, was recently introduced and should be well suited for systems where noncovalent interactions, such as hydrogen bonding, are significant.[56] With ωB97X-D/6-311++G**, protonation at the carbonyl oxygen atom of PABAOMeH$^+$•$(H_2O)_2$ is lower in energy by 6.6 kJ mol^{-1} compared to protonation at the amine nitrogen. For PABAOMeH$^+$ with three water molecules attached, protonation at the amine nitrogen is favored, although it is predicted to be nearly isoenergetic (to within ~1 kJ mol^{-1}) with protonation of the carbonyl oxygen atom. Thus, the change in structure from O to N protonation for PABAOMeH$^+$ with two and three water molecules observed in the experiment is correctly predicted by ωB97X-D/6-311++G**.

A similar comparison between different levels of theory for PABAH$^+$•$(H_2O)_6$ (Table 2.1), where a mixture of both the gas- and solution-phase isomers were observed in the IRPD spectrum, was performed. Increasing the basis set with B3LYP has a relatively small effect on the relative energies, and protonation of the carbonyl oxygen atom is favored by 20 kJ mol^{-1} with B3LYP/6-311++G**. By contrast, protonation of the amine nitrogen is 29 kJ mol^{-1} *lower* in energy with MP2/6-311++G**. This is a 49 kJ mol^{-1} difference in the relative energies predicted by these two methods. With ωB97X-D/6-311++G**, protonation of the carbonyl oxygen atom is only 2.5 kJ mol^{-1} higher in energy, consistent with the observed presence of both isomers. As

Table 2.1. Calculated relative Gibbs free energies at 133 K in kJ mol^{-1} of selected structures.

	B3LYP/ 6-31+G**	B3LYP/ 6-311++G**	ωB97X-D/ 6-311++G**	MP2/ 6-311++G**
PABAOMe_S_2a	22	19	6.6	0
PABAOMe_G_2a	0	0	0	14
PABAOMe_S_3a	19	13	0	0
PABAOMe_G_3a	0	0	1.1	–
PABAOMe_G_3b	14	10	12	33
PABA_S_6a	22	20	0	0
PABA_G_6a	0	0	2.5	29

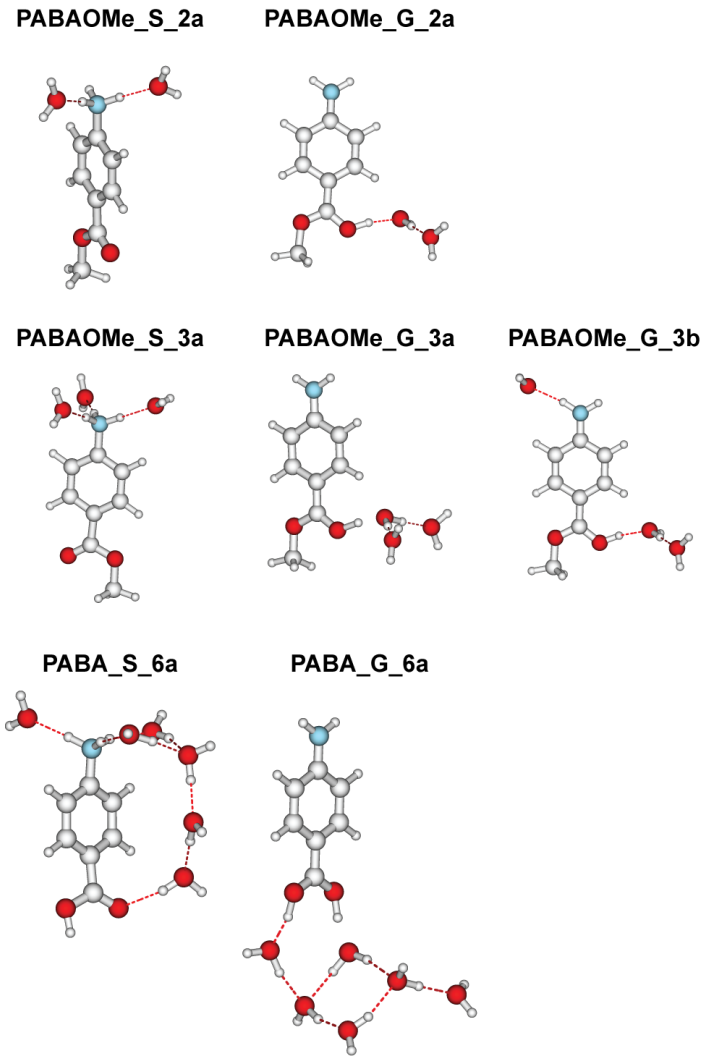

Figure 2.8. Low-energy structures for PABAOMeH$^+$•$(H_2O)_{2,3}$ and PABAH$^+$•$(H_2O)_6$ minimized at the B3LYP/6-31+G** level of theory. With the exception of **PABAOMe_G_3a**, structures obtained at higher levels of theory are nearly identical.

was the case for $PABAOMeH^+•(H_2O)_{2,3}$, the ωB97X-D/6-311++G** level of theory is in closest agreement with the experimental data.

To the extent that these ωB97X-D/6-311++G** calculations are accurate, this indicates that ions are not kinetically trapped in higher-energy structures in these experiments. For $PABAH^+•(H_2O)_6$, **PABA_S_6a** (Figure S2.1), in which the water molecules form a bridge between the two protonation sites, is the lowest energy structure at the MP2/6-311++G** and ωB97X-D/6-311+G** levels of theory. This and similar structures should make proton transfer between the two protonation sites facile, reducing the possibility of kinetic trapping. A water bridge between two charges sites is unfavorable for $PABAOMeH^+•(H_2O)_{2,3}$, yet the experimental results show that these ions are protonated at different sites. The excellent agreement between experiment and the ωB97X-D/6-311++G** calculations for both ions suggests that low-energy structures are formed in these experiments even without water bridging. Additional higher level calculations will ultimately be required to more definitively answer this question.

2.6. Conclusion

IRPD spectra of hydrated, protonated PABA were measured in the region from 2600 to 3900 cm^{-1} in order to study the relative stabilities of the preferred isolated gas- and solution-phase isomers as a function of hydration state. The preferred gas-phase isomer was observed for $PABAH^+•(H_2O)_{1–5}$, but both the solution- and gas-phase isomers are present for $PABAH^+•(H_2O)_6$. For $PABAOMeH^+$, protonation of the carbonyl oxygen atom occurs with one and two water molecules attached, but protonation of the amine occurs with three water molecules attached. The spectral assignments for these ions were confirmed by measuring IRPD spectra of structurally related compounds. Results from calculations depend strongly on the method used. B3LYP and MP2 with the 6-311++G** basis set give widely opposing results, neither of which is in line with results from these experiments. In contrast, the ωB97X-D/6-311++G** level of theory gave relative energies that are much more consistent with the experimental data.

Fewer water molecules are necessary to stabilize protonation at the amine of $PABAOMeH^+$ compared to $PABAH^+$, indicating that the more favorable HB in the latter ion is more important in stabilizing protonation of a carboxyl group than the higher GB of this site in PABAOMe. Protonation of the carbonyl oxygen atom in the isolated ion is favored due to the conjugation between the carboxyl and amine groups. When the carboxyl group is protonated, the neutral amine donates electron density into the conjugated π system, delocalizing and stabilizing the positive charge associated with a protonated carbonyl oxygen atom.

This is the first study to report a change in protonation from the most favorable site in the gas phase to the most favorable site in aqueous solution with increasing hydration state. These results provide insight into how water stabilizes protonation sites in molecules and structural transitions that can occur during the desolvation process in ESI.

2.7. References

1. Locke, M. J.; McIver, R. T. *J. Am. Chem. Soc.* **1983**, *105*, 4226-4232.
2. Skurski, P.; Gutowski, M.; Barrios, R.; Simons, J. *Chem. Phys. Lett.* **2001**, *337*, 143-150.
3. Linder, R.; Seefeld, K.; Vavra, A.; Kleinermanns, K. *Chem. Phys. Lett.* **2008**, *453*, 1-6.
4. Jockusch, R. A.; Price, W. D.; Williams, E. R. *J. Phys. Chem. A.* **1999**, *103*, 9266-9274.
5. Bush, M. F.; O'Brien, J. T.; Prell, J. S.; Saykally, R. J.; Williams, E. R. *J. Am. Chem. Soc.* **2007**, *129*, 1612-1622.
6. Forbes, M. W.; Bush, M. F.; Polfer, N. C.; Oomens, J.; Dunbar, R. C.; Williams, E. R.; Jockusch, R. A. *J. Phys. Chem. A.* **2007**, *111*, 11759-11770.
7. Dunbar, R. C.; Polfer, N. C.; Oomens, J. *J. Am. Chem. Soc.* **2007**, *129*, 14562-14563.
8. Wu, R. H.; McMahon, T. B. *Angew. Chem. Int. Ed.* **2007**, *46*, 3668-3671.
9. Armentrout, P. B.; Rodgers, M. T.; Oomens, J.; Steill, J. D. *J. Phys. Chem. A.* **2008**, *112*, 2248-2257.
10. O'Brien, J. T.; Prell, J. S.; Berden, G.; Oomens, J.; Williams, E. R. *Int. J. Mass Spectrom.* **2010**, *297*, 116-123.
11. Mino, W. K.; Szczepanski, J.; Pearson, W. L.; Powell, D. H.; Dunbar, R. C.; Eyler, J. R.; Polfer, N. C. *Int. J. Mass Spectrom.* **2010**, *297*, 131-138.
12. Prell, J. S.; O'Brien, J. T.; Steill, J. D.; Oomens, J.; Williams, E. R. *J. Am. Chem. Soc.* **2009**, *131*, 11442-11449.
13. Schnier, P. D.; Price, W. D.; Jockusch, R. A.; Williams, E. R. *J. Am. Chem. Soc.* **1996**, *118*, 7178-7189.
14. Freitas, M. A.; Marshall, A. G. *Int. J. Mass Spectrom.* **1999**, *182*, 221-231.
15. Jockusch, R. A.; Schnier, P. D.; Price, W. D.; Strittmatter, E. F.; Demirev, P. A.; Williams, E. R. *Anal. Chem.* **1997**, *69*, 1119-1126.
16. Skinner, O. S.; McLafferty, F. W.; Breuker, K. *J. Am. Soc. Mass Spectrom.* **2012**, *23*, 1011-1014.
17. Brauman, J. I.; Riveros, J. M.; Blair, L. K. *J. Am. Chem. Soc.* **1971**, *93*, 3914-3918.
18. Aue, D. H.; Webb, H. M.; Bowers, M. T. *J. Am. Chem. Soc.* **1976**, *98*, 311-317.
19. Trotman-Dickenson, A. F. *J. Am. Chem. Soc.* **1949**, 1293-1297.
20. Brown, H. C. *Science* **1946**, *103*, 385-387.
21. Hall, H. K. *J. Am. Chem. Soc.* **1957**, *79*, 5441-5444.
22. Wang, G. D.; Cole, R. B. *Anal. Chim. Acta.* **2000**, *406*, 53-65.
23. Chen, R. D.; Cheng, X. H.; Mitchell, D. W.; Hofstadler, S. A.; Wu, Q. Y.; Rockwood, A. L.; Sherman, M. G.; Smith, R. D. *Anal. Chem.* **1995**, *67*, 1159-1163.
24. Fuerstenau, S. D.; Benner, W. H.; Thomas, J. J.; Brugidou, C.; Bothner, B.; Siuzdak, G. *Angew. Chem. Int. Ed.* **2001**, *40*, 542-544.
25. Rodriguez-Cruz, S. E.; Klassen, J. S.; Williams, E. R. *J. Am. Mass. Spectrom.* **1999**, *10*, 958-968.
26. Nonose, S.; Iwaoka, S.; Mori, K.; Shibata, Y.; Fuke, K. *Eur. Phys. J. D.* **2005**, *34*, 315-319.
27. Donald, W. A.; Demireva, M.; Leib, R. D.; Aiken, M. J.; Williams, E. R. *J. Am. Chem. Soc.* **2010**, *132*, 4633-4640.
28. O'Brien, J. T.; Prell, J. S.; Bush, M. F.; Williams, E. R. *J. Am. Chem. Soc.* **2010**, *132*, 8248-8249.

29. Prell, J. S.; O'Brien, J. T.; Williams, E. R. *J. Am. Chem. Soc.* **2011**, *133*, 4810-4818.
30. Nagornova, N. S.; Rizzo, T. R.; Boyarkin, O. V. *Science*. **2012**, *336*, 320-323.
31. Wang, F.; Freitas, M. A.; Marshall, A. G.; Sykes, B. D. *Int. J. Mass Spectrom.* **1999**, *192*, 319-325.
32. Gross, D. S.; Zhao, Y. X.; Williams, E. R. *J. Am. Soc. Mass Spectrom.* **1997**, *8*, 519-524.
33. Lin, H.; Dass, C. *Rapid Commun. Mass Spectrom.* **2001**, *15*, 2341-2346.
34. Covey, T.; Douglas, D. J. *J. Am. Mass. Spectrom.* **1993**, *4*, 616-623.
35. Cox, K. A.; Julian, R. K.; Cooks, R. G.; Kaiser, R. E. *J. Am. Mass. Spectrom.* **1994**, *5*, 127-136.
36. Hudgins, R. R.; Woenckhaus, J.; Jarrold, M. F. *Int. J. Mass Spectrom.* **1997**, *165*, 497-507.
37. Pierson, N. A.; Chen, L. X.; Valentine, S. J.; Russell, D. H.; Clemmer, D. E. *J. Am. Chem. Soc.* **2011**, *133*, 13810-13813.
38. Tian, Z. X.; Wang, X. B.; Wang, L. S.; Kass, S. R. *J. Am. Chem. Soc.* **2009**, *131*, 1174-1181.
39. Steill, J. D.; Oomens, J. *J. Am. Chem. Soc.* **2009**, *131*, 13570-13571.
40. Tian, Z. X.; Kass, S. R. *Angew. Chem. Int. Ed.* **2009**, *48*, 1321-1323.
41. Schmidt, J.; Meyer, M. M.; Spector, I.; Kass, S. R. *J. Phys. Chem. A.* **2011**, *115*, 7625-7632.
42. Kumler, W. D.; Strait, L. A. *J. Am. Chem. Soc.* **1943**, *65*, 2349-2354.
43. Tang, M.; Isbell, J.; Hedges, B.; Brodbelt, J. *J. Mass. Spectrom.* **1995**, *30*, 977-984.
44. Wong, R. L.; Paech, K.; Williams, E. R. *Int. J. Mass Spectrom.* **2004**, *232*, 59-66.
45. Prell, J. S.; O'Brien, J. T.; Williams, E. R. *J. Am. Mass. Spectrom.* **2010**, *21*, 800-809.
46. Shao, Y.; et al. *Phys. Chem. Chem. Phys.* **2006**, *8*, 3172-3191.
47. Kamariotis, A.; Boyarkin, O. V.; Mercier, S. R.; Beck, R. D.; Bush, M. F.; Williams, E. R.; Rizzo, T. R. *J. Am. Chem. Soc.* **2006**, *128*, 905-916.
48. Prell, J. S.; Chang, T. M.; O'Brien, J. T.; Williams, E. R. *J. Am. Chem. Soc.* **2010**, *132*, 7811-7819.
49. Prell, J. S.; Correra, T. C.; Chang, T. M.; Biles, J. A.; Williams, E. R. *J. Am. Chem. Soc.* **2010**, *132*, 14733-14735.
50. Chang, H. C.; Wang, Y. S.; Lee, Y. T. *Int. J. Mass Spectrom.* **1998**, *180*, 91-102.
51. Huisken, F.; Kaloudis, M.; Kulcke, A. *J. Chem. Phys.* **1996**, *104*, 17-25.
52. Prell, J. S.; Williams, E. R. *J. Am. Chem. Soc.* **2009**, *131*, 4110-4119.
53. Wang, Y. S.; Jiang, J. C.; Cheng, C. L.; Lin, S. H.; Lee, Y. T.; Chang, H. C. *J. Chem. Phys.* **1997**, *107*, 9695-9698.
54. Cimas, A.; Vaden, T. D.; de Boer, T.; Snoek, L. C.; Gaigeot, M. P. *J. Chem. Theory Comput.* **2009**, *5*, 1068-1078.
55. Hunter, E. P.; Lias, S. G. Proton Affinity Evaluation. In *NIST Chemistry WebBook, NIST*; Linstrom, P. J., Mallard, W. G., Eds.; National Institute of Standards and Technology: Gaithersburg, MD, November 1998 (http://webbook.nist.gov).
56. Chai, J. D.; Head-Gordon, M. *Phys. Chem. Chem. Phys.* **2008**, *10*, 6615-6620.

2.8. Supplementary Figures

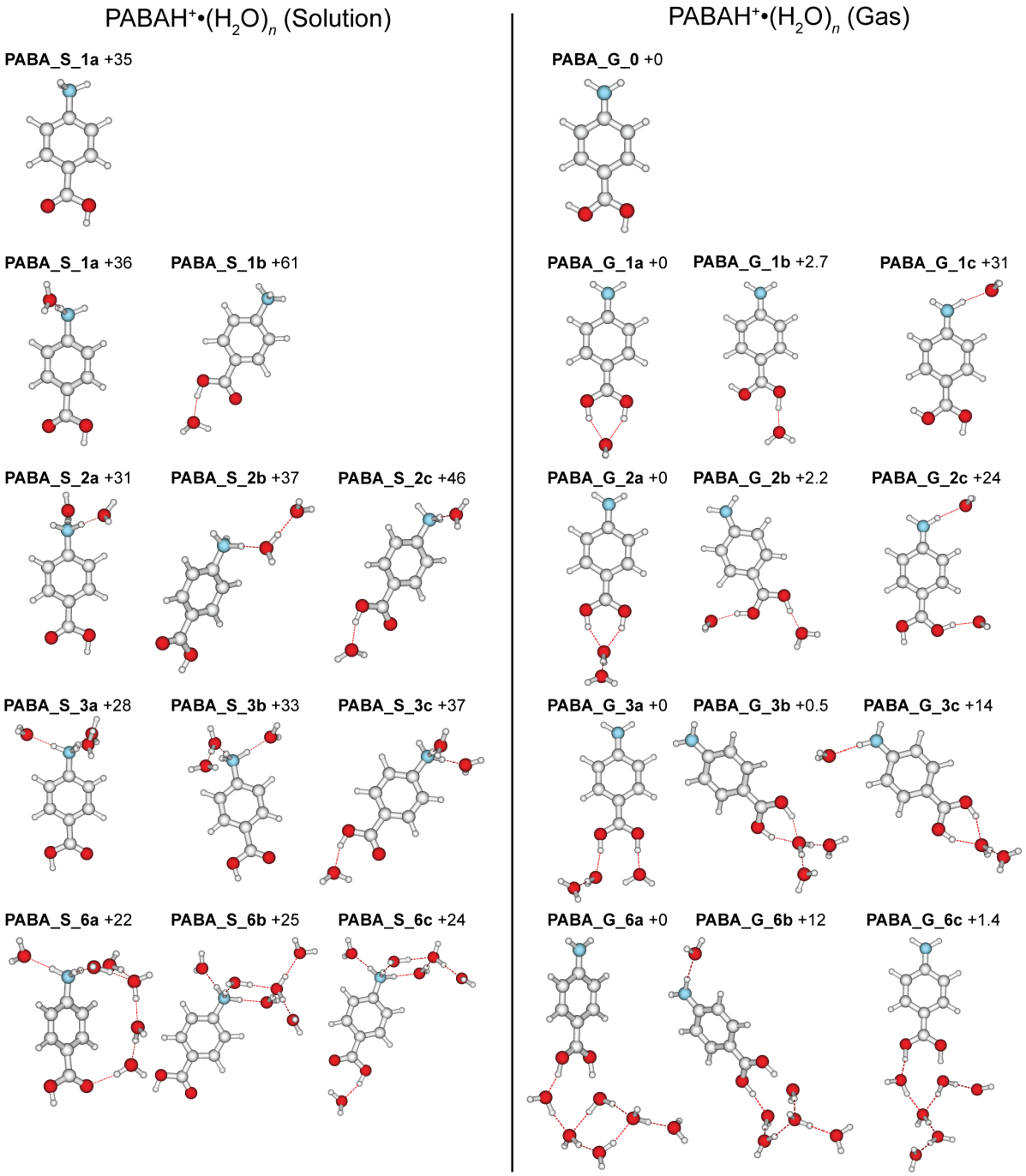

Figure S2.1. Calculated structures and relative 133 K Gibbs free energies (kJ mol^{-1}) for PABAH$^+$•$(H_2O)_{0–3,6}$. Relative energies were calculated at the B3LYP/6-31+G** level of theory . Structures are designated by **PABA_*X*_*nx***. ***X*** is designated either **S** for structures with a aqueous-solution isomer or **G** for structures with a gas-phase isomer. The ***n*** indicates the hydration state and the ***x*** distinguishes between different conformers with the same protonation site and hydration state.

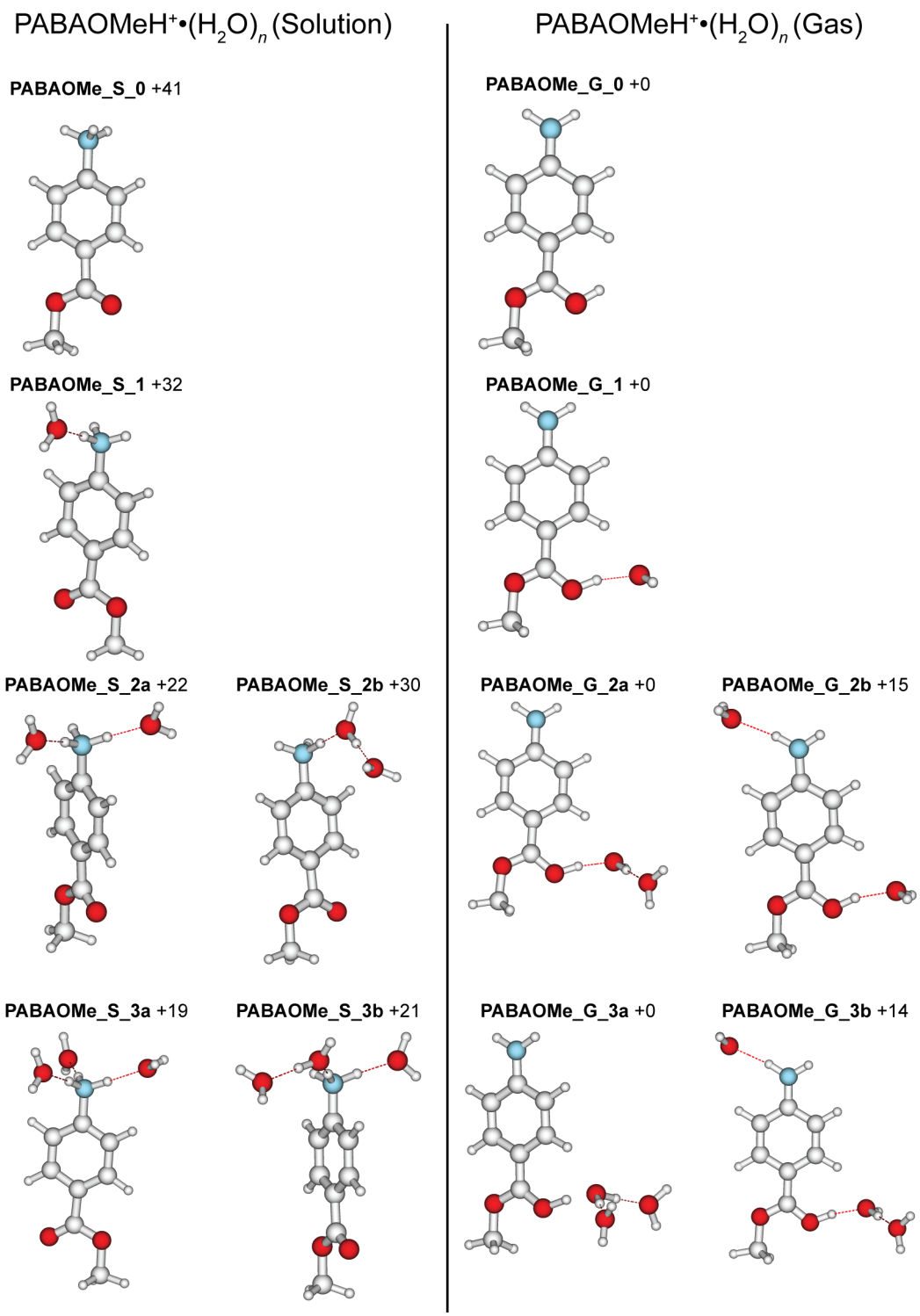

Figure S2.2. Calculated structures and 133 K relative Gibbs free energies (kJ mol^{-1}) for $PABAOMeH^+•(H_2O)_{0–3}$. Relative energies are calculated at the B3LYP/6-31+G** level of theory. Structures are designated by **PABAOMe_*X*_*nx***. ***X*** is designated either **S** for structures with a aqueous-solution isomer or **G** for structures with a gas-phase isomer. The ***n*** indicates the hydration state and the ***x*** distinguishes between different conformers with the same protonation site and hydration state when necessary.

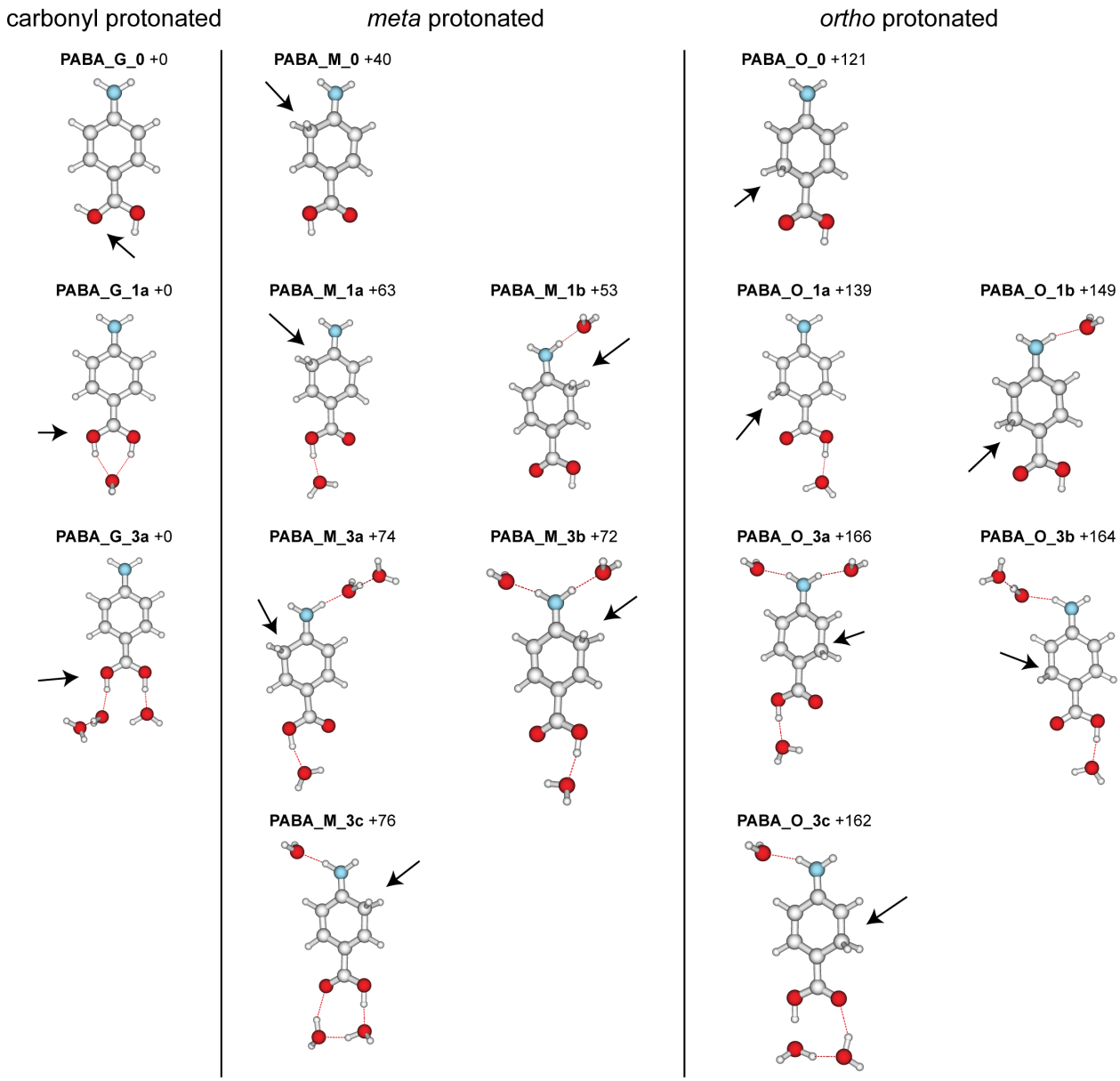

Figure S2.3. Calculated structures and relative 133 K Gibbs free energies (kJ mol^{-1}) for $PABAH^+•(H_2O)_{0,1,3}$ ions protonated at the carbonyl oxygen or the aromatic ring. Relative energies were calculated at the B3LYP/6-31+G** level of theory . Structures are designated by **PABA_*X*_*nx***. ***X*** is designated **G** for structures with a gas-phase isomer, **M** for protonation at the *meta* position, or **O** for protonation at the *ortho* position. The protonation site is also indicated with an arrow. The ***n*** indicates the hydration state and the ***x*** distinguishes between different conformers with the same protonation site and hydration state.

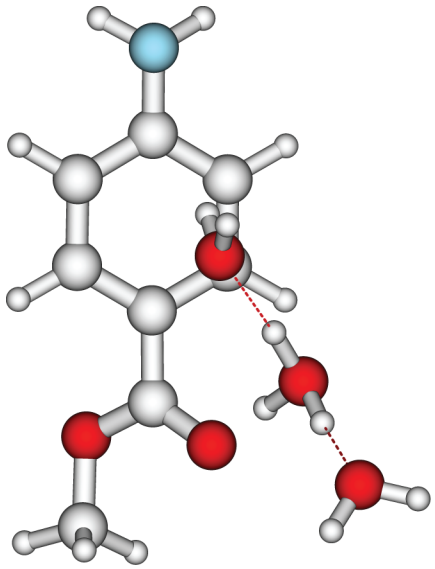

Figure S4. Structure of **PABAOMe_G_3a** minimized at the MP2/6-311++G** level of theory.

Chapter 3. Hydration of Gaseous *meta*-Aminobenzoic Acid: Ionic vs. Neutral Hydrogen Bonding and Water Bridges

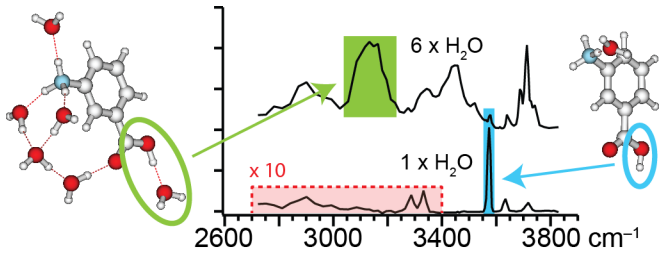

This chapter has been submitted to the Journal of the American Chemical Society

3.1. Abstract

Hydration of a protonated amine and a neutral carboxylic acid were investigated for protonated *meta*-aminobenzoic acid ($MABAH^+$) with up to 15 water molecules attached using infrared photodissociation spectroscopy, laser induced dissociation kinetics, and computational chemistry. A free COO–H stretch in the spectra of $MABAH^+•(H_2O)_{1–5}$ indicates that water does not bind to the carboxylic acid H atom. This band is absent in the spectrum of $MABAH^+$ with six or more water molecules attached, and there is a hydrogen bonded (HB) COO–H stretch indicating that water hydrogen bonds to the carboxylic acid H atom for these larger clusters. Photodissociation kinetic data for $MABAH^+•(H_2O)_6$ indicate that ≥74% of the ion population consists of the HB COO–H isomer. These results are consistent with calculations at the B3LYP/6-31+G** level of theory that indicate that the HB COO–H isomer is ~3 kJ mol^{-1} lower in Gibbs free energy (133 K) than the free COO–H isomer. Lower effective ion heating rates, either by attenuation of the laser power or irradiating the ions at a lower frequency result in more time for interconversion between the free and HB COO–H isomers. These data suggest that the barrier to dissociation for the free COO–H isomer is less than that for the HB COO–H isomer but greater than the barrier for interconversion between the two isomers. These results show the competition between hydration of a primary protonated amine vs. a neutral carboxylic acid and the effect of water bridging between the two functional groups, which provide valuable insight into the hydration of protonated amino acids and establish rigorous benchmarks for theoretical modeling of water-biomolecule interactions.

3.2. Introduction

Water plays an important role in many different physical properties of molecules in solution. In the aqueous solution, the basicities of methylamines follow the order $NH_3 < Me_3N < MeNH_2 \approx Me_2NH$,[1-3] whereas the gas-phase basicities of these molecules follow the order $NH_3 < MeNH_2 < Me_2NH < Me_3N$.[4,5] The difference in the ordering between the gas- and solution-phase basicities of these molecules is due to the ability of water to effectively stabilize charge, which is hindered by the presence of multiple methyl groups. Such solvent-ion interactions can change the intrinsic structures and reactivities of ions.

Water can also influence the protonation[6-9] or deprotonation[10-12] sites of molecules. Protonation of isolated *para*-aminobenzoic acid occurs at the carbonyl O atom[6,7] as a result of resonant stabilization of the positive charge,[9] but protonation of the amine N atom occurs in water.[8] This solution-phase structure is observed for gaseous ions with six or more water molecules attached.[9] Water also affects the stabilities of the zwitterionic forms of amino acids. In the gas phase, amino acids are nonzwitterionic,[13,14] whereas these molecules are zwitterionic in water over a wide range of pH. Results from spectroscopic studies of hydrated gaseous Trp indicate that it is nonzwitterionic with up to four water molecules attached, but there is a population of the zwitterionic form with five or six water molecules attached.[15] The nonzwitterionic form of Gly is calculated to be lowest in energy for $Gly•(H_2O)_{1–6}$, but the zwitterionic form is the lowest-energy structure for $Gly•(H_2O)_{7,8}$.[16] Similarly, water can stabilize the zwitterionic forms of amino acid cation complexes. Results from IR photodissociation spectroscopy of $Arg•Li^+$ indicate that Arg is nonzwitterionic,[17,18] whereas the zwitterionic form of Arg, in which the side chain is protonated and the carboxylic acid is deprotonated, is more stable with the attachment of a single water molecule to this complex.[19] These results demonstrate that interactions between an ion and even one water molecule can significantly affect ion structure.

An advantage of studying hydration of ions in the gas phase is that effects of each water molecule on molecular structure can be probed. The sequential binding energies of individual water molecules to protonated[20-23] and cationized[24-29] amino acids have been measured using a variety of thermochemical methods. Structural information can be inferred from these data, but more detailed information is typically obtained by computations. Results from hydration equilibrium experiments for $PheH^+•(H_2O)_n$, $TrpH^+•(H_2O)_n$ and $TyrH^+•(H_2O)_n$ ($n = 1 – 5$) show that the sequential water binding enthalpies decrease from 54 kJ $mol^{–1}$ to 33 kJ $mol^{–1}$ with increasing hydration.[22] Low-energy structures computed for these ions indicate that a single water molecule binds more strongly to the protonated amine by only 4 kJ $mol^{–1}$ compared to the binding at the neutral carboxylic acid H atom. Interactions between the phenyl ring and the carbonyl O atom with two of the H atoms of the protonated amine reduce the water binding affinities to these amine H atoms.

Detailed information about ion-water interactions can be directly obtained from ion spectroscopy,[9,19,30-44] which can be used in combination with laser dissociation kinetics experiments to measure relative populations of non-interconverting isomers, from which accurate relative binding energies can be obtained.[42,43] Spectroscopic and kinetic data for $PheH^+•(H_2O)_1$ indicate that the attachment of a single water molecule to the neutral carboxylic

acid H is only 1 kJ mol^{-1} higher in Gibbs free energy than to the fully exposed H atom of the protonated anime.[42] For $ProH^+•(H_2O)_1$, hydration of the C-terminal H atom is enthalpically favored due to the ability for the water molecule to form a second, weak hydrogen bond (HB) to the carbonyl O atom of the carboxylic acid, and is the preferred binding site at low temperature.[43]

Here, the competitive solvation of a protonated amine and a neutral carboxylic acid is investigated for hydrated, protonated *meta*-aminobenzoic acid ($MABAH^+$) using infrared photodissociation (IRPD) spectroscopy, laser induced dissociation kinetics, and computational chemistry. Unlike *para*-aminobenzoic acid, protonation of the carbonyl O atom at the carboxylic acid is not resonantly stabilized, and the amine is calculated to be the favored gas-phase protonation site.[45] A HB cannot be formed between theses two functional groups, making $MABAH^+$ an excellent model for investigating the intrinsic competition between the hydration of a protonated amine and neutral carboxylic acid. These results provide insight into how water interacts with both charged and neutral functional groups.

3.3. Experimental

3.3.1. IRPD Spectroscopy

The IRPD spectra of hydrated, protonated MABA and *meta*-aminobenzoic acid methyl ester (MABAOMe) were measured using a 7.0 T Fourier-transform ion cyclotron resonance (FT/ICR) mass spectrometer. The compounds (Sigma-Aldrich, St. Louis, MO, U.S.A.) were dissolved in water purified by a Milli-Q purification system (Millipore, MA) to a concentration of ~4 mM. Sample solutions were transferred into borosilicate capillaries that were pulled to an inner tip diameter of ~2 μm. Electrospray was induced by applying a ~700 V difference between a platinum filament that is in contact with the solution and the heated metal capillary entrance of the mass spectrometer. Electrostatic lenses guide the hydrated ions through five stages of differential pumping into the ion cell. A copper jacket surrounding the cell is maintained at a temperature of ~133 K by a regulated flow of liquid nitrogen. Dry nitrogen gas is pulsed into the vacuum chamber to enhance thermalization and trapping of the ions. Between 6 and 11 s after ions are trapped, the cell pressure is $<10^{-8}$ Torr. Ions of interest are isolated by a stored waveform inverse Fourier transform. Photodissociation was induced by irradiating the precursor ions using an OPO/OPA (LaserVision, Bellevue, WA, USA) pumped by the fundamental of a Nd: YAG laser (Continuum Surelight I-10, Santa Clara, CA, USA) at a repetition rate of 10 Hz. Irradiation times of 5 – 60 s were used for spectroscopy and up to 120 s to measure more accurate laser induced dissociation kinetic data at a fixed laser frequency. First order dissociation rate constants, obtained from the precursor and product ion abundances after irradiation and corrected for laser power and absorption of ~133 K blackbody photons, are plotted as a function of laser frequency to generate IRPD spectra.[46]

3.3.2. Computational Chemistry

Macromodel 9.1 (Schrodinger, Inc., Portland, OR) was used for Monte Carlo conformational searches for $MABAH^+$ with up to six water molecules attached to generate at least 2000 initial geometries for each hydration state. A selection of the low-energy conformers as well as structures obtained from chemical intuition that represent different hydrogen-bonding patterns were used as starting geometries for density functional calculations. Q-Chem 4.0[47] (Q-

Chem, Inc., Pittsburgh, PA) was used to perform a geometry optimization as well as vibrational frequency and intensity calculations at the B3LYP/6-31+G** level of theory. Calculated vibrational frequencies were scaled by 0.955 and convolved with a 30 and 15 cm^{-1} fwhm Gaussian for the 2700 – 3550 and 3350 – 3900 cm^{-1} regions, respectively. Zero-point energies, enthalpy, and entropy corrections at 133 K were calculated for these structures using unscaled B3LYP/6-31+G** harmonic oscillator vibrational frequencies.

3.4. Results and Discussion

3.4.1. Protonation Site for $MABAH^+$

Hydration of $MABAH^+$ with up to 15 water molecules attached was investigated using IRPD spectroscopy in the region from 2700 – 3900 cm^{-1} and by computational chemistry. Protonation of the N atom of the amine for isolated $MABAH^+$ is favored over protonation at the carbonyl O atom of the carboxylic acid by 8 kJ mol^{-1} at the B3LYP/6-31+G** level of theory. These results are consistent with those from previous PM3 calculations,[45] and the difference between the two forms of the protonated ion is expected to increase with increasing hydration state.

The IRPD spectrum of $MABAH^+•(H_2O)_1$ (Figure 1a) has bands at 3287 and 3332 cm^{-1} corresponding to the free N–H symmetric and asymmetric stretches (s.s. and a.s., respectively) of a protonated amine that donates a HB to a single water molecule. These frequencies are within 10 cm^{-1} for the free N–H and O–H stretches and within 50 cm^{-1} for the HB N–H stretch of the corresponding peaks in the IRPD spectrum of $anilinium^+•(H_2O)_1$.[9] These results indicate that the amine group is protonated and that the water molecule attaches at this site.

There is an intense and relatively sharp band in the IRPD spectrum of $MABAH^+•(H_2O)_1$ at 3573 cm^{-1}. This feature corresponds to the carboxylic acid free COO–H stretch, which occurs near 3560 cm^{-1} in the spectra of hydrated, protonated amino acids.[19,42-44] The IRPD spectrum of *para*-aminobenzoic acid, for which hydration and protonation occur at the carboxylic acid group, has a free N–H s.s. and a.s. at 3443 and 3553 cm^{-1},[6,9] respectively. There is no significant dissociation in the spectrum of $MABAH^+•(H_2O)_1$ from 3360 – 3550 cm^{-1}, the region where the free N–H s.s. for a neutral amine should appear. Thus, there is no significant population of ions that are protonated and hydrated at the carboxyl group. These data support our conclusion that both the proton and the water molecule are located at the amine group.

The lowest-energy structures for N-protonated $MABAH^+•(H_2O)_1$ with water attached to either the protonation site or the carboxylic acid are shown in Figure 1b. The structure where the water molecule forms an ionic HB to the protonated amine (**MABAH1a**) is 25 kJ mol^{-1} lower in energy than the one in which the water molecule accepts a neutral HB from the carboxylic acid hydroxyl group (**MABAH1b**). The calculated frequencies for the free N–H and COO–H stretches for **MABAH1a** are within 15 cm^{-1} of the corresponding bands in the measured spectrum. The computed frequencies for the hydrogen bonded (HB) N–H stretch as well as the s.s. and a.s. of a water molecule that accepts a single HB (single-acceptor, SA water molecule) are within 6 – 25 cm^{-1} of the peaks in the measured spectrum at 2901, 3634 and 3718 cm^{-1}, respectively. There is a greater difference in the calculated and measured frequencies for the HB

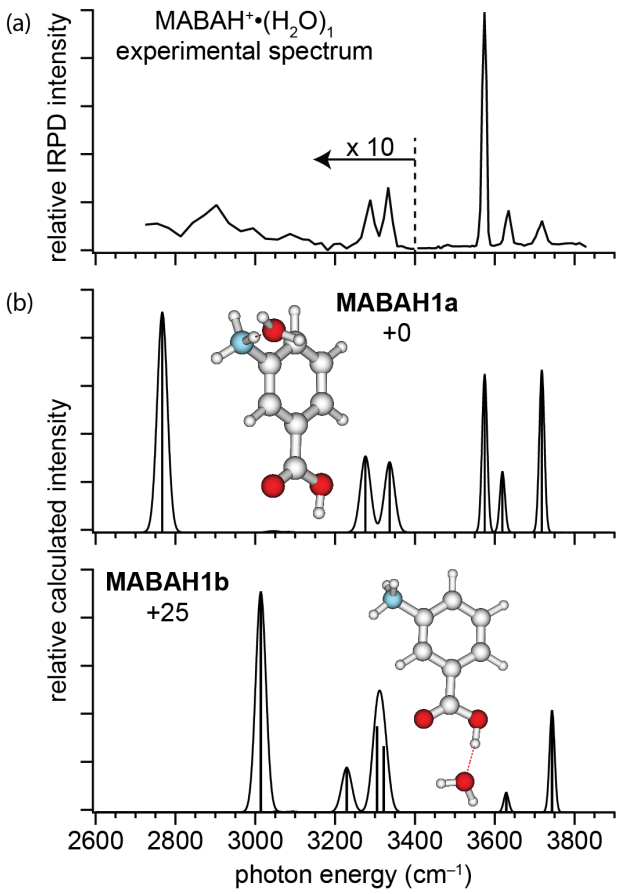

Figure 1. (a) IRPD spectrum of $MABAH^+•(H_2O)_1$ measured at 133 K and (b) calculated spectra of two isomers. 133 K relative Gibbs free energies (in kJ mol^{-1}) calculated at the B3LYP/6-31+G** level of theory are inset.

N–H band that can be attributed to the greater anharmonic nature of vibrational modes that participate in HBs compared to free N–H or O–H stretches.[48] The calculated spectrum for **MABAH1a** is a good frequency match to the measured spectrum whereas the calculated spectrum for **MABAH1b** is not. The free COO–H band is absent from the spectrum of the **MABAH1b** isomer, and there is an extra free N–H stretch feature at 3229 cm^{-1}. These results indicate that the water molecule forms an ionic HB to the protonated amine group.

3.4.2. Water-Ammonium vs. Water-Water Hydrogen Bonding

$MABAH^+$ has four H atoms that can donate HBs to water molecules: the three H atoms of the ammonium group and the hydroxyl H atom of the carboxylic acid. The IRPD spectrum for $MABAH^+•(H_2O)_2$ (Figure 2a) has an intense carboxylic acid free COO–H stretch, indicating that water does not bind to this hydration site. There is only one distinguishable free N–H stretch at ~3325 cm^{-1}, indicating that two H atoms of the ammonium group each donate a HB. The SA

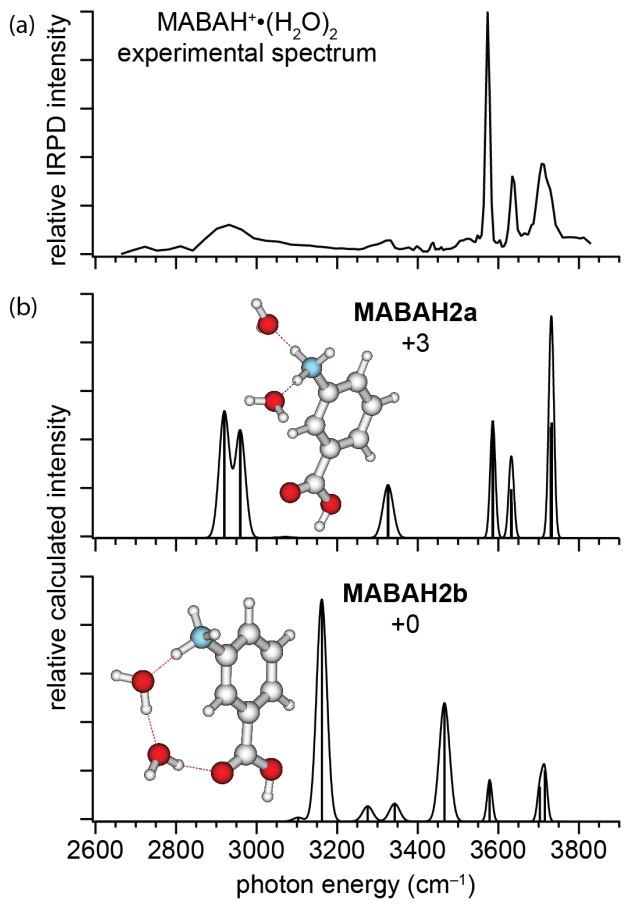

Figure 2. (a) IRPD spectrum of $MABAH^+•(H_2O)_2$ measured at 133 K and (b) calculated spectra of two isomers. 133 K relative Gibbs free energies (in kJ mol^{-1}) calculated at the B3LYP/6-31+G** level of theory are inset.

water s.s. and a.s. that appear in the measured spectrum of $MABAH^+•(H_2O)_1$ are also present for $MABAH^+•(H_2O)_2$. These results are consistent with each of the two water molecules accepting a HB from the protonated amine group for $MABAH^+•(H_2O)_2$.

Two low-energy structures computed for $MABAH^+•(H_2O)_2$ are shown in Figure 2b. In **MABAH2a**, both water molecules bind to the protonated amine, whereas in **MABAH2b**, the water molecules form a bridge between the amine and the carbonyl O atom of the carboxylic acid. The Gibbs free energies of these two structures differ by only 3 kJ mol^{-1}. The calculated spectrum for the higher energy structure, **MABAH2a,** matches the IRPD spectrum well, with the vibrational frequencies near the measured frequencies (to within 10 cm^{-1} for the free N–H and O–H stretches and to within 30 cm^{-1} for the HB N–H stretch). The close frequency match results indicate that the ion population for $MABAH^+$ with two water molecules attached predominantly consists of **MABAH2a**, but the bands computed for this structure do not fully account for the IRPD spectrum.

The free N–H and O–H features at ~3330 and ~3720 cm^{-1}, respectively, have shoulders, indicating the presence of more than one band. The calculated spectrum for **MABAH2b** has two free N–H stretches at 3276 and 3342 cm^{-1} and a free O–H stretch of water molecules that accept and donate a HB (acceptor-donor, AD water molecules) near 3710 cm^{-1}. It is possible that the shoulders in the measured spectrum are a result of a minor population of isomers similar to **MABAH2b**. There is also some dissociation measured from 3000 – 3200 cm^{-1} and a minor band near 3440 cm^{-1} that can be explained by the HB O–H stretches computed for this structure near 3160 and 3470 cm^{-1}. These results suggest that there may be a small population of structures similar to **MABAH2b** for $MABAH^+•(H_2O)_2$. There is a small, broad peak at ~3530 cm^{-1}, and the width of this feature suggests that is due to HB O–H stretches. The appearance of this band indicates that a small population of an unidentified isomer may also be present, or it may be an overtone or combination band. This feature also overlaps with a peak in the measured spectrum of $MABAH^+•(H_2O)_3$ (Figure 3a) at ~3520 cm^{-1}, but the former is wider than the latter. It is unclear whether these two bands originate from similar vibrational modes.

The IRPD spectrum of $MABAH^+•(H_2O)_3$ (Figure 3a) has a relatively sharp and intense band at 3708 cm^{-1} that corresponds to the free O–H stretch of an AD water molecule. There are also features in the region from 3150 – 3550 cm^{-1} that correspond to HB O–H stretches, although there may be contributions from free N–H stretches in this region as well. The AD free O–H and HB O–H bands occur from 3700 – 3730 cm^{-1} and 3250 – 3450 cm^{-1}, respectively, for hydrated anilinium$^+$ and NH_4^+,[9,49] consistent with the assignment of these features in the spectrum of $MABAH^+•(H_2O)_3$. These bands indicate the presence of water-water HBs. The ion population for $MABAH^+•(H_2O)_{1,2}$ predominantly consists of structures where the water molecules coordinate directly to the protonated amine. For $MABAH^+•(H_2O)_3$, the formation of water-water HBs is more favorable than the formation of an additional HB to the H atom of either the ammonium or the carboxylic acid group. In contrast, the major isomer for anilinium$^+•(H_2O)_3$ has all three water molecules hydrogen bonded to the ammonium group, although there is a minor population of isomers where one water molecule forms a second solvation shell, and the ammonium group for protonated *para*-aminobenzoic acid methyl ester with three water molecules attached is also fully hydrogen-bonded.[9] The stability of structures with water-water HBs for $MABAH^+•(H_2O)_3$ is enhanced owing to the ability to form a hydrogen-bonding bridge to the carboxylic acid group.

The IRPD spectrum for $MABAH^+$ with three water molecules attached is similar to that for $MABAH^+•(H_2O)_4$ (Figure 4a, bottom). Both spectra have the same features in the HB and free O–H regions (3200 – 3900 cm^{-1}). The similarities between the two spectra indicate that $MABAH^+•(H_2O)_4$ also adopt structures where there are water-water HBs. The carboxylic acid free COO–H stretch remains a major feature, indicating that water does not coordinate to the carboxylic acid H atom.

The HB N–H stretch for $MABAH^+•(H_2O)_3$ is relatively weak and appears at ~3000 cm^{-1}, whereas this feature is much more intense and centered at ~3050 cm^{-1} for $MABAH^+•(H_2O)_4$. The greater relative intensity and the frequency of the HB N–H stretch for $MABAH^+•(H_2O)_4$ is indicative of the HB N–H stretches of a fully hydrogen-bonded ammonium group. The IRPD spectrum of anilinium$^+$ with three water molecules attached, for which the ammonium group is fully hydrogen-bonded, has HB N–H stretches from 2950 – 3150 cm^{-1} (Figure 4a, top),[9]

consistent with the results for $MABAH^+•(H_2O)_4$. These data indicate that the fourth water molecule hydrates the third and remaining H atom of the ammonium group.

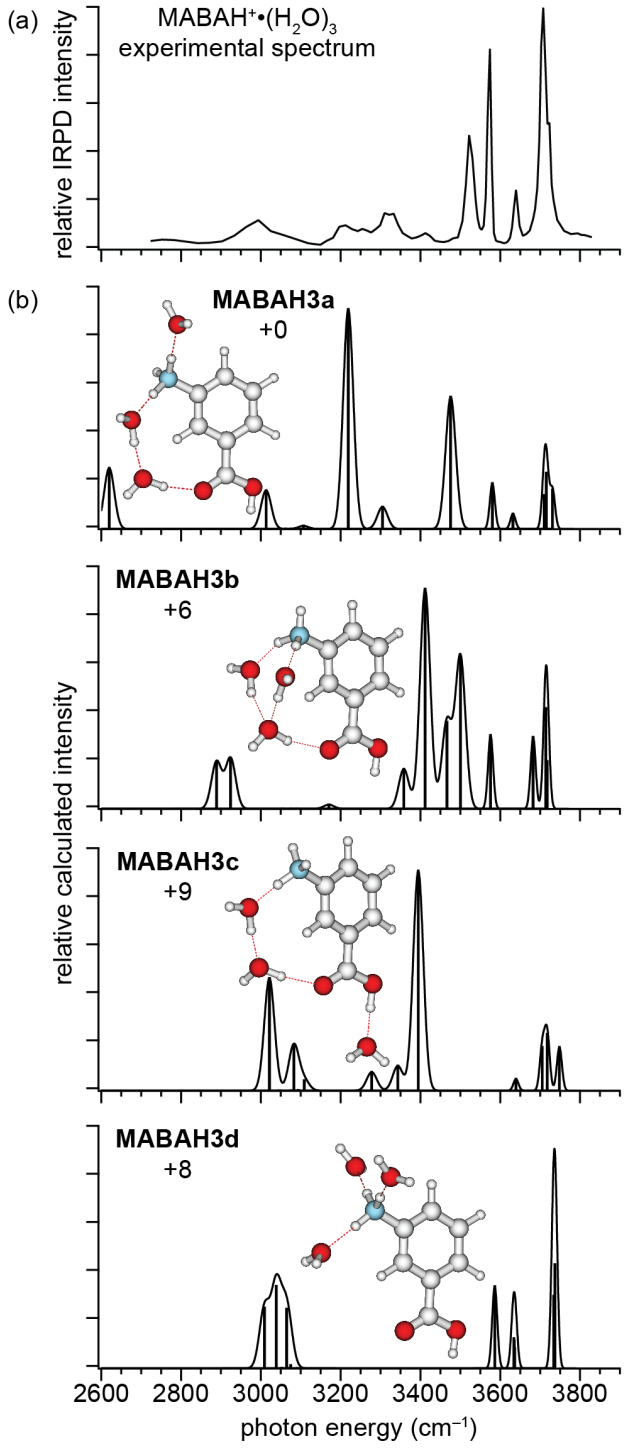

Figure 3. (a) IRPD spectrum of $MABAH^+•(H_2O)_3$ measured at 133 K and (b) calculated spectra of four isomers. 133 K relative Gibbs free energies (in kJ mol^{-1}) calculated at the B3LYP/6-31+G** level of theory are inset.

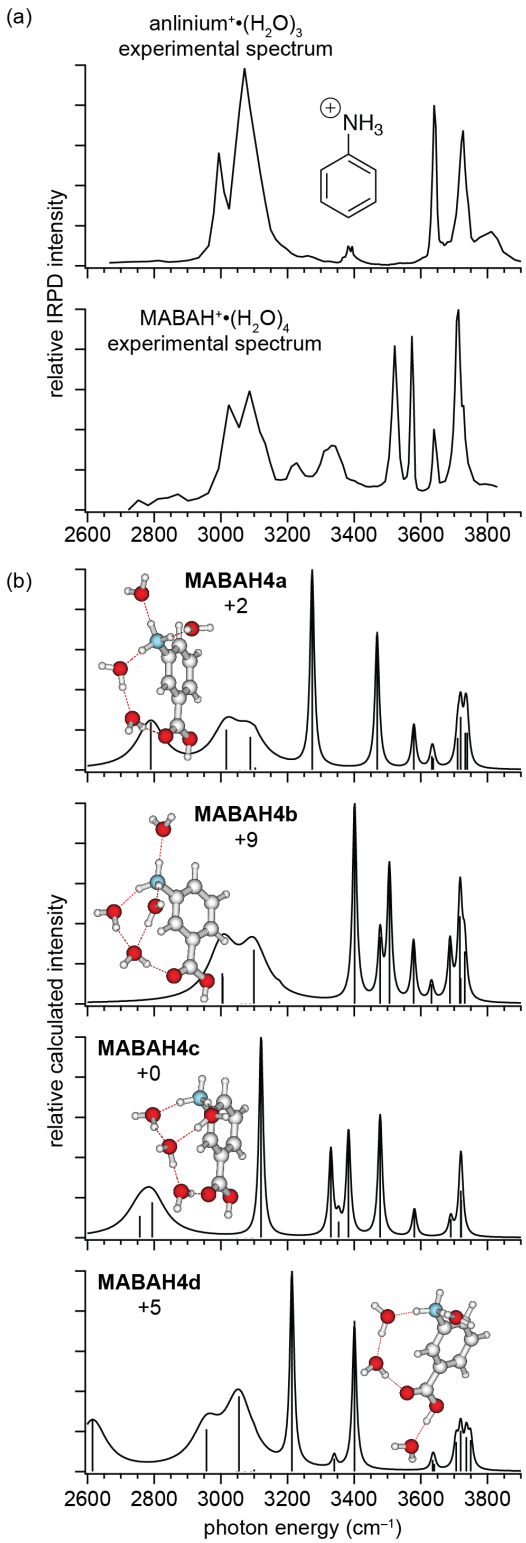

Figure 4. (a) IRPD spectra of anilinium^{+}•$(H_2O)_3$ reproduced from ref. 9 and MABAH^{+}•$(H_2O)_4$ (top and bottom, respectively) measured at 133 K. (b) Calculated spectra of four isomers. 133 K relative Gibbs free energies (in kJ mol^{-1}) calculated at the B3LYP/6-31+G** level of theory are inset.

Low-energy structures identified for $MABAH^+•(H_2O)_{3,4}$ (**MABAH3a – c** and **MABAH4a – d**, shown in Figure 3b and 4b, respectively) have a water bridge and are either the lowest-energy structure or are within 9 kJ mol^{-1} of the lowest-energy structure. **MABAH3a** (the lowest-energy structure) and **MABAH3b** (+6 kJ mol^{-1}) have two water molecules coordinated to the protonated amine, and the third water molecule forms the water bridge. **MABAH3a** has a SA water molecule whereas all three water molecules participate in the water bridge in **MABAH3b**. There is also a water bridge in **MABAH3c** (+9 kJ mol^{-1}), but a third water molecule forms a HB to the carboxylic acid H atom. In contrast to **MABAH3a – c**, all three water molecules attach to an H atom at the protonated amine in **MABAH3d** (+8 kJ mol^{-1}), and there are no water-water HBs. **MABAH4a** and **MABAH4b** (+2 and +9 kJ mol^{-1}, respectively) are similar to **MABAH3a** and **MABAH3b**, respectively, except there is a water molecule that accepts a third HB from the ammonium group, i.e., the protonated amine is fully hydrogen-bonded. All four water molecules participate in the water bridge for **MABAH4c** (the lowest energy structure). **MABAH4d** (+5 kJ mol^{-1}) is similar to **MABAH3a**, but with a water molecule attached at the carboxylic acid H atom.

The calculated spectrum for **MABAH3a** (Figure 3b) is a good frequency match to the measured spectrum. In contrast, the spectra for **MABAH3b – d** poorly match the IRPD spectrum. **MABAH3b** does not have any SA s.s. or a.s. stretches, which are in the measured spectrum. In addition the HB O–H stretches occur between 3400 and 3500 cm^{-1}, whereas they appear in a broader range, from 3200 – 3550 cm^{-1}, in the measured spectrum. The spectra for **MABAH3c** has a HB COO–H stretch at ~3020 cm^{-1}, overlaps with the HB N–H stretch at ~3000 cm^{-1}, but is typically an intense feature in IRPD spectra.[42-44] Water-water HBs are absent from **MABAH3d**. Despite the differences between the measured spectrum and those calculated for **MABAH3b – d**, minor contributions from these three structures cannot be ruled out. Similarly, the calculated spectrum for **MABAH4a** is most consistent with the measured spectrum for $MABAH^+•(H_2O)_4$, but contributions from minor populations of **MABAH4b – d** may be possible. The comparisons between the measured and simulated spectra indicate that the ion population for $MABAH^+$ with three and four water molecules attached consists of isomers that have a water bridge between the ammonium and carboxylic acid functional groups.

3.4.3. Hydration of the Carboxylic Acid H Atom

The carboxylic acid free COO–H stretch, which appears in the IRPD spectra for $MABAH^+•(H_2O)_{1-4}$, is also a major feature in the measured spectrum for $MABAH^+•(H_2O)_5$ (Figure 5). These data indicate that a substantial population of ions, where water does not form a HB to the carboxylic acid H atom, remains for $n = 5$. In contrast, the carboxylic acid free COO–H stretch is a relatively weak band in the spectrum of $MABAH^+•(H_2O)_6$, and there are two broad bands below 3200 cm^{-1}. The band at ~3150 cm^{-1} is blue shifted from the HB N–H stretches for $MABAH^+•(H_2O)_{4,5}$ (~3050 and ~3120 cm^{-1}, respectively), but it is also significantly more intense. The higher intensity is attributed to the presence of a HB COO–H stretch, which occurs between 2800 and 3200 cm^{-1} for hydrated, protonated phenylalanine.[42] These results indicate that there is a significant population of ions where the carboxylic acid H atom participates in a HB when six water molecules are attached, and that $MABAH^+$ is fully hydrogen-bonded to water molecules.

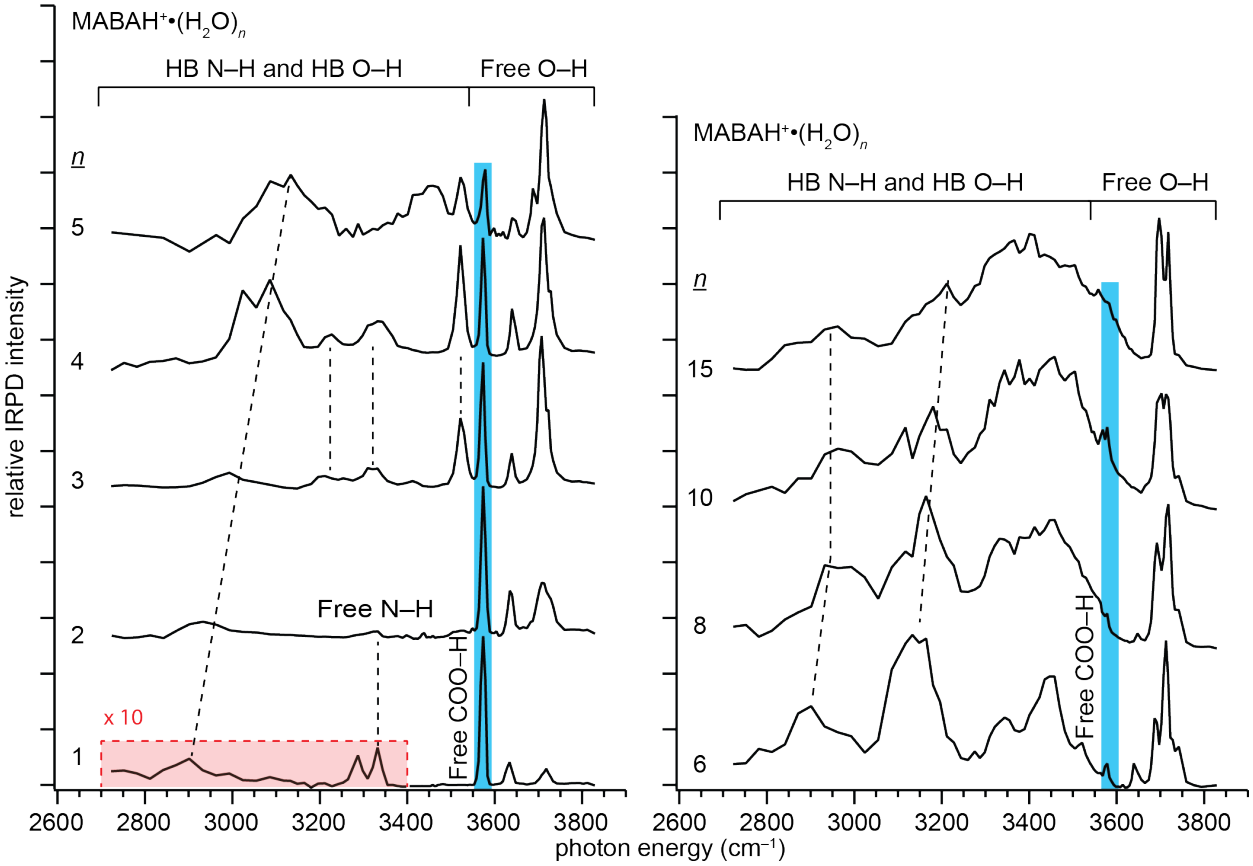

Figure 5. IRPD spectra of $MABAH^+•(H_2O)_n$ with up to 15 water molecules attached measured at 133 K. Regions corresponding to free O–H, HB N–H and HB O–H stretches are labeled. The free N–H and free COO–H stretches are also indicated.

The band at ~2900 cm^{-1} in the IRPD spectrum of $MABAH^+•(H_2O)_6$ is too low in energy for a HB O–H stretch. Thus, this feature is attributed to HB N–H stretches. It is likely that this band is due to the stretching motion of N–H bonds that donate HBs to AD water molecules involved in the water bridge. The frequency of this vibrational mode is calculated to be between 2350 and 3100 cm^{-1} in the low-energy structures for $MABAH^+•(H_2O)_{2-4}$ where the water bridge is present, and this absorption may be below the range of the measured spectra for $MABAH^+•(H_2O)_{2-5}$ or may be too weak to induce measureable dissociation in these experiments.

The HB COO–H stretch is also present in the IRPD spectra for $MABAH^+•(H_2O)_{8,15}$, and the free COO–H stretch is nearly or entirely eliminated. These results indicate that the vast majority of the ion population for these hydration states consists of isomers where the $MABAH^+$ ion is fully hydrogen-bonded. There is a HB COO–H stretch in the measured spectrum for $MABAH^+$ with 10 water molecules attached, but there are also two sharp bands near 3575 cm^{-1} that are within 5 cm^{-1} of the free COO–H stretch that appears for $MABAH^+•(H_2O)_{1-6}$. These bands are also present in the spectrum of the methyl ester form of this ion ($MABAOMeH^+$) with 10 water molecules attached (Figure S1). The appearance of these bands for both $MABAH^+•(H_2O)_{10}$ and $MABAOMeH^+•(H_2O)_{10}$ indicates that these features do not correspond to

a free COO–H stretch but may be due to HB O–H stretches or overtones. These features in the spectrum of $MABAH^+•(H_2O)_{10}$ are much more narrow than typical HB O–H bands, but they also appear to be of similar peak width to the HB O–H stretches near 3520 cm^{-1} for $MABAH^+•(H_2O)_{3,4}$. It is possible that bands in the spectrum of $MABAH^+•(H_2O)_{10}$ have similar origins to those for $MABAH^+•(H_2O)_{3,4}$.

3.4.4. Confirmation of Band Assignments

To confirm the band assignments for hydrated $MABAH^+$, the IRPD spectra for hydrated $MABAOMeH^+$ with up to 10 water molecules attached were measured. The basicity of the carbonyl O atom is higher for MABAOMe than for MABA due to the methyl group's greater polarizability compared to the carboxylic H atom.[4,5] Calculations indicate that protonation of the carbonyl O atom for MABAOMe is lower in Gibbs free energy by 5 kJ mol^{-1} compared to protonation at the amine. In contrast, protonation of the amine is calculated to be favored by 6 kJ mol^{-1} when one water molecule is attached. The IRPD spectrum for $MABAOMeH^+•(H_2O)_1$ (Figure 6) is nearly identical to that of $MABAH^+$ with one water molecule attached, but the carboxylic acid free COO–H stretch is notably absent from the former. These results indicate that protonation and hydration for $MABAOMeH^+•(H_2O)_1$ occurs at the amine and confirm the assignment of the free COO–H stretch in the spectra of $MABAH^+•(H_2O)_{1-6}$.

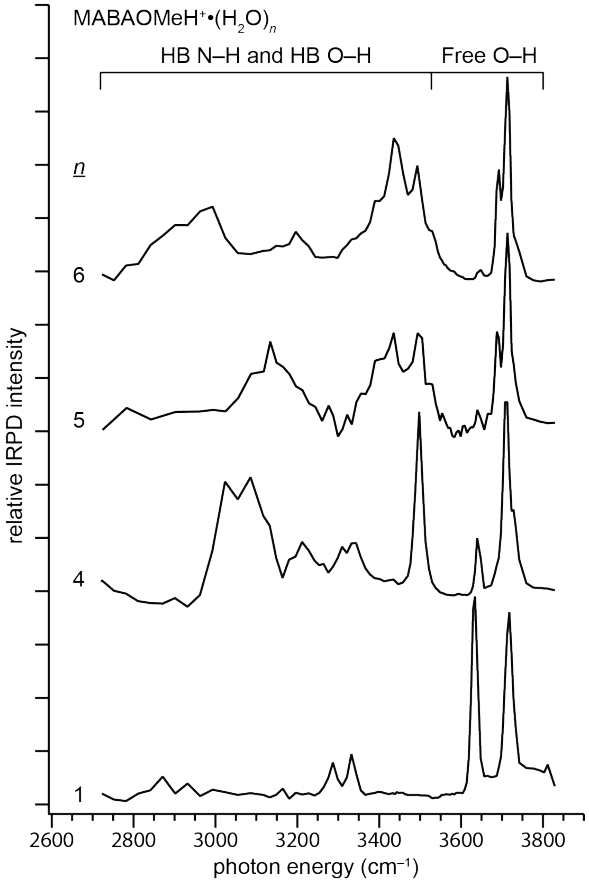

Figure 6. IRPD spectra of $MABAOMeH^+•(H_2O)_n$ with up to six water molecules attached measured at 133 K. Regions corresponding to the HB N–H and O–H stretches as well as the free O–H stretches are indicated.

The spectra of $MABAOMeH^+•(H_2O)_{4,5}$ are identical to those for $MABAH^+•(H_2O)_{4,5}$ except for the absence of a free COO–H stretch. These results indicate that the hydration structures of both ions are the same with up to five water molecules attached, and that the carboxylic acid H atom does not participate in hydrogen-bonding. The spectra of $MABAH^+$ and $MABAOMeH^+$ with six water molecules attached are also similar except both the HB and the free COO–H stretch bands at 3133 cm^{-1} and 3578 cm^{-1}, respectively, are absent from the latter. These results confirm the band assignments and that the majority of the ion population of $MABAH^+$ is fully hydrogen-bonded with six water molecules attached. In sum, the confirmation of the band assignments in the spectra of hydrated $MABAH^+$ suggest that the ion is fully hydrogen-bonded when solvated by six or more water molecules.

3.4.5. Identifying Multiple Isomers

When more than one isomer is present in an ion population, the relative contribution of each isomer to an IRPD spectrum can be challenging to determine. Calculated band intensities can differ significantly from those measured in IRPD spectra,[50] and isomers may have significantly different fragmentation efficiencies, which can affect the contribution of each isomer to an IRPD spectrum unless the entire ion population is dissociated.[6,50,51] Dissociation kinetics have been used to determine the relative contributions of different isomers to ion populations,[52] and the method has been recently applied to IRPD spectroscopy.[6,42,43,50,51]

Based on the calculated relative Gibbs free energies, only a single structure for $MABAH^+•(H_2O)_1$, **MABAH1a** (Figure 1b), is expected under these experimental conditions. Irradiation of the ion packet at the free COO–H stretch at 3573 cm^{-1}, should lead to selective dissociation of **MABAH1a** but not **MABAH1b** (Figure 1b), which does not have a free COO–H stretch. Dissociation kinetics obtained by irradiating these ions at 3573 cm^{-1} are first order up to 98% depletion of the precursor population (Figure 7a). This is consistent with the exclusive presence of isomer **MABAH1a** or the presence of rapidly interconverting structures. These results also demonstrate that there is excellent overlap between the laser beam and the ion cloud.

The two isomers for $MABAH^+•(H_2O)_2$, **MABAH2a** and **MABAH2b** (Figure 2b), are only 3 kJ mol^{-1} different in energy. To distinguish between these two nearly isoenergetic isomers, dissociation kinetics were measured at 3622 cm^{-1}, corresponding to SA water OH s.s. band for the **MABAH2a** isomer. **MABAH2b**, which lacks SA water molecules, does not absorb at this frequency. The data (Figure 7b) fit first order kinetics up to 92% depletion. This indicates the presence of a single dominant conformer corresponding to **MABAH2a**. Therefore, attachment of a water molecule to the protonated amine group is preferred over formation of the HB bridge to the carboxylic group. The remaining ~8% of the ion population may be attributable to **MABAH2b**.

3.4.6. Partially vs. Fully Hydrogen-Bonded Isomers of $MABAH^+(H_2O)_6$

Calculations indicate that structures of $MABAH^+•(H_2O)_{1-4}$, with a water molecule attached to the carboxylic acid H atom, are 5 – 25 kJ mol^{-1} higher in energy than partially hydrogen-bonded structures with a free COO–H. However, the lowest-energy structure for $MABAH^+•(H_2O)_6$ is fully hydrogen-bonded with a water molecule at the carboxylic acid H atom. The lowest-energy structure with a free COO–H is only 3 kJ mol^{-1} higher in Gibbs free energy at 133 K (Figure S2). These results indicate that the fully and partially hydrogen-bonded isomers

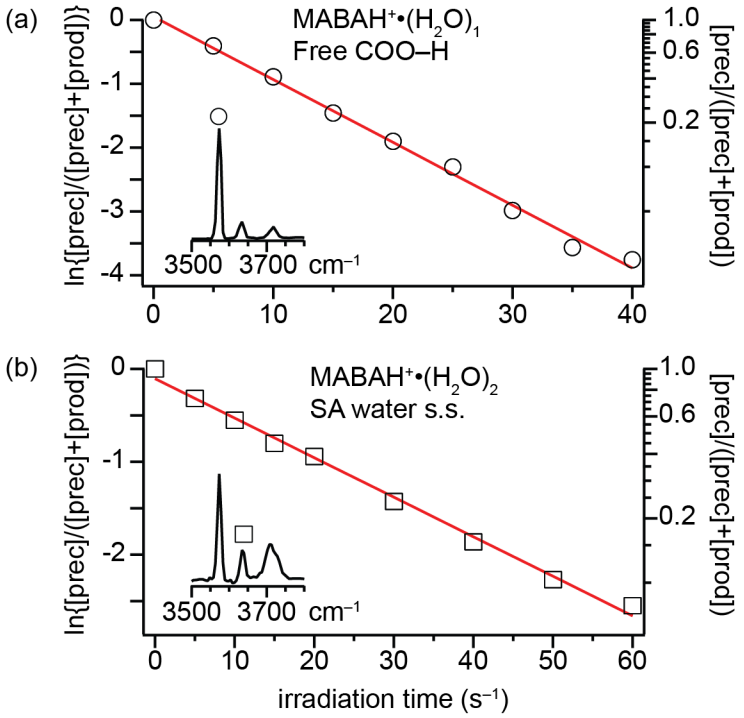

Figure 7. Laser photodissociation kinetic data for (a) $MABAH^+•(H_2O)_1$ at 3573 cm^{-1} (open circles) and (b) $MABAH^+•(H_2O)_2$ at 3622 cm^{-1} (open squares) measured at 133 K. Partial IRPD spectra inset (see Figures 1 and 2) showing the corresponding bands for resonant excitation. Lines are least-squares fits to the first order kinetic data.

are energetically competitive and likely co-exist. Dissociation kinetics were measured to determine the relative contributions of these isomers to the ion population.

Irradiation of the free COO–H stretch at 3578 cm^{-1} results in biexponential kinetics (Figure 8a). This can be attributed to the presence of two isomers, one which dissociates quickly owing to resonance absorption at this frequency, and another which does not absorb strongly at this frequency. The relative populations of the resonant partially hydrogen-bonded (free COO–H) and off-resonant fully hydrogen-bonded isomers are 26% and 74%, respectively.

Photodissociation kinetics for $MABAH^+•(H_2O)_6$ were also measured at 3133 cm^{-1}, corresponding to the stretch frequency of HB COO–H in isomers where $MABAH^+$ is fully hydrogen-bonded. The fit is first order to ~98% precursor depletion (Figure 8b), suggesting the exclusive presence of ions that are solvated at the carboxylic group or two rapidly interconverting isomers. However, the kinetic data from the free COO–H stretch excitation at 3578 cm^{-1} indicates two coexisting isomers that do not interconvert rapidly when excited at this higher energy.

The different kinetic behavior at these two frequencies is likely due to a difference in the dissociation rates. The rate constant at 3578 cm^{-1} (the free COO–H stretch) is 0.393 s^{-1} but only 0.101 s^{-1} at 3133 cm^{-1} (the HB COO–H stretch). The difference in dissociation rate constants is

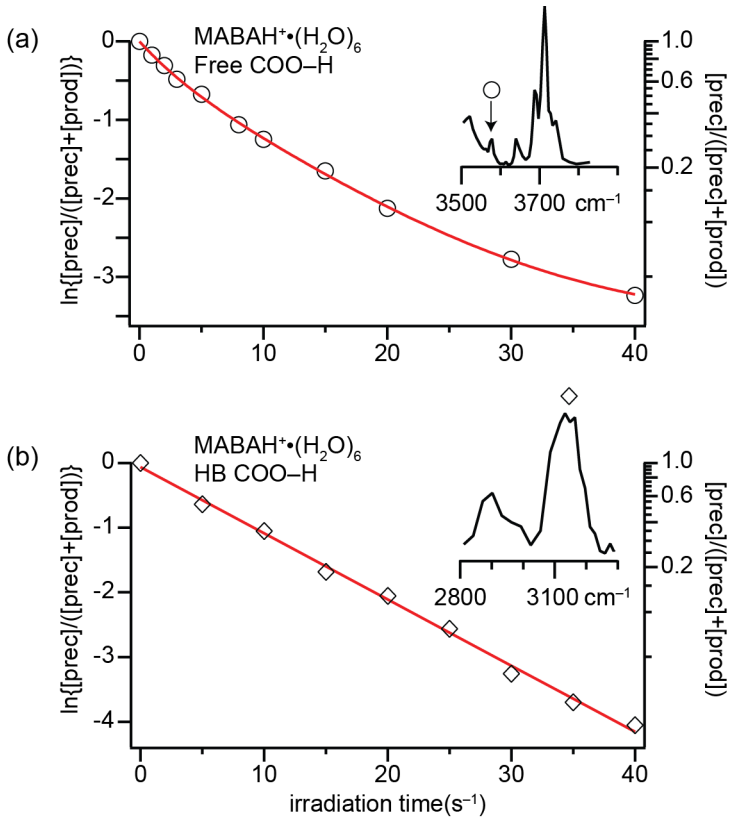

Figure 8. Laser photodissociation kinetic for $MABAH^+•(H_2O)_6$ at (a) 3578 cm^{-1} and at (b) 3133 cm^{-1} (open diamonds and circles, respectively) measured at 133 K. Partial IRPD spectra inset (see Figure 5) showing the corresponding bands for resonant excitation. Least-squares biexponential fit to the kinetic data measured at 3578 cm^{-1} indicate the presence of two isomers that interconvert on a slower time scale than dissociation. A least-squares fit to first order kinetic data measured at 3133 cm^{-1} indicate the presence of a single isomer or two rapidly interconverting isomers.

not accurately reflected by the peak intensities of the absorption bands in the IRPD spectrum. The OPO/OPA system has a higher power output at 3578 cm^{-1} than at 3133 cm^{-1}, but the IRPD spectral intensities are corrected to account for the frequency dependent variation in laser power. Therefore, further kinetic studies were carried out with attenuated power at 3578 cm^{-1} to investigate the influence of lower energy deposition on relative rates of dissociation and interconversion between the isomers. The relative abundance of the free COO–H isomer determined form these power dependent kinetic measurements increases from 26% at 1.6 mJ $pulse^{-1}$ to 95% at 0.12 mJ $pulse^{-1}$ (Figure S3 and Table 1).

Slower dissociation at lower laser powers result in different measured isomer abundances owing to increased extent of interconversion between isomers because of the longer ion lifetimes. Figure 9 is a qualitative illustration of relative stabilities of the isomers and their fragmentation thresholds deduced from these kinetic data. Clusters in which $MABAH^+$ is fully hydrogen-bonded, i.e., a water molecule is bound to the COO–H group, are the most stable and constitute ≥74% of the ion population as indicated by kinetic data at 3578 cm^{-1}. Photon absorption at 3578 cm^{-1} drives dissociation of the isomer with the free COO–H at a rate faster than interconversion, both as a result of higher laser power and higher photon energy (Figure 9a).

Table 1. Relative populations for resonant and off-resonant isomers (irradiating at 3578 cm^{-1}) for $MABAH^+•(H_2O)_6$ measured at different laser powers.

laser power ($mJ\ pulse^{-1}$)	relative population (%)	
	resonant	off-resonant
1.6	26	74
0.7	57	43
0.12	95	5

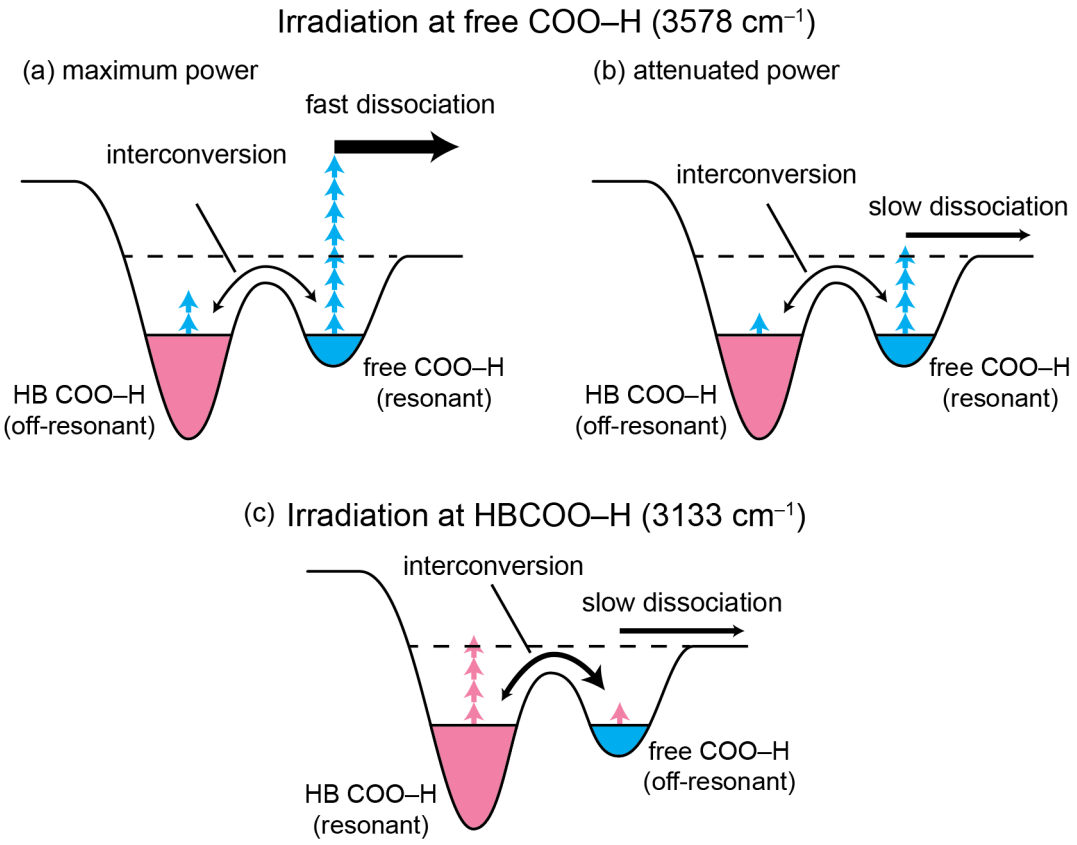

Figure 9. Illustration of the potential energy surface for the dissociation of $MABAH^+(H_2O)_6$ at two laser powers and at two different photon energies. (a) Irradiation of the free COO–H stretch at 3578 cm^{-1} at maximum power results in biexponential kinetics owing to the rapid depletion of the resonant isomer compared to the slow replenishment via off-resonant excitation and interconversion. (b) Irradiation at lower laser fluence, results in slower depletion of the resonant isomer so that replenishment via excitation and interconversion of the off-resonant isomer occurs more rapidly in comparison. (c) Irradiating at the HB COO–H stretch (3133 cm^{-1}) results in relatively slow heating followed by interconversion and subsequent slow dissociation.

When the laser power at 3578 cm^{-1} is reduced, the measured relative abundance of the isomer with a free COO–H is greater owing to replenishment of the population by isomerization of the isomer with the HB COO–H due to off-resonant excitation of (Figure 9b). These results indicate that the isomerization barrier between the isomers is lower than either of their dissociation thresholds.

Resonant excitation of the HB COO–H stretch frequency at 3133 cm^{-1} deposits energy in the HB COO–H isomer but slowly owing to the lower laser fluence and photon energy compared to excitation of the isomer with the free O–H stretch at full laser power. The dissociation barrier of the HB COO–H isomer is likely higher than that of the free COO–H isomer so that fragmentation proceeds through the latter isomer. The result is the appearance of a single isomer from the kinetic data (Figure 9c) at 3133 cm^{-1}. A more accurate estimate of the relative population of these isomers could be obtained at higher laser powers sufficient to induce prompt dissociation of the resonant structure before its population can be replenished by interconversion between isomers.

3.5. Conclusion

Hydration of the protonated amine and neutral carboxylic acid functional groups of $MABAH^+$ was investigated using IRPD spectroscopy, laser induced dissociation kinetics, and computational chemistry. These two functional groups are oriented so that they cannot form a HB to each other. For $MABAH^+$ with six or more water molecules attached, the vast majority of the ion population consists of isomers where the carboxylic acid H atom donates a HB to a water molecule whereas results for $MABAH^+•(H_2O)_{1–5}$ indicate there is no water molecule attached to this hydration site for these ions. In contrast, results for $ProH^+$ and $PheH^+$, where N- and C-termini interact with each other, indicate that isomers where a water is hydrogen bonded to the carboxylic acid H atom are present even with one water molecule attached.[42,43] These results indicate that the interaction of N-terminus with the C-termini or a side chain can significantly influence the propensity for a water molecule to bind to the N- or C-terminus an amino acid.

The formation of a water bridge between the protonated amine and the carbonyl O atom for $MABAH^+•(H_2O)_3$ is more favorable than the attachment of a water molecule at each of the H atoms of the protonated amine. In contrast, the dominant isomers for protonated aniline or *para*-aminobenzoic acid methyl ester with three water molecules attached have an ammonium group that is fully hydrogen-bonded.[9] These results show that a water bridge to a nearby carboxylic acid can be more favorable than solvating each H atom of a protonated amine.

Photodissociation kinetics data for $MABAH^+•(H_2O)_{1,2}$ are first order to >90% precursor depletion, indicating the vast majority of the ion population for these two ions consists of a single isomer or rapidly interconverting structures. Dissociation induced by irradiating $MABAH^+•(H_2O)_6$ at the HB COO–H stretch are also first order, whereas data measured at the free COO–H stretch of the same ion are biexponential and indicate that the fully solvated isomer is predominant. Irradiation at the free COO–H stretch with lower laser power results in slower dissociation which allows more time for interconversion between isomers. These data are consistent with the results obtained at the HB COO–H stretch frequency, where the laser has lower power compared to that at the free COO–H stretch, and indicate that the first order kinetics

observed for HB COO–H stretch excitation are due to interconversion over the time scale of the experiment.

These results show that, although laser induced kinetics data can provide information about the relative populations of the isomers in an ion population, it is possible for resonant and off-resonant isomers to interconvert when the dissociation rate is small. By increasing laser power, dissociation can occur more rapidly than interconversion, leading to more accurate information about the relative abundances of isomers. The results from this study illustrate the competition between water binding to a protonated primary amine vs. a neutral carboxylic acid and the formation of water bridges between the two functional groups. These results provide new insights into hydration of protonated amino acids and provide stringent benchmarks for modeling biomolecule-water interactions.

3.6. References

1. Brown, H. C. *Science* **1946**, *103*, 385-387.
2. Trotman-Dickenson, A. F. *J. Am. Chem. Soc.* **1949**, 1293-1297.
3. Hall, H. K. *J. Am. Chem. Soc.* **1957**, *79*, 5441-5444.
4. Brauman, J. I.; Riveros, J. M.; Blair, L. K. *J. Am. Chem. Soc.* **1971**, *93*, 3914-3918.
5. Aue, D. H.; Webb, H. M.; Bowers, M. T. *J. Am. Chem. Soc.* **1976**, *98*, 311-317.
6. Schmidt, J.; Meyer, M. M.; Spector, I.; Kass, S. R. *J. Phys. Chem. A.* **2011**, *115*, 7625-7632.
7. Tian, Z. X.; Kass, S. R. *Angew. Chem. Int. Ed.* **2009**, *48*, 1321-1323.
8. Kumler, W. D.; Strait, L. A. *J. Am. Chem. Soc.* **1943**, *65*, 2349-2354.
9. Chang, T. M.; Prell, J. S.; Warrick, E. R.; Williams, E. R. *J. Am. Chem. Soc.* **2012**, *134*, 15805-15813.
10. Tian, Z. X.; Wang, X. B.; Wang, L. S.; Kass, S. R. *J. Am. Chem. Soc.* **2009**, *131*, 1174-1181.
11. Steill, J. D.; Oomens, J. *J. Am. Chem. Soc.* **2009**, *131*, 13570-13571.
12. Yamdagni, R.; McMahon, T. B.; Kebarle, P. *J. Am. Chem. Soc.* **1974**, *96*, 4035-4037.
13. Skurski, P.; Gutowski, M.; Barrios, R.; Simons, J. *Chem. Phys. Lett.* **2001**, *337*, 143-150.
14. Linder, R.; Seefeld, K.; Vavra, A.; Kleinermanns, K. *Chem. Phys. Lett.* **2008**, *453*, 1-6.
15. Blom, M. N.; Compagnon, I.; Polfer, N. C.; von Helden, G.; Meijer, G.; Suhai, S.; Paizs, B.; Oomens, J. *J. Phys. Chem. A* **2007**, *111*, 7309-7316.
16. Aikens, C. M.; Gordon, M. S. *J. Am. Chem. Soc.* **2006**, *128*, 12835-12850.
17. Bush, M. F.; O'Brien, J. T.; Prell, J. S.; Saykally, R. J.; Williams, E. R. *J. Am. Chem. Soc.* **2007**, *129*, 1612-1622.
18. Forbes, M. W.; Bush, M. F.; Polfer, N. C.; Oomens, J.; Dunbar, R. C.; Williams, E. R.; Jockusch, R. A. *J. Phys. Chem. A.* **2007**, *111*, 11759-11770.
19. Bush, M. F.; Prell, J. S.; Saykally, R. J.; Williams, E. R. *J. Am. Chem. Soc.* **2007**, *129*, 13544-13553.
20. Liu, D. F.; Wyttebach, T.; Barran, P. E.; Bowers, M. T. *J. Am. Chem. Soc.* **2003**, *125*, 8458–8464.
21. Wincel, H. *Int. J. Mass Spectrom.* **2006**, *251*, 23-31.
22. Gao, B.; Wyttenbach, T.; Bowers, M. T. *J. Am. Chem. Soc.* **2009**, *131*, 4695-4701.
23. Wyttenbach, T.; Bowers, M. T. *Chem. Phys. Lett.* **2009**, *480*, 1–16.
24. Lemoff, A. S.; Bush, M. F. *J. Am. Chem. Soc.* **2003**, *125*, 13576–13584.
25. Lemoff, A. S.; Williams, E. R. *J. Am. Mass. Spectrom.* **2004**, *15*, 1014–1024.
26. Lemoff, A. S.; Bush, M. F.; Wu, C. C.; Williams, E. R. *J. Am. Chem. Soc.* **2005**, *127*, 10276–10286.
27. Wincel, H. *J. Phys. Chem. A* **2007**, *111*, 5784-5791.
28. Wincel, H. *J. Am. Soc. Mass Spectrom.* **2007**, *18*, 2083-2089.
29. Ye, S. J.; Moision, R. M.; Armentrout, P. B. *Int. J. Mass Spectrom.* **2006**, *253*, 288-304.
30. Miyazaki, M.; Fujii, A.; Ebata, T.; Mikami, N. *Science* **2004**, *304*, 1134-1137.
31. Shin, J.-W.; Hammer, N. I.; Diken, E. G.; Johnson, M. A.; Walters, R. S.; Jaeger, T. D.; Duncan, M. A.; Christie, R. A.; Jordan, K. D. *Science* **2004**, *304*, 1137-1140.
32. Diken, E. G.; Hammer, N. I.; Johnson, M. A.; Christie, R. A.; Jordan, K. D. *J. Chem. Phys.* **2005**, *123*, 164309.

33. Miller, D. J.; Lisy, J. M. *J. Am. Chem. Soc.* **2008**, *130*, 15393-15404.
34. Douberly, G. E.; Walters, R. S.; Cui, J.; Jordan, K. D.; Duncan, M. A. *J. Phys. Chem. A* **2010**, *114*, 4570-4579.
35. O'Brien, J. T.; Prell, J. S.; Bush, M. F.; Williams, E. R. *J. Am. Chem. Soc.* **2010**, *132*, 8248-8249.
36. Mizuse, K.; Fujii, A. *Phys. Chem. Chem. Phys.* **2011**, *13*, 7129-7135.
37. Prell, J. S.; O'Brien, J. T.; Williams, E. R. *J. Am. Chem. Soc.* **2011**, *133*, 4810-4818.
38. Demireva, M.; O'Brien, J. T.; Williams, E. R. *J. Am. Chem. Soc.* **2012**, *134*, 11216-11224.
39. O'Brien, J. T.; Williams, E. R. *J. Am. Chem. Soc.* **2012**, *134*, 10228-10236.
40. Cooper, R. J.; Chang, T. M.; Williams, E. R. *J. Phys. Chem. A* **2013**, *117*, 6571–6579.
41. Ke, H.; van der Linde, C.; Lisy, J. M. *J. Phys. Chem. A* **2014**, *118*, 1363-1373.
42. Prell, J. S.; Chang, T. M.; O'Brien, J. T.; Williams, E. R. *J. Am. Chem. Soc.* **2010**, *132*, 7811-7819.
43. Prell, J. S.; Correra, T. C.; Chang, T. M.; Biles, J. A.; Williams, E. R. *J. Am. Chem. Soc.* **2010**, *132*, 14733-14735.
44. Kamariotis, A.; Boyarkin, O. V.; Mercier, S. R.; Beck, R. D.; Bush, M. F.; Williams, E. R.; Rizzo, T. R. *J. Am. Chem. Soc.* **2006**, *128*, 905-916.
45. Pankratov, A. N.; Uchaeva, I. M. *J. Serb. Chem. Soc.* **2002**, *67*, 111-113.
46. Prell, J. S.; O'Brien, J. T.; Williams, E. R. *J. Am. Mass. Spectrom.* **2010**, *21*, 800-809.
47. Shao, Y.; et al. *Phys. Chem. Chem. Phys.* **2006**, *8*, 3172-3191.
48. Cimas, A.; Vaden, T. D.; de Boer, T.; Snoek, L. C.; Gaigeot, M. P. *J. Chem. Theory Comput.* **2009**, *5*, 1068-1078.
49. Chang, H. C.; Wang, Y. S.; Lee, Y. T. *Int. J. Mass Spectrom.* **1998**, *180*, 91-102.
50. Prell, J. S.; Chang, T. M.; Biles, J. A.; Berden, G.; Oomens, J.; Williams, E. R. *J. Phys. Chem. A* **2011**, *115*, 2745-2751.
51. Schmidt, J.; Kass, S. R. *J. Phys. Chem. A* **2013**, *117*, 4863-4869.
52. Schnier, P. D.; Williams, E. R. *Anal. Chem.* **1998**, *70*, 3033-3041.

3.7. Supporting Figures

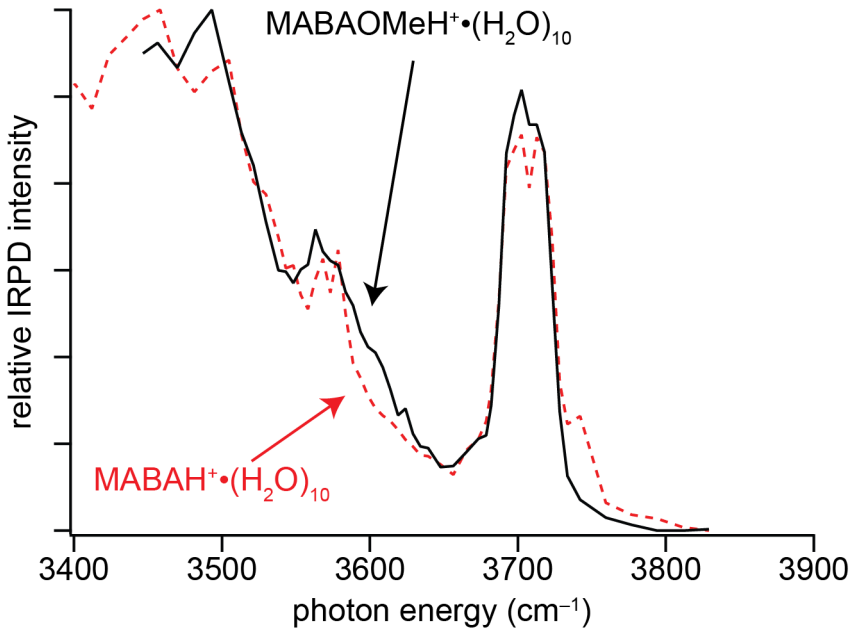

Figure S1. IRPD spectra of $MABAH^+$ (dashed red) and $MABAOMeH^+$ (solid black) with 10 water molecules attached at 133 K.

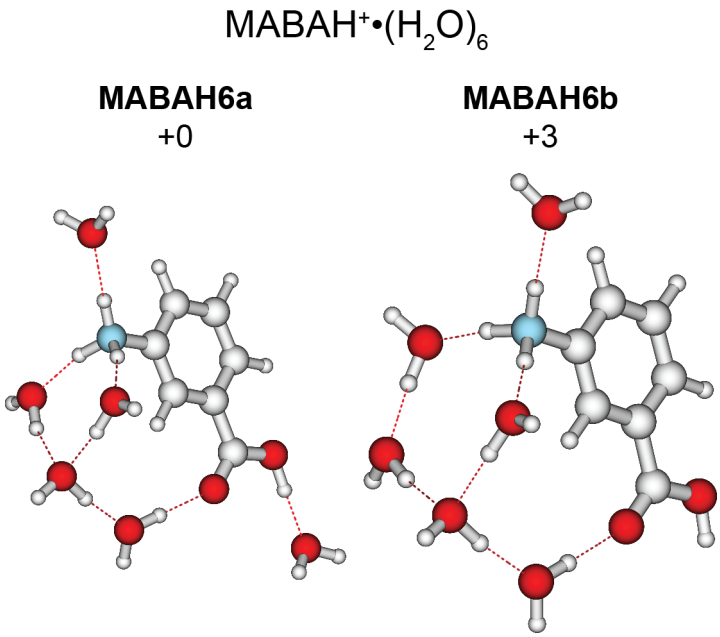

Figure S2. Selected low energy structures calculated for $MABAH^+•(H_2O)_6$. **MABAH6a** is the global minimum, whereas **MABAH6b** is the lowest energy structure where the hydroxyl H atom of the carboxylic acid does not donate a HB, i.e., the $MABAH^+$ ion is partially hydrogen-bonded. Relative Gibbs free energies (in kJ mol^{-1}) were calculated at the B3LYP/6-31+G** level of theory.

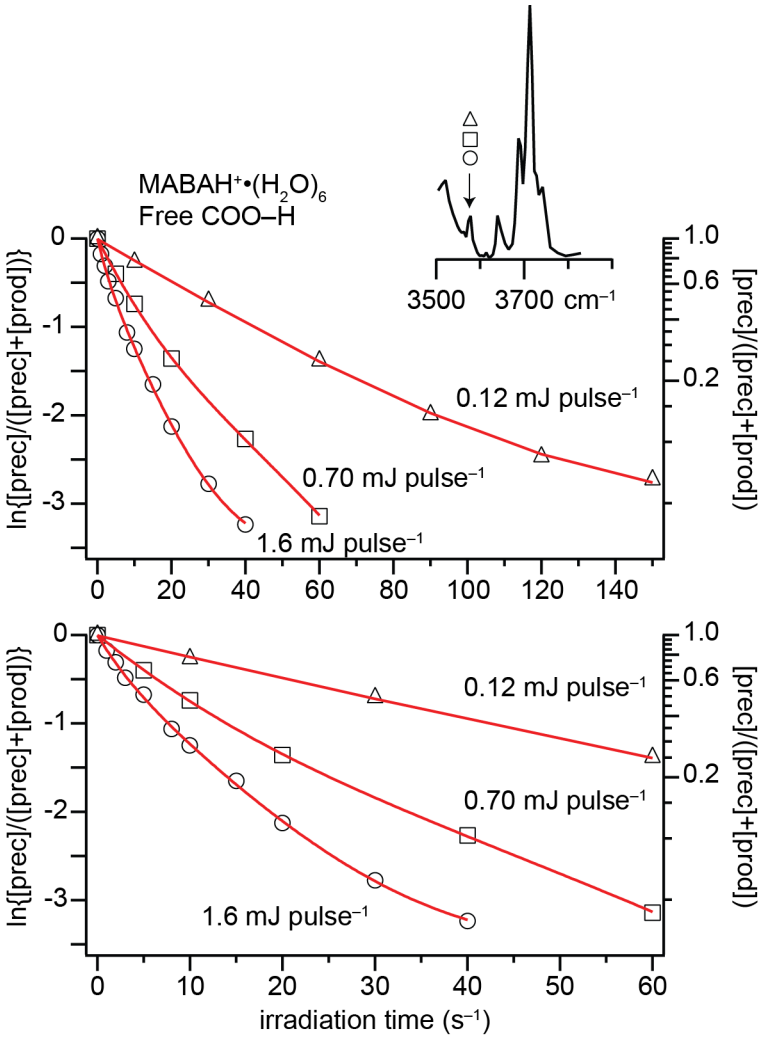

Figure S3. Laser photodissociation kinetics at 133 K for $MABAH^+•(H_2O)_6$ at 3578 cm^{-1} measured at varying laser fluences (top). Laser powers of 1.6, 0.70, and 0.12 mJ $pulse^{-1}$ are indicated with open circles, open squares, and open triangles, respectively. Partial IRPD spectrum inset (see Figure 3). Least-squares biexponential fit to the % precursor remaining for irradiation at 3578 cm^{-1} are shown. The bottom plot is an expansion of the dissociation kinetics from 0 – 60 s. Note that the data are plotted on a logarithmic scale.

Chapter 4. Locating Protonated Amines in Clathrates

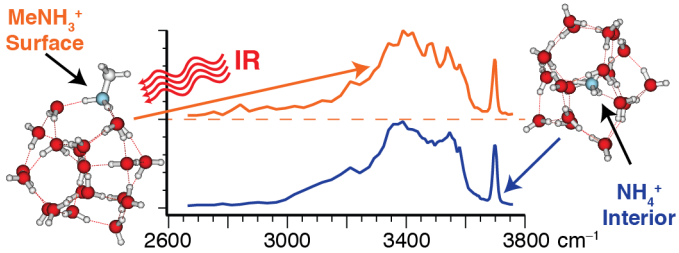

Originally published in the Journal of the American Chemical Society
http://dx.doi.org/10.1021/ja407414d

4.1. Abstract

The structures and inherent stabilities of hydrated, protonated ammonia, select protonated primary, secondary and tertiary amines as well as tetramethylammonium with 19 – 21 water molecules were investigated using infrared photodissociation (IRPD) spectroscopy and blackbody infrared radiative dissociation (BIRD) at 133 K. Magic number clusters (MNCs) with 20 water molecules were observed for all ions except tetramethylammonium, and the BIRD results indicate that these clusters have stable structures, which are relatively unaffected by addition of one water molecule but are disrupted in clusters with one less water molecule. IRPD spectra in the water free O–H stretch region are consistent with clathrate structures for the MNCs with 20 water molecules, whereas nonclathrate structures are indicated for tetramethylammonium as well as ions at the other cluster sizes. The locations of protonated ammonia and the protonated primary amines either in the interior or at the surface of a clathrate were determined by comparing IRPD spectra of these ions to those of reference ions; Rb^+ and protonated *tert*-butylammonia with 20 water molecules were used as references for an ion in the interior and at the surface of a clathrate, respectively. These results indicate that protonated ammonia is in the interior of the clathrate whereas protonated methyl- and *n*-heptylamine are at the surface. Calculations suggest that the number of hydrogen bonds in these clusters does not directly correlate with structural stability, indicating that both the number and orientation of the hydrogen bonds are important. These experimental results should serve as benchmarks for computational studies aimed at elucidating ion effects on the hydrogen-bonding network of water molecules and the surface activity of ions.

4.2. Introduction

Interfaces are important in many different chemical and biochemical processes, ranging from drug delivery,[1-3] protein folding,[4,5] and assembly of macromolecular complexes,[6,7] to reactions at aerosol surfaces relevant to atmospheric chemistry.[8-11] Hydrogen-bonding networks of water are affected by interfaces, such as those between water and air or water and proteins. Hydrogen-bonding networks are also influenced by ions,[12-18] and ion-water interactions play an important role in the Hofmeister phenomena[19-21] as well as the surface activity of ions.[22] The latter can significantly affect reaction rates at surfaces. For example, formation of Br_2 from the surface active ion, Br^-, occurs up to 4 orders of magnitude faster at the surface of an aerosol than it does in solution.[8] The surface activity of an ion depends on several factors, including the ion's polarizability[23,24] and charge state.[25] Investigating how ions interact with solvating water molecules can lead to a better understanding of both surface activity and the extent to which ions can influence the hydrogen-bonding network of water.

Detailed information about ion-water interactions can be obtained from studies of gas-phase hydrated ions, where clusters can be size selected and subsequently characterized by a wide variety of structural methods. Inner shell coordination numbers,[14,26-30] sequential water molecule binding energies[31-39] and the effect of hydration on molecular structure[40-43] have been investigated. IR spectroscopy is a powerful technique for obtaining structural information and has been used to investigate the effect of water on zwitterion stability,[40] molecular folding,[43,44] and ion effects on the hydrogen-bonding network of water molecules.[14-18,26-30,45-49]

Some hydrated ions in cluster distributions can have enhanced abundances compared to adjacent sized clusters.[47-59] These ions, often referred to as magic number clusters (MNCs), often indicate especially stable structures. MNCs with 20 water molecules have been reported for a variety of ions, including H_3O^+, NH_4^+, K^+, Rb^+ and Cs^+, and have been attributed to the formation of cage-like clathrate structures.[46-49,51,59-79] Clathrates are common in nature where they have been implicated in global climate change[80] and blocking of oil pipelines.[81] Clathrates also have potential practical applications, such as sequestration of greenhouse gases,[82-84] and are a significant reservoir of natural gas.[85-87]

One of the most widely investigated MNCs is $H_3O^+•(H_2O)_{20}$, for which a clathrate structure has been deduced from computational chemistry,[59,68-75] IR spectroscopy[46,47] and ion molecule reactivity.[79] The IR spectrum of this ion has a single peak in the free O–H stretch region corresponding to water molecules that accept two hydrogen bonds (HBs) and donate one HB to adjacent water molecules (acceptor-acceptor-donor, or AAD, water molecules), which is characteristic of a clathrate structure.[46,47] However, the location of the proton, whether in the interior or at the surface of a clathrate structure, could not be determined from these experiments alone. Early computational studies indicated that the proton is located in the interior,[59,68-70] but more recent calculations suggest that the proton is at the surface.[71-75] Both experimental[48] and computational[64-67] results indicate that larger alkali metal ions fit into a clathrate cage when hydrated by 20 water molecules, but Na^+ does not. Results for $Li^+•(H_2O)_{20}$ suggest that a fraction of the ion population adopts clathrate structures, indicating that these structures depend both on the ion size and how the ions affect the hydrogen-bonding network of the water molecules.[48,88]

$NH_4^+•(H_2O)_{20}$ is also a MNC, and the IR spectrum of this ion reported by Diken et al. has the characteristic AAD free O–H stretch indicative of clathrate structure.[49] As was the case for $H_3O^+•(H_2O)_{20}$, the location of the ion could not be determined solely from the spectroscopy data. Computed enthalpies of formation for various structures suggest that it is more favorable for the ion to be located at the surface than in the interior by ~40 kJ mol^{-1},[49] consistent with a previous computational study.[76] However, formation enthalpies from recent computational studies indicate that structures with NH_4^+ in the interior are more favorable by ~10 kJ mol^{-1}.[77,78] Computations suggest that the charge is localized on the ammonium moiety (vs. neutral ammonia and a hydronium ion),[76] whereas an excess proton is highly mobile in a pure water network,[89-92] even at the surface of $H_3O^+•(H_2O)_{20}$ clathrates.[61] This may affect the preferred location of an ion in a clathrate.

Here, the locations of the ions either at the surface or in the interior of a clathrate structure when hydrated by 20 water molecules were determined by comparing spectra of $NH_4^+•(H_2O)_{20}$ and $RNH_3^+•(H_2O)_{20}$ (R = methyl- and *n*-heptyl- alkyl groups) to spectra of reference ions for which the location of the ion can be confidently assigned. From these comparisons, we conclude that $NH_4^+•(H_2O)_{20}$ is in the interior of a clathrate whereas primary alkylamines are at the surface of a clathrate. This is the first experimental evidence for the location of these ions either in the interior or at the surface of clathrates. These results provide insight into clathrate structures and how guest ions affect the hydrogen-bonding network of water molecules in these structures.

4.3. Experimental

4.3.1. Mass Spectrometry and Spectroscopy

All experimental data were obtained using a 7.0 T Fourier transform ion cyclotron resonance (FT/ICR) mass spectrometer. This instrument is based on a 2.75 T FT/ICR instrument described elsewhere[93] but with a higher field strength magnet and modified vacuum chamber. The protonated forms of the following molecules: NH_3, methyl-, *n*-heptyl-, *tert*-butyl-, dimethyl- and trimethylammonia ($MonMA^+$, nHA^+, tBA^+, $DiMA^+$ and $TriMA^+$, respectively) as well as tetramethylammonium ions ($TetMA^+$) (Figure 4.1) were formed by nanoelectrospray (nanoESI) from 3 – 5 mM solutions using water purified by a Milli-Q purification system (Millipore, Billerica, MA). All chemicals were obtained from Sigma-Aldrich (St. Louis, MO). Borosilicate capillaries that are pulled to an inner tip diameter of ~1 μm and filled with the analyte-containing aqueous solution are used to form ions by nanoESI. A platinum filament in contact with the sample solution is held at a potential of 700 – 900 V relative to the heated metal capillary of the nanoESI interface. Ions are guided by electrostatic lenses through five stages of differential pumping into the ion cell. The temperature of the ion cell is controlled by a surrounding copper jacket that is cooled by a regulated flow of liquid nitrogen.[94] Prior to experiments, the cell is cooled to 133 K for a minimum of 8 h. A pulse of dry nitrogen gas (~10^{-6} Torr) is introduced into the vacuum chamber containing the ion cell for ~5 s to improve ion trapping and thermalization. After a ~7 s pumpdown delay following the introduction of pulse gas, the pressure inside the cell is <10^{-8} Torr. Precursor ions are subsequently mass selected using a stored waveform inverse Fourier transform.

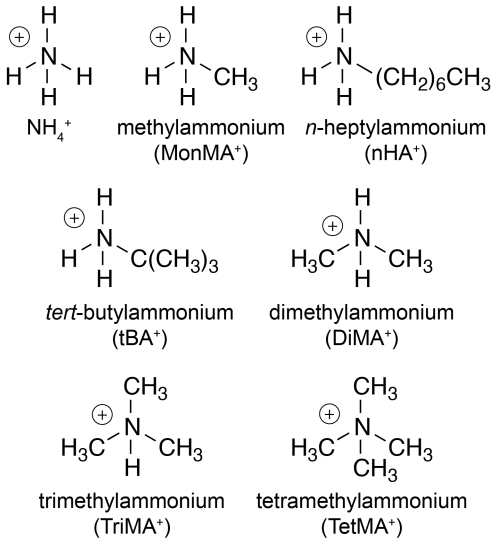

Figure 4.1. Structures and abbreviations for ammonium and alkylammonium ions investigated.

Blackbody infrared radiative dissociation (BIRD) rate constants are obtained from the precursor and product ion abundances as a result of dissociation from absorption of blackbody photons from the ion cell and cell jacket for times between 0.5 and 5.0 s. Infrared photodissociation (IRPD) spectra are measured by irradiating the mass selected precursor ions with tunable IR photons generated by an OPO/OPA system (LaserVision, Bellevue, WA) that is pumped by the 1064 nm fundamental of a Nd:YAG laser (Continuum Surelight I-10, Santa Clara, CA) pulsed at a 10 Hz repetition rate. The IRPD rate constants are corrected for frequency dependent variations in laser power as well as BIRD.[95] Irradiation times were chosen so that substantial, but not complete, dissociation of the precursor occurred. The relative intensities of bands in the free O–H region (~3640 – 3780 cm^{-1}) were determined from the integrated areas of Gaussian peaks fitted to the experimental data using Igor v 6.00 (Wavemetrics, Portland, OR).

4.3.2. Computational Chemistry

Conformational searches for tBA^+, $DiMA^+$, $TriMA^+$ and $TetMA^+$ with 20 water molecules attached were performed with Macromodel 9.1 (Schrödinger, Inc., Portland, OR, U.S.A.) using MMFFs or OPLS2005 force fields. The ten lowest-energy structures from each conformational search were then optimized at the B3LYP/6-31+G** level of theory using Q-Chem 4.0 (Q-Chem, Inc., Pittsburgh, PA).[96] Additional structures based on those reported for $H_3O^+•(H_2O)_{20}$ were also optimized at the same level of theory.[47] Relative Gibbs free energies at 133 K were calculated from zero-point energies, enthalpy and entropy corrections using unscaled B3LYP/6-31+G** harmonic oscillator vibrational frequencies.

4.4. Results and Discussion

4.4.1. Magic Number Clusters for Hydrated Ammonium Ions

A broad distribution of hydrated ions: NH_4^+, $MonMA^+$, nHA^+, tBA^+, $DiMA^+$, $TriMA^+$ and $TetMA^+$ can be readily produced by nanoESI from aqueous solutions, and these distributions can be shifted to smaller or larger average sizes by varying experimental conditions. The relative abundances of these different hydrated ions as a function of cluster size, measured with the same experimental conditions, are shown in Figure 4.2. The abundances of several clusters are higher than those of adjacent clusters. Most notably, the abundances of clusters with 20 water molecules are significantly higher than those of $n = 19$ or 21 for all ions except $TetMA^+$ and only marginally so for $DiMA^+$. These MNCs at $n = 20$ are consistent with previous studies on hydrated ammonium, alkylammonium and NH_4^+•pyridine ions,[49,53-55,58] with the exception of $TriMA^+•(H_2O)_{20}$, for which a MNC was not observed.[58] The appearance of a MNC for this ion may be due to the longer time scale or lower ion temperature of our experiments. Some clusters at other sizes have enhanced abundances as well. For example, $n = 18$ is a MNC for most of the ions, consistent with previous results for ammonium[54,55] and also observed for some alkali metal ions.[48,56,57,64] The enhanced abundance is most pronounced for $tBA^+•(H_2O)_{18}$, but $DiMA^+•(H_2O)_{18}$ is less abundant than adjacent clusters.

A MNC can occur owing to the inherent stability of an ion with respect to water loss, but it can also be due to the inherent instability of neighboring clusters. To distinguish between these possibilities, BIRD rate constants (133 K) with 19 – 21 water molecules attached were measured, and the values for each of the ions are shown in Figure 4.3. BIRD rate constants depend on the rates of radiative absorption and emission as well as the rates of dissociation. In this limited size range, the rates of radiative absorption and emission of the different hydrated ions are expected to be similar. In the absence of specific structural effects, the BIRD rate constants should increase very slightly with increasing cluster size, owing to increasing radiative rates[97] and decreasing threshold dissociation energies for the loss of a water molecule.[98] For $TetMA^+•(H_2O)_n$, which has no apparent enhanced abundance at $n = 20$, and for $DiMA^+•(H_2O)_n$, for which the abundance of the $n = 20$ cluster is only slightly enhanced, the BIRD rate constants are nearly the same and increase only slightly with increasing cluster size (Figure 3, top). The rate constants for these ions are similar to those measured under the same conditions for the same size nanodrops containing either Li^+ or Na^+, for which cluster abundances in this size range show minimal or no enhancement.[48]

In contrast, the rate constants for NH_4^+, $MonMA^+$, nHA^+, tBA^+ and $TriMA^+$ do not increase monotonically with increasing cluster size (Figure 3, bottom). The clusters with 20 water molecules are significantly more stable than the adjacent size clusters. The average BIRD rate constants for hydrated $DiMA^+$ and $TetMA^+$, for which there are no significant magic numbers in this size range, are plotted as a dashed line in Figure 3, bottom, and this line provides a reference for the expected stability of clusters in the absence of specific structural effects. These data indicate that $Amm•(H_2O)_{19}$ clusters, Amm = NH_4^+, $MonMA^+$, nHA^+, tBA^+ and $TriMA^+$, are only slightly less stable than the $DiMA^+$ and $TetMA^+$ containing clusters at this size. In contrast, the former ions are significantly more stable at $n = 20$ and significantly less stable at $n = 21$. These results indicate that the origin of the MNCs at $n = 20$ for NH_4^+, $MonMA^+$, nHA^+,

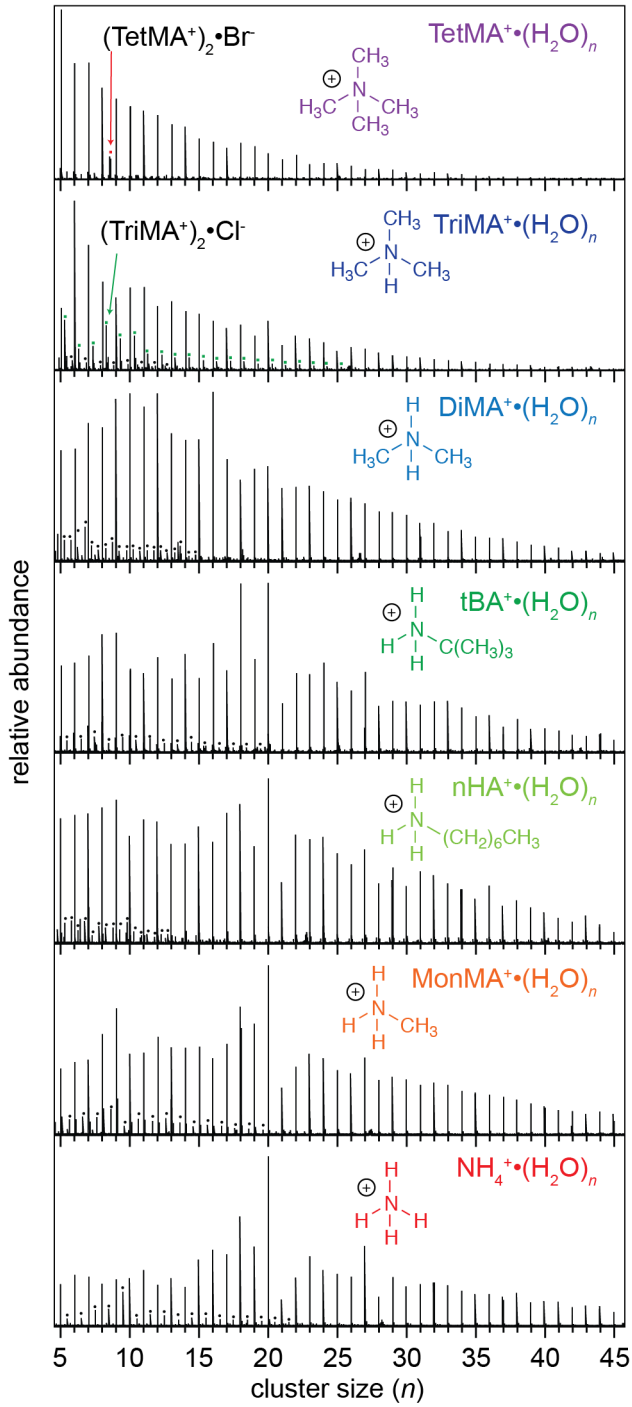

Figure 4.2. Abundances of hydrated ammonium ions formed by nanoESI as a function of cluster size (n). Chemical interferences are labeled with red or green squares corresponding to $(TetMA^+)_2•Br^-$ and $(TriMA^+)_2•Cl^-$, respectively. Second harmonics are labeled with black circles.

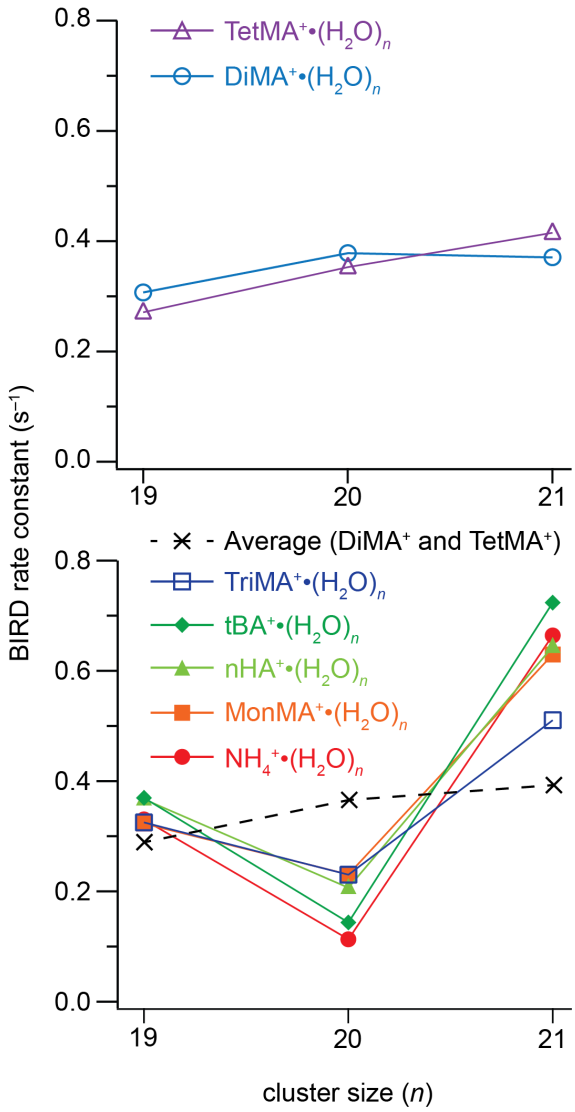

Figure 4.3. BIRD rate constants (133 K) for hydrated ammonium ions with 19 – 21 water molecules attached. The dotted line (bottom) indicates average BIRD rate constants for $DiMA^+$ and $TetMA^+$ as a function of cluster size. NH_4^+, $MonMA^+$, nHA^+, tBA^+ and $TriMA^+$ with $n = 20$ have BIRD rate constants that are significantly lower than the average, indicating higher inherent stability, whereas these values for these same ions are significantly higher than the average at $n = 21$, indicating a significant inherent instability.

tBA^+ and $TriMA^+$ (Figure 4.2) is a result of both significant stability of the $n = 20$ clusters and significant instability of the $n = 21$ clusters. The relatively low binding energy of water to the $n = 21$ cluster suggests that addition of a water molecule to the $n = 20$ cluster may not significantly change the structure of this cluster, i.e., the core structure that makes the clusters with 20 water molecules especially stable and provides greater stability than what can be gained by optimizing HBs to the additional water molecule in the $n = 21$ cluster. Although the clusters at $n = 19$ are less stable than those at $n = 20$ (Figure 4.3, bottom), the $n = 19$ clusters show comparable stability to clusters that do not exhibit magic numbers (Figure 4.3, top), suggesting that removal of a water molecule from the $n = 20$ cluster significantly disrupts this core structure.

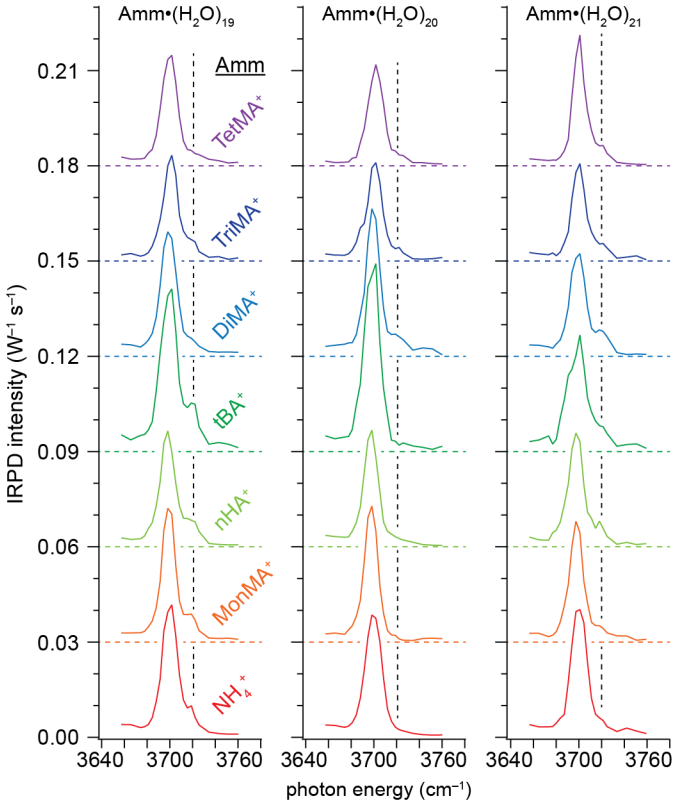

Figure 4.4. IRPD spectra in the free O–H region for Amm•$(H_2O)_n$ measured at 133 K, where Amm = NH_4^+, $MonMA^+$, nHA^+, tBA^+, $DiMA^+$, $TriMA^+$ or $TetMA^+$. Horizontal dashed lines indicate a vertical offset of 0.03 W^{-1} s^{-1}.

4.4.2. Spectroscopic Signature for Magic Numbers

IRPD spectra can provide useful insights into structural motifs associated with MNCs. Results from prior IR spectroscopy studies of hydrated H_3O^+,[46,47] NH_4^+ [49] and some alkali metal ions[48] indicate that stable clathrate or cage-like structures are formed at n = 20. The IRPD spectra in the free O–H region (~3640 – 3780 cm^{-1}) of hydrated ammonium ions with 19 – 21 water molecules are shown in Figure 4.4. Bands that appear in this region correspond to stretches of free O–H oscillators, i.e., those that are not hydrogen bonding, and these frequencies are sensitive to the local hydrogen-bonding environment of water molecules at the nanodrop surface.[26,41,46-49,99-103] The spectrum of NH_4^+ with 19 water molecules attached (Figure 4.4, bottom left) has a band near 3700 cm^{-1} and a shoulder near 3720 cm^{-1}. The 3700 and 3720 cm^{-1} bands correspond to the free O–H stretches of AAD water molecules and water molecules that accept a single HB and donate a single HB (acceptor-donor or AD water molecules), respectively.[26,46-49,100-103] Both of these bands also occur for NH_4^+•$(H_2O)_{21}$. In contrast, the spectrum of NH_4^+•$(H_2O)_{20}$ has only the AAD free O–H feature. These data indicate that there are AD water molecules for clusters at n = 19 and 21 but not at n = 20, consistent with the results of Diken et al. for this ion.[49] IR spectra of the other ions investigated here have not been previously reported. The spectra of $MonMA^+$, nHA^+ and tBA^+ also have both AD and AAD free O–H bands for n = 19 and 21, but only the AAD free O–H band is present for n = 20.

The spectra of $DiMA^+$, $TriMA^+$ and $TetMA^+$ with n = 19 – 21 (Figure 4.4) as well as tBA^+ and $DiMA^+$ at n = 18 (Figure S4.1) each contain both AD and AAD free O–H bands. Thus, these ions do not exhibit the same spectral simplification that occurs for hydrated NH_4^+, $MonMA^+$, nHA^+ and tBA^+ at n = 20. Although $TriMA^+\bullet(H_2O)_{20}$ and $tBA^+\bullet(H_2O)_{18}$ are MNCs, the small shoulder near 3720 cm^{-1} indicates the presence of AD water molecules, which is not the case for the other MNCs. $TriMA^+$ at n = 20 is the least stable of the MNCs at this size but the most stable at n = 21. Both the presence of AD water molecules and lower relative stability for $TriMA^+\bullet(H_2O)_{20}$ suggest that there may be a mixture of two or more structural families, some of which are less stable.

4.4.3. Integrated Ratios of the AD and AAD Bands

In order to more readily compare the free O–H spectra of these clusters, the ratios of integrated intensities for the AD and AAD features at each hydration state were determined by fitting the spectral bands to two Gaussian peaks centered near 3720 and 3700 cm^{-1}, respectively, and these values are shown in Figure 4.5. The AD/AAD ratios for $NH_4^+\bullet(H_2O)_{20}$, $MonMA^+\bullet(H_2O)_{20}$ and $tBA^+\bullet(H_2O)_{20}$ are <0.01, indicating that there is no measurable contribution from an AD free O–H stretch to these spectra. The AD/AAD ratios for $M^+\bullet(H_2O)_{20}$ (M = K, Rb and Cs), also MNCs, are ≤ 0.01.[48] There is no apparent shoulder near 3720 cm^{-1} in the spectrum of $nHA^+\bullet(H_2O)_{20}$, but the integrated ratio is 0.03, which is substantially larger than that of NH_4^+, $MonMA^+$ and tBA^+. The higher ratio for $nHA^+\bullet(H_2O)_{20}$ can be attributed to the asymmetric peak shape of the AAD free O–H band, which may be due to contributions from a minor population of structures containing AD water molecules. In contrast, the AD/AAD ratios for the spectra of NH_4^+, $MonMA^+$, nHA^+ and tBA^+ with n = 19 or 21 are ≥ 0.04. These data also show a minimum in the AD/AAD ratio at n = 20 for all of these ions, indicating that the stability of the MNC is related to the absence (or minimization) of the number of AD water molecules.

Interestingly, although the spectra of $TriMA^+\bullet(H_2O)_n$ each contain both the AD and AAD free O–H features, the AD/AAD ratios also exhibit a local minimum at n = 20, suggesting that the relative number of AD water molecules is significantly lower at n = 20 than at n = 19 or 21. In contrast, the AD/AAD ratios for $DiMA^+$ and $TetMA^+$ increase monotonically with increasing hydration state. These data indicate that the minimum in the AD/AAD ratio of $TriMA^+\bullet(H_2O)_{20}$ is associated with its enhanced abundance in the mass spectrum. In addition, both spectra of tBA^+ and $DiMA^+$ with 18 water molecules attached have the AD and AAD free O–H bands, but the AD/AAD ratio for $tBA^+\bullet(H_2O)_{18}$ is significantly lower than that of $DiMA^+\bullet(H_2O)_{18}$. This indicates that there is more extensive hydrogen bonding for $tBA^+\bullet(H_2O)_{18}$ than $DiMA^+\bullet(H_2O)_{18}$, consistent with a lower BIRD rate constant for the former ion and its appearance as a MNC in the mass spectrum.

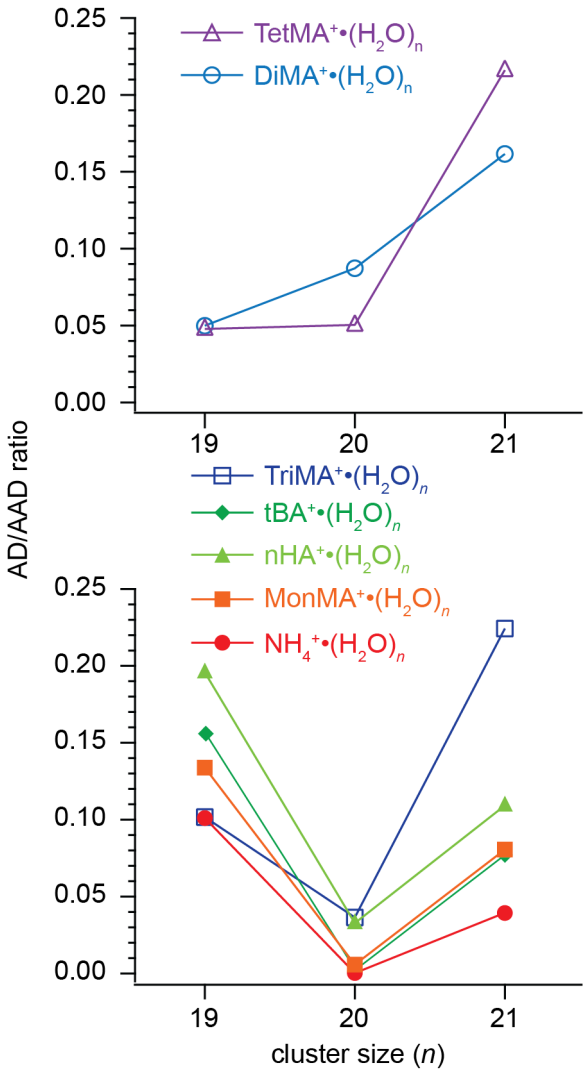

Figure 4.5. AD/AAD ratio of integrated areas plotted as a function of hydration state. Integrated areas of the AD and AAD bands were calculated from Gaussians centered near 3720 and 3700 cm^{-1}, respectively, that were fitted to the IRPD spectra of each ion in the free O–H region (Figure 4.4).

4.4.4. Dodecahedral Clathrate Structures

Previous computational studies of $NH_4^+•(H_2O)_{20}$ indicate that it is favorable for the cluster to form a dodecahedral clathrate structure for which the ion can reside either at the surface or in the interior of the clathrate,[49,76-78] and representative structures are shown in Figure 4.6a and 4.6b, respectively. These clathrate structures have only three and four coordinate water molecules at the surface of nanodrop. Thus, clusters that adopt a dodecahedral structure should only have an AAD band in the free O–H region. The presence of only the AAD band in the spectra of NH_4^+, $MonMA^+$, nHA^+ and tBA^+ at $n = 20$ is consistent with a clathrate hydration structure, but both dodecahedral and nondodecahedral clathrate structures have just the AAD band.

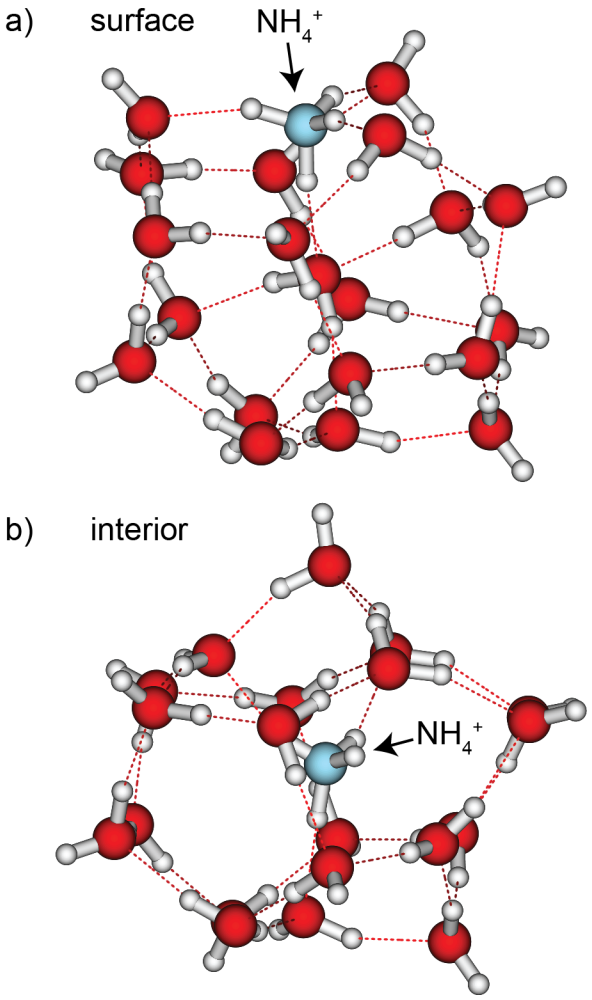

Figure 4.6. Representative structures for $NH_4^+•(H_2O)_{20}$ with the ion located at the a) surface or b) interior of a dodecahedral clathrate structure calculated at the B3LYP/6-31+G** level of theory. Initial geometries were modified from those computed for $H_3O^+•(H_2O)_{20}$.[47]

Although the IR spectra in the free O–H region provide information about whether a cluster adopts a clathrate structure, the location of ion in the clathrate is more difficult to determine. For NH_4^+, the AD band is predicted to be absent regardless of whether NH_4^+ is located at the surface or the interior.[49] Diken et al. concluded that the location of the ion could not be determined from the IR spectrum of $NH_4^+•(H_2O)_{20}$ alone, but a structure with NH_4^+ at the surface was calculated to be lowest in energy.[49]

4.4.5. Full IRPD Spectra of Hydrated Ammonium Ions

The hydrogen bonded (HB) O–H region (~2600 – 3650 cm^{-1}) of the spectrum can provide additional information about the structures of these clusters. The full IRPD spectrum, including the free O–H region, of each ammonium ion with 20 water molecules is shown in Figure 4.7. The spectra generally appear quite similar, each containing a relatively sharp band near 3700 cm^{-1} corresponding to the AAD free O–H stretch as well as a broad series of unresolved bands below 3650 cm^{-1} corresponding to HB O–H stretches. Analysis of an individual spectrum is complicated by spectral congestion, but a comparison of the spectra of all

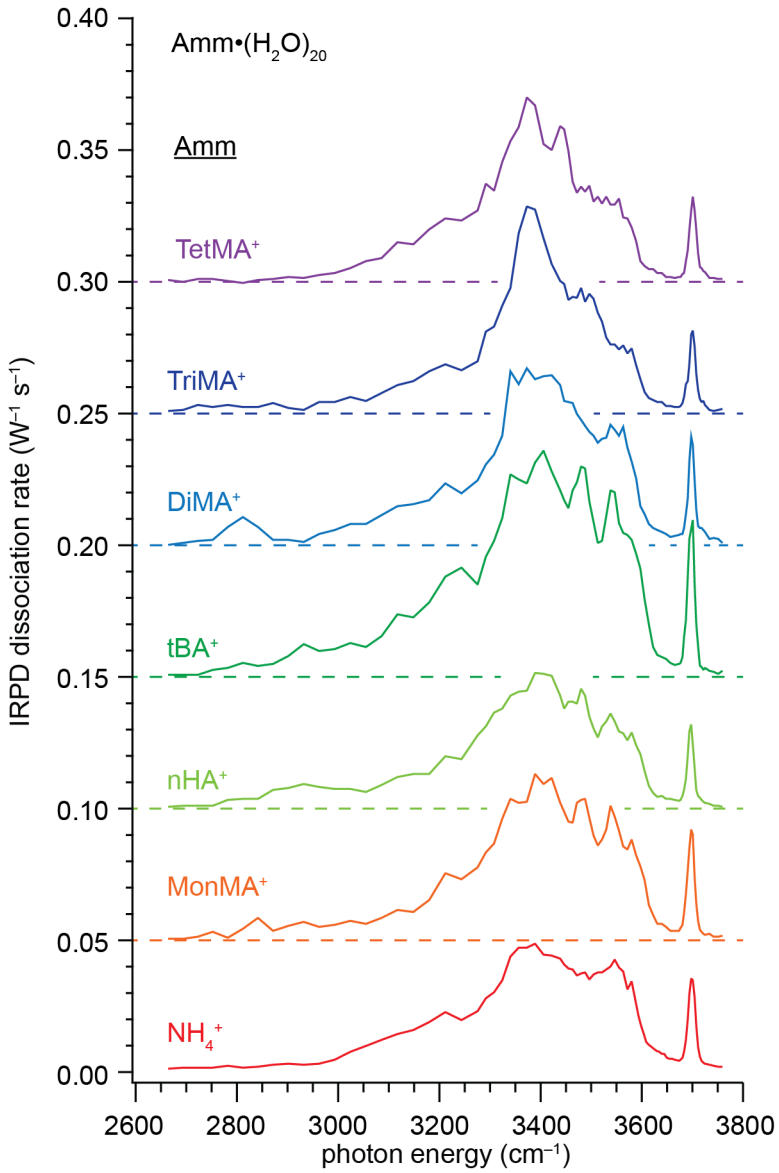

Figure 4.7. IRPD spectra of Amm•$(H_2O)_{20}$ in both the HB and free O–H regions measured at 133 K, where Amm = NH_4^+, MonMA$^+$, nHA$^+$, tBA$^+$, DiMA$^+$, TriMA$^+$ or TetMA$^+$. Horizontal dashed lines indicate a vertical offset of 0.05 W^{-1} s^{-1}.

the ammonium ions at n = 20 reveals subtle differences. Specifically, each spectrum has two dominant features near 3400 and 3550 cm^{-1} that are similar to those observed for $M^+•(H_2O)_{20}$, where M = Li, Na, K, Rb and Cs.[48] The band near 3400 cm^{-1} can be assigned to coupled HB O–H stretches,[46-49,102-104] whereas the feature near 3550 cm^{-1} corresponds to the HB O–H stretches of an acceptor-donor-donor (ADD) water molecule.[46-48] The relative intensities of the these features depend on the identity of the ion. Information about whether an ion is at the surface or in the interior of the cluster can be obtained by comparing these spectra to reference spectra of ions for which the locations of the ion can be confidently assigned.

4.4.6. Structures of Reference Clusters

The use of reference spectra can aid the analysis of complex spectra of hydrated ions.[40,42,105,106] Recent IRPD results from Cooper et al. as well as computations indicate that K^+, Rb^+, and Cs^+ are located in the interior of clathrates when hydrated by 20 water molecules.[48,64-67] Rb^+ has the same ionic radius as NH_4^+ (1.48 Å),[107] making it a good reference for an ion located at the interior of a clathrate. tBA^+ is very likely to be at the surface of a clathrate owing to the hydrophobic *tert*-butyl group, which disrupts the water hydrogen-bonding network if the ion is in the center. Calculations at the B3LYP/6-31+G** level of theory indicate that structures with tBA^+ in the interior of a clathrate are 86 kJ mol^{-1} or more higher in relative Gibbs free energy (133 K) compared to a structure where the ion is located at the surface (Figure 4.8). Non-clathrate structures with tBA^+ at the surface are calculated to be 18 – 35 kJ mol^{-1} higher in energy than a dodecahedral clathrate structure with the ion also at the surface. These results indicate $tBA^+•(H_2O)_{20}$ should be a good reference for an ammonium ion located at the surface of a clathrate.

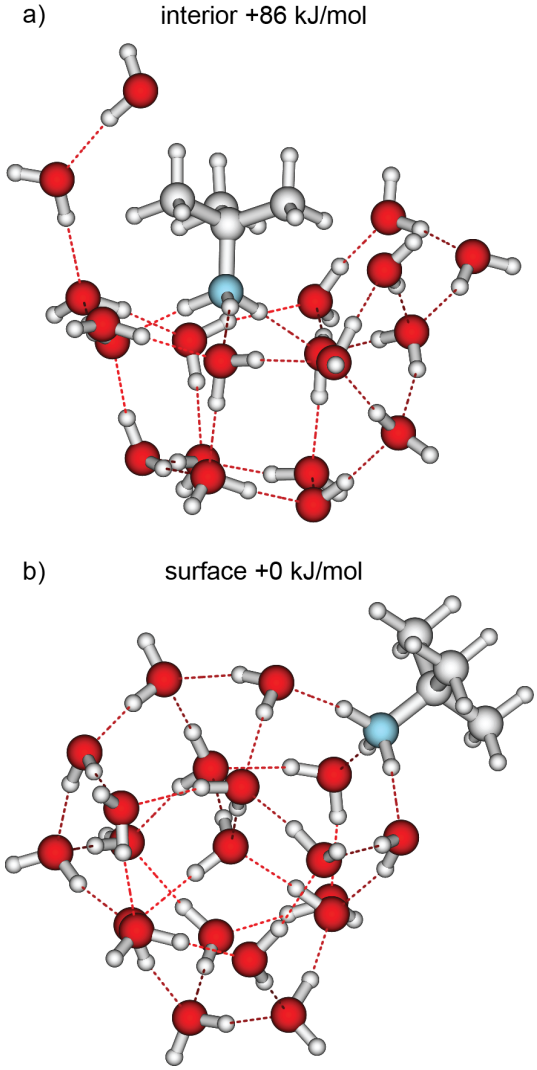

Figure 4.8. Structures for $tBA^+•(H_2O)_{20}$ with tBA^+ at the a) interior and at the b) surface of the droplet. Relative Gibbs free energies (133 K) calculated at the B3LYP/6-31+G** level of theory.

4.4.7. Location of Protonated Primary Amines in a Clathrate Structure

In order to determine how an alkyl group might disrupt the hydrogen-bonding network of a water nanodrop, the locations of $MonMA^+$ and nHA^+ when hydrated by 20 water molecules were determined using the reference spectra. The spectrum of $MonMA^+$ is compared to both reference spectra in Figure 4.9a. The reference spectra are intensity normalized to one, and the spectrum of $MonMA^+$ is scaled to minimize the residuals (Figure 4.9a, bottom). The spectra of $MonMA^+$ and tBA^+ with 20 water molecules are nearly the same. In contrast, $MonMA^+$ is a poor match to Rb^+. Compared to Rb^+, the spectrum of $MonMA^+•(H_2O)_{20}$ has an extra band near 3450 cm^{-1}, there is a small shift in the band at 3400 cm^{-1} and the two bands near 3550 cm^{-1} have slightly different shapes.

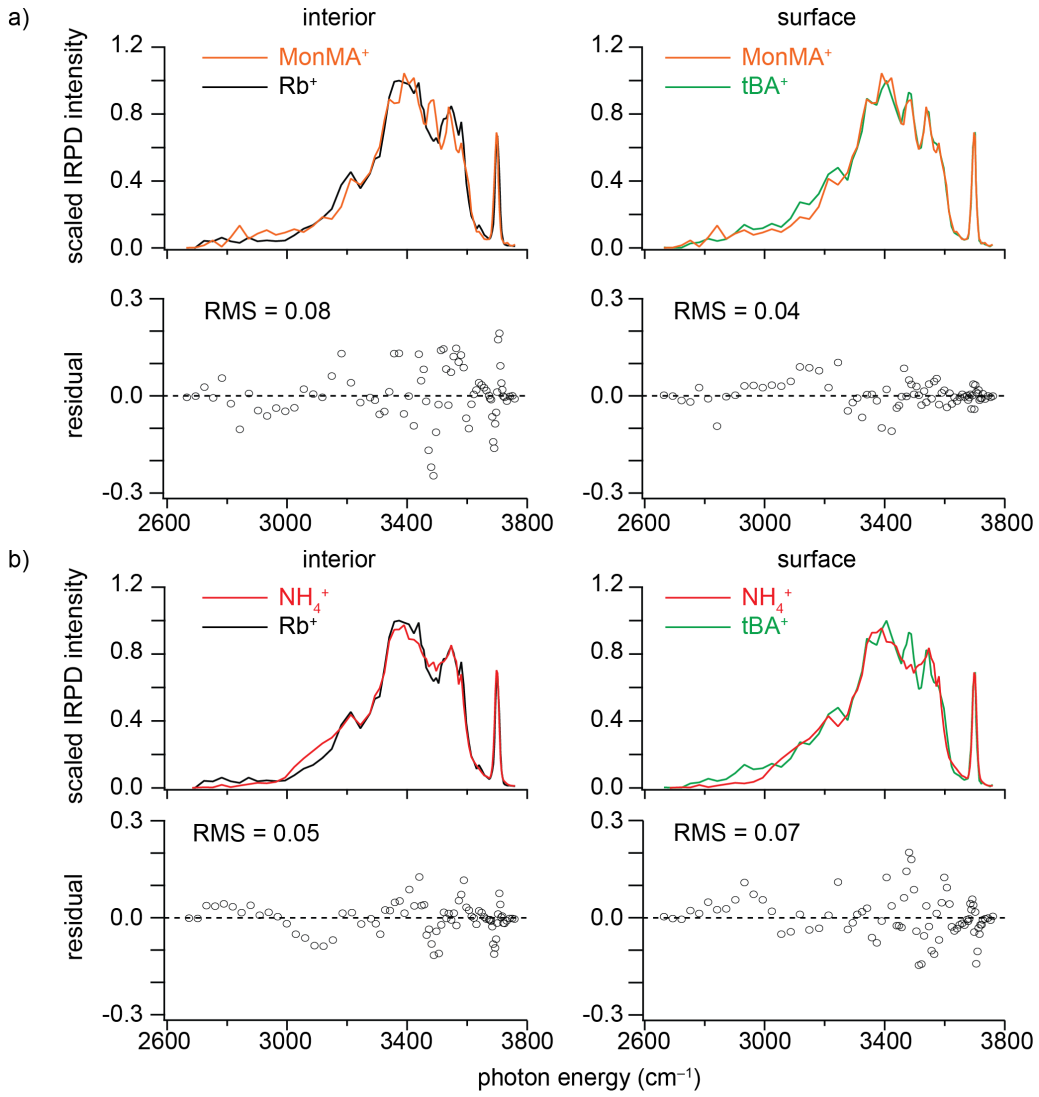

Figure 4.9. Comparisons of the IRPD spectra of a) $MonMA^+•(H_2O)_{20}$ and b) $NH_4^+•(H_2O)_{20}$ with $Rb^+•(H_2O)_{20}$, which is a reference of a clathrate structure with the ion in the interior, and $tBA^+•(H_2O)_{20}$, which is a reference for a clathrate structure with the ion at the surface. The root mean squares of the residuals (RMS) are below. The high similarity between the IRPD spectra of $MonMA^+•(H_2O)_{20}$ and $tBA^+(H_2O)_{20}$ indicates that $MonMA^+$ is at the surface of a clathrate structure. In contrast, the similarity between the IRPD spectra of $NH_4^+•(H_2O)_{20}$ and $Rb^+•(H_2O)_{20}$ indicates that ammonium is located in the center of a clathrate structure.

Table 4.1. Calculated RMS of residuals for comparisons with reference spectra.

	Interior (Rb^+)	Surface (tBA^+)
NH_4^+	0.05	0.07
$MonMA^+$	0.08	0.04
nHA^+	0.10	0.04
$DiMA^+$	0.08	0.08
$TriMA^+$	0.14	0.14
$TetMA^+$	0.13	0.15

The quality of a match between two spectra is reflected by the RMS value of the residuals (Table 4.1). These data indicate that the spectrum of $MonMA^+•(H_2O)_{20}$ is more similar to $tBA^+•(H_2O)_{20}$ (RMS = 0.04) than to $Rb^+•(H_2O)_{20}$ (RMS = 0.08). By comparison, two spectra of $NH_4^+•(H_2O)_{20}$ measured on different days had a RMS = 0.04, indicating the limit of reproducibility in these experiments. Even though tBA^+ has three methyl groups compared to one for $MonMA^+$, the spectra are essentially indistinguishable. C–H stretches appear between 2950 and 3150 cm^{-1}, yet there is little difference in intensity in this region, consistent with prior observations that these are typically weak bands in IRPD spectra.[41,43,105,108] The close match between $MonMA^+•(H_2O)_{20}$ and $tBA^+•(H_2O)_{20}$ suggests that they adopt similar structures in which $MonMA^+$ is located at the surface of a clathrate. Similarly, the RMS values obtained for nHA^+ (Table 4.1) indicate that nHA^+ closely matches tBA^+ (RMS = 0.04) and is a poor match to Rb^+ (RMS = 0.10). This indicates that nHA^+ is also located at the clathrate surface. If nHA^+ is used instead of tBA^+ as the reference for an ion at the surface, the RMS from a comparison to $MonMA^+$ is also 0.04. Thus, the same result is obtained whether tBA^+ or nHA^+ is used as the reference for an ion at the surface. These comparisons suggest that protonated primary amines are at the surface of a clathrate irrespective of the length or size of the alkyl group attached to the nitrogen atom.

4.4.8. Location of Ammonium in a Clathrate Structure

In contrast to $MonMA^+$ and nHA^+ at n = 20, the spectrum of $NH_4^+•(H_2O)_{20}$ is nearly identical to that of $Rb^+•(H_2O)_{20}$ (Figure 4.9b). Both spectra have similar bands near 3400 and 3550 cm^{-1}, and neither has a significant band at ~3450 cm^{-1} observed for primary amines and for tBA^+. The RMS value between NH_4^+ and Rb^+ is 0.05, but this relatively high value can be attributed to a fundamental difference between these two ions. The residuals near 3100 cm^{-1} are consistent with HB N–H stretches[102] for $NH_4^+•(H_2O)_{20}$, which are absent for $Rb^+•(H_2O)_{20}$. The residuals near 3700 cm^{-1} are due to a shift in the free O–H band, which can be attributed to NH_4^+ forming HBs to water molecules, whereas Rb^+ cannot. These HBs can cause slight differences in the hydrogen-bonding environment of the AAD water molecules resulting in the small shift in the free O–H frequency. The spectra of $NH_4^+•(H_2O)_{20}$ and $Rb^+•(H_2O)_{20}$ closely match, whereas the spectra of $NH_4^+•(H_2O)_{20}$ and $tBA^+•(H_2O)_{20}$ do not match nearly as well (RMS = 0.07). There is poor overlap between the bands at ~3400 and ~3550 cm^{-1}, and the spectrum of $tBA^+•(H_2O)_{20}$ has the extra band near 3450 cm^{-1}. A comparison between nHA^+ and NH_4^+ also yields the same RMS value (0.07) as between tBA^+ and NH_4^+. These results show that $NH_4^+•(H_2O)_{20}$ adopts a similar structure to that of $Rb^+•(H_2O)_{20}$, indicating that NH_4^+ is located in the interior of a clathrate.

4.4.9. Reference Comparisons to Other Alkylammonium Ions

Similar comparisons were performed for $DiMA^+$, $TriMA^+$ and $TetMA^+$ with $n = 20$. The RMS values obtained from these comparisons (Table 4.1) are ≥ 0.08, indicating that $DiMA^+$, $TriMA^+$ and $TetMA^+$ are poor matches to either reference ion. The poor matches can be attributed to the presence of nonclathrate structures. The free O–H spectra of $DiMA^+$, $TriMA^+$ and $TetMA^+$ for $n = 20$ have an AD free O–H band, indicating that a significant fraction of the ion population adopts nonclathrate structures. In contrast, the absence of this band for of Rb^+ and tBA^+ with 20 water molecules suggests that these ions form clathrate structures nearly exclusively. Because $DiMA^+$, $TriMA^+$ and $TetMA^+$ adopt nonclathrate structures when hydrated by 20 water molecules, Rb^+ and tBA^+ are unsuitable reference ions.

4.4.10. Relative Energies of Clathrate vs. Nonclathrate Structures

The origin of nonclathrate structures present for $DiMA^+$, $TriMA^+$ and $TetMA^+$ at $n = 20$ was investigated with computational chemistry to determine the relative energy differences between clathrate and nonclathrate structures. The relative energies and the number of water-water HBs of low-energy structures calculated for $DiMA^+$, $TriMA^+$ and $TetMA^+$ are shown in Figure 4.10 and are summarized in Table 4.2. For all three ions, a dodecahedral clathrate structure (Figure S4.2) was found to be lowest in energy, and this structure has the highest number of HBs. The difference in Gibbs free energy (133 K) between a clathrate and nonclathrate structure for $TriMA^+$ is calculated to be 18 kJ mol^{-1}. In contrast, the relative energy differences for $DiMA^+$ and $TetMA^+$ are significantly lower (13 and 3 kJ mol^{-1}, respectively). The lower differences in relative Gibbs free energies for $DiMA^+•(H_2O)_{20}$ and $TetMA^+•(H_2O)_{20}$ in comparison to that for $TriMA^+•(H_2O)_{20}$ are consistent with the trends in relative intensities of the AD free O–H band observed for these ions. There is a noticeable shoulder corresponding to the AD free O–H for $DiMA^+•(H_2O)_{20}$ and $TetMA^+•(H_2O)_{20}$, whereas this is only a minor feature for $TriMA^+•(H_2O)_{20}$. Although dodecahedral structures maximize the number of HBs, structures with fewer HBs were found to energetically competitive. In addition, there does not appear to be a direct correlation between the relative energy of a structure and the number of HBs. These results indicate the relative stabilities of clathrate structures are not solely a result of maximizing the number of HBs. Other factors, such as the orientation and thus the strength of HBs in the water network, contribute to the overall stabilities of clathrate structures.

Table 4.2. Range and mean (in parentheses) of relative Gibbs free energies (133 K) in kJ mol^{-1} for calculated structures (B3LYP/6-31+G** level of theory) with a given number of water-water hydrogen bonds (WW HBs) within the cluster.

WW HBs	$DiMA^+•(H_2O)_{20}$	$TriMA^+•(H_2O)_{20}$	$TetMA^+•(H_2O)_{20}$
27	–	33	–
28	13-14 (13.8)	21–44 (28.8)	3–28 (12.8)
29	25–37 (30.8)	18–41 (31.6)	8–25 (13.8)
30	18–51 (34.4)	22–52 (32.5)	12–25 (27.0)
31	0–45 (22.5)	0	0

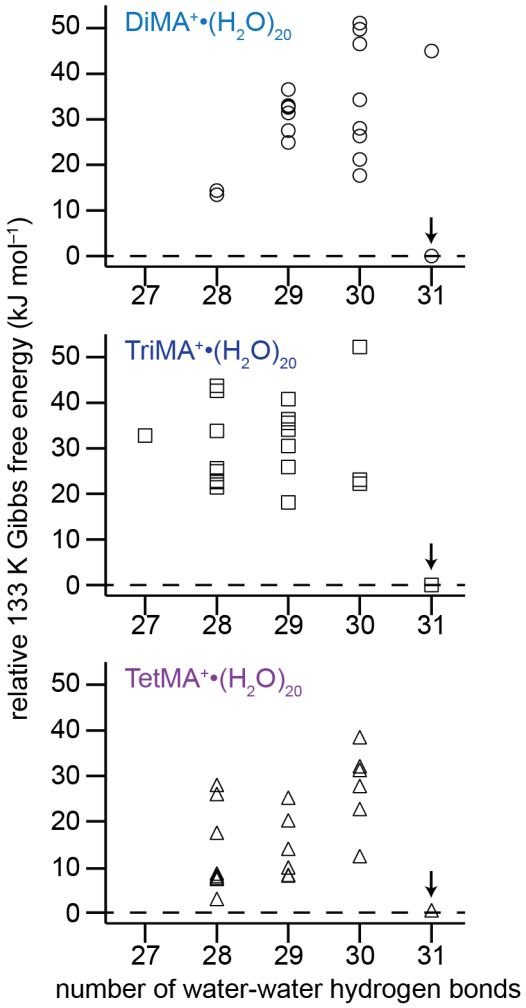

Figure 4.10. Relative 133 K Gibbs free energies (kJ mol^{-1}) of low-energy structures for Amm•$(H_2O)_{20}$ (Amm = $DiMA^+$, $TriMA^+$ and $TetMA^+$) calculated at the B3LYP/6-31+G** level of theory plotted as a function of the number of water-water hydrogen bonds in the cluster. The lowest-energy dodecahedral clathrate structures are indicated with an arrow.

4.5. Conclusion

IRPD spectroscopy in the region between 2600 and 3800 cm–1 was used to distinguish whether protonated primary amines and ammonia are located at the surface or in the interior of a clathrate consisting of 20 water molecules. For these ions, clathrate structures are indicated by the characteristic AAD free O–H stretch and the absence of an AD free O–H stretch. However, the location of these ions cannot be determined from these data alone. A comparison of IRPD spectra that includes HB O–H stretches shows subtle but important differences. The location of the ion at the surface or in the interior of the nanodrop is elucidated by comparisons to IRPD spectra of reference ions for which the location of the ion can be confidently assigned. Rb^+ is used as a reference for an ion at the interior of the clathrate[48] due to its similar ionic radius as NH_4^+,[107] and protonated *tert*-butylamine is used as a reference for an ion at the surface of the nanodrop. IRPD spectra indicate that the latter ion is a clathrate, and structures with the ion in

the interior are calculated to be 86 kJ mol^{-1} higher in energy than those with the ion at the surface. Results from these comparisons indicate that protonated ammonia is located in the interior of the clathrate whereas protonated methylamine and protonated *n*-heptylamine are at the surface. Results for protonated secondary and tertiary amines as well as $TetMA^+$ were ambiguous because structures other than clathrates are competitive for these ions making Rb^+ and tBA^+ unsuitable as references.

The interior location of NH_4^+ and Rb^+ in a clathrate structure with 20 water molecules compared to the surface location for $MonMA^+$, nHA^+ and tBA^+ is likely a result of the propensity of the latter ions to adversely affect the hydrogen-bonding network of the very stable clathrate structure when these ions are located in the interior. There is no direct correlation between stability and the number of HBs in a structure, indicating that the orientation of the hydrogen-bonding network as well as the overall number of HBs are critical to stability. These are the first experimental results showing that NH_4^+ is in the interior of a clathrate structure with 20 water molecules, and these results should provide a benchmark for future computational studies aimed at determining the propensity for ions to be surface active.

4.6. References

1. Schreier, S.; Malheiros, S. V. P.; de Paula, E. *Biochim. Biophys. Acta* **2000**, *1508*, 210-234.
2. Jin, Y. G.; Chen, S. F.; Xin, R.; Zhou, Y. S. *Colloids Surf., B* **2008**, *64*, 229-235.
3. Kabir-ud-Din; Khan, A. B.; Naqvi, A. Z. *Phys. Chem. Liq.* **2012**, *50*, 478-494.
4. Tsai, C. J.; Nussinov, R. *Protein Sci.* **1997**, *6*, 1426-1437.
5. Vanhee, P.; Stricher, F.; Baeten, L.; Verschueren, E.; Lenaerts, T.; Serrano, L.; Rousseau, F.; Schymkowitz, J. *Structure* **2009**, *17*, 1128-1136.
6. Krishnaswamy, S. R.; Williams, E. R.; Kirsch, J. F. *Protein Sci.* **2006**, *15*, 1465-1475.
7. Percy, A. J.; Rey, M.; Burns, K. M.; Schriemer, D. C. *Anal. Chim. Acta* **2012**, *721*, 7-21.
8. Hunt, S. W.; Roeselova, M.; Wang, W.; Wingen, L. M.; Knipping, E. M.; Tobias, D. J.; Dabdub, D.; Finlayson-Pitts, B. J. *J. Phys. Chem. A* **2004**, *108*, 11559-11572.
9. Nissenson, P.; Packwood, D. M.; Hunt, S. W.; Finlayson-Pitts, B. J.; Dabdub, D. *Atmos. Environ.* **2009**, *43*, 3951-3962.
10. Richards, N. K.; Wingen, L. M.; Callahan, K. M.; Nishino, N.; Kleinman, M. T.; Tobias, D. J.; Finlayson-Pitts, B. J. *J. Phys. Chem. A* **2011**, *115*, 5810-5821.
11. Jubb, A. M.; Hua, W.; Allen, H. C. *Annu. Rev. Phys. Chem.* **2012**, *63*, 107-130.
12. Li, R. H.; Jiang, Z. P.; Chen, F. G.; Yang, H. W.; Guan, Y. T. *J. Mol. Struct.* **2004**, *707*, 83-88.
13. Guardia, E.; Laria, D.; Marti, J. *J. Phys. Chem. B* **2006**, *110*, 6332-6338.
14. Miller, D. J.; Lisy, J. M. *J. Am. Chem. Soc.* **2008**, *130*, 15393-15404.
15. O'Brien, J. T.; Prell, J. S.; Bush, M. F.; Williams, E. R. *J. Am. Chem. Soc.* **2010**, *132*, 8248-8249.
16. O'Brien, J. T.; Williams, E. R. *J. Am. Chem. Soc.* **2012**, *134*, 10228-10236.
17. Prell, J. S.; O'Brien, J. T.; Williams, E. R. *J. Am. Chem. Soc.* **2011**, *133*, 4810-4818.
18. Marcus, Y. *Pure Appl. Chem.* **2010**, *82*, 1889-1899.
19. Hofmeister, F. *Arch. Exp. Pathol. Pharmacol.* **1888**, *24*, 247–260.
20. Baldwin, R. L. *Biophys. J.* **1996**, *71*, 2056-2063.
21. Rembert, K. B.; Paterova, J.; Heyda, J.; Hilty, C.; Jungwirth, P.; Cremer, P. S. *J. Am. Chem. Soc.* **2012**, *134*, 10039-10046.
22. Stuart, S. J.; Berne, B. J. *J. Phys. Chem. A* **1999**, *103*, 10300-10307.
23. Jungwirth, P.; Tobias, D. J. *Chem. Rev.* **2006**, *106*, 1259-1281.
24. Ishiyama, T.; Morita, A. *J. Phys. Chem. C* **2007**, *111*, 721-737.
25. Hagberg, D.; Brdarski, S.; Karlstrom, G. *J. Phys. Chem. B* **2005**, *109*, 4111-4117.
26. Walters, R. S.; Pillai, E. D.; Duncan, M. A. *J. Am. Chem. Soc.* **2005**, *127*, 16599-16610.
27. O'Brien, J. T.; Williams, E. R. *J. Phys. Chem. A* **2011**, *115*, 14612-14619.
28. Cooper, T. E.; O'Brien, J. T.; Williams, E. R.; Armentrout, P. B. *J. Phys. Chem. A* **2010**, *114*, 12646-12655.
29. Misaizu, F.; Sanekata, M.; Fuke, K.; Iwata, S. *J. Chem. Phys.* **1994**, *100*, 1161-1170.
30. Robertson, W. H.; Diken, E. G.; Price, E. A.; Shin, J. W.; Johnson, M. A. *Science* **2003**, *299*, 1367-1372.
31. Gao, B.; Wyttenbach, T.; Bowers, M. T. *J. Am. Chem. Soc.* **2009**, *131*, 4695-4701.
32. Lemoff, A. S.; Bush, M. F.; Wu, C. C.; Williams, E. R. *J. Am. Chem. Soc.* **2005**, *127*, 10276–10286.

33. Gao, B.; Wyttenbach, T.; Bowers, M. T. *J. Phys. Chem. B* **2009**, *113*, 9995-10000.
34. Lemoff, A. S.; Williams, E. R. *J. Am. Mass. Spectrom.* **2004**, *15*, 1014–1024.
35. Klassen, J. S.; Blades, A. T.; Kebarle, P. *J. Phys. Chem.* **1995**, *99*, 15509–15517.
36. Meot-Ner, M.; Field, F. H. *J. Am. Chem. Soc.* **1974**, *96*, 3168–3171.
37. Wincel, H. *J. Phys. Chem. A* **2007**, *111*, 5784-5791.
38. Ye, S. J.; Moision, R. M.; Armentrout, P. B. *Int. J. Mass Spectrom.* **2006**, *253*, 288-304.
39. Carl, D. R.; Armentrout, P. B. *ChemPhysChem* **2013**, *14*, 681-697.
40. Bush, M. F.; Prell, J. S.; Saykally, R. J.; Williams, E. R. *J. Am. Chem. Soc.* **2007**, *129*, 13544-13553.
41. Kamariotis, A.; Boyarkin, O. V.; Mercier, S. R.; Beck, R. D.; Bush, M. F.; Williams, E. R.; Rizzo, T. R. *J. Am. Chem. Soc.* **2006**, *128*, 905-916.
42. Chang, T. M.; Prell, J. S.; Warrick, E. R.; Williams, E. R. *J. Am. Chem. Soc.* **2012**, *134*, 15805-15813.
43. Demireva, M.; O'Brien, J. T.; Williams, E. R. *J. Am. Chem. Soc.* **2012**, *134*, 11216-11224.
44. Wende, T.; Wanko, M.; Jiang, L.; Meijer, G.; Asmis, K. R.; Rubio, A. *Angew. Chem. Int. Ed.* **2011**, *50*, 3807-3810.
45. Ayotte, P.; Bailey, C. G.; Weddle, G. H.; Johnson, M. A. *J. Phys. Chem. A* **1998**, *102*, 3067-3071.
46. Miyazaki, M.; Fujii, A.; Ebata, T.; Mikami, N. *Science* **2004**, *304*, 1134-1137.
47. Shin, J.-W.; Hammer, N. I.; Diken, E. G.; Johnson, M. A.; Walters, R. S.; Jaeger, T. D.; Duncan, M. A.; Christie, R. A.; Jordan, K. D. *Science* **2004**, *304*, 1137-1140.
48. Cooper, R. J.; Chang, T. M.; Williams, E. R. *J. Phys. Chem. A* **2013**, *117*, 6571–6579.
49. Diken, E. G.; Hammer, N. I.; Johnson, M. A.; Christie, R. A.; Jordan, K. D. *J. Chem. Phys.* **2005**, *123*, 164309.
50. Lin, S. S. *Rev. Sci. Instrum.* **1973**, *44*, 516-517.
51. Searcy, J. Q.; Fenn, J. B. *J. Chem. Phys.* **1974**, *61*, 5282-5288.
52. Wu, C. C.; Lin, C. K.; Chang, H. C.; Jiang, J. C.; Kuo, J. L.; Klein, M. L. *J. Chem. Phys.* **2005**, *122*, 074315.
53. Shinohara, H.; Nagashima, U.; Tanaka, H.; Nishi, N. *J. Chem. Phys.* **1985**, *83*, 4183-4192.
54. Schmidt, M.; Masson, A.; Brechignac, C.; Cheng, H. P. *J. Chem. Phys.* **2007**, *126*, 154315.
55. Ryding, M. J.; Ruusuvuori, K.; Andersson, P. U.; Zatula, A. S.; McGrath, M. J.; Kurten, T.; Ortega, I. K.; Vehkamaki, H.; Uggerud, E. *J. Phys. Chem. A* **2012**, *116*, 4902-4908.
56. Selinger, A.; Castleman, A. W. *J. Phys. Chem.* **1991**, *95*, 8442-8444.
57. Lee, S. W.; Freivogel, P.; Schindler, T.; Beauchamp, J. L. *J. Am. Chem. Soc.* **1998**, *120*, 11758-11765.
58. Nguyen, V. Q.; Chen, X. G.; Yergey, A. L. *J. Am. Soc. Mass Spectrom.* **1997**, *8*, 1175-1179.
59. Nagashima, U.; Shinohara, H.; Nishi, N.; Tanaka, H. *J. Chem. Phys.* **1986**, *84*, 209-214.
60. Kassner, J. L.; Hagen, D. E. *J. Chem. Phys.* **1976**, *64*, 1860-1861.
61. Holland, P. M.; Castleman, A. W. *J. Chem. Phys.* **1980**, *72*, 5984.
62. Hermann, V.; Kay, B. D.; Castleman, A. W. *Chem. Phys.* **1982**, *72*, 185-200.
63. Silveira, J. A.; Servage, K. A.; Gamage, C. M.; Russell, D. H. *J. Phys. Chem. A* **2013**, *117*, 953-961.

64. Steel, E. A.; Merz, K. M.; Selinger, A.; Castleman, A. W. *J. Phys. Chem.* **1995**, *99*, 7829-7836.
65. Khan, A. *Chem. Phys. Lett.* **2004**, *388*, 342-347.
66. Schulz, F.; Hartke, B. *ChemPhysChem* **2002**, *3*, 98-106.
67. Schulz, F.; Hartke, B. *Theor. Chem. Acc.* **2005**, *114*, 357-379.
68. Buffey, I. P.; Brown, W. B. *Chem. Phys. Lett.* **1984**, *109*, 59-65.
69. Kozack, R. E.; Jordan, P. C. *J. Chem. Phys.* **1993**, *99*, 2978-2984.
70. Khan, A. *Chem. Phys. Lett.* **1994**, *217*, 443-450.
71. Khan, A. *Chem. Phys. Lett.* **2000**, *319*, 440-450.
72. Hodges, M. P.; Wales, D. J. *Chem. Phys. Lett.* **2000**, *324*, 279-288.
73. Iyengar, S. S.; Petersen, M. K.; Day, T. J. F.; Burnham, C. J.; Teige, V. E.; Voth, G. A. *J. Chem. Phys.* **2005**, *123*, 084309.
74. Singh, N. J.; Park, M.; Min, S. K.; Suh, S. B.; Kim, K. S. *Angew. Chem., Int. Ed.* **2006**, *45*, 3795-3800.
75. Kus, T.; Lotrich, V. F.; Perera, A.; Bartlett, R. J. *J. Chem. Phys.* **2009**, *131*, 104313.
76. Khan, A. *Chem. Phys. Lett.* **2001**, *338*, 201-207.
77. Douady, J.; Calvo, F.; Spiegelman, F. *J. Chem. Phys.* **2008**, *129*, 154305.
78. Willow, S. Y.; Singh, N. J.; Kim, K. S. *J. Chem. Theory Comput.* **2011**, *7*, 3461-3465.
79. Wei, S.; Shi, Z.; Castleman, A. W. *J. Chem. Phys.* **1991**, *94*, 3268-3270.
80. Kennett, J. P.; Cannariato, K. G.; Hendy, I. L.; Behl, R. J. *Science* **2000**, *288*, 128-133.
81. Koh, C. A.; Sloan, E. D.; Sum, A. K.; Wu, D. T. *Annu. Rev. Chem. Biomol. Eng.* **2011**, *2*, 237-257.
82. Seo, Y.; Kang, S. P. *Chem. Eng. J.* **2010**, *161*, 308-312.
83. Zhang, B. Y.; Wu, Q. *Energy Fuels* **2010**, *24*, 2530-2535.
84. Eslamimanesh, A.; Mohammadi, A. H.; Richon, D.; Naidoo, P.; Ramjugernath, D. *J. Chem. Thermodyn.* **2012**, *46*, 62-71.
85. Booth, J. S.; Rowe, M. M.; Fischer, K. M. US Geological Survey, Open File Report 1, **1996**, pp. 96-272.
86. Collett, T. S. *AAPG Bull.* **2002**, *86*, 1971-1992.
87. Milkov, A. V. *Earth Sci. Rev.* **2004**, *66*, 183-197.
88. Gonzalez, B. S.; Hernandez-Rojas, J.; Wales, D. J. *Chem. Phys. Lett.* **2005**, *412*, 23-28.
89. Agmon, N. *Chem. Phys. Lett.* **1995**, *244*, 456-462.
90. Tuckerman, M.; Laasonen, K.; Sprik, M.; Parrinello, M. *J. Phys. Chem.* **1995**, *99*, 5749-5752.
91. Geissler, P. L.; Dellago, C.; Chandler, D.; Hutter, J.; Parrinello, M. *Science* **2001**, *291*, 2121-2124.
92. Lockwood, G. K.; Garofalini, S. H. *J. Phys. Chem. B* **2013**, *117*, 4089-4097.
93. Bush, M. F.; O'Brien, J. T.; Prell, J. S.; Saykally, R. J.; Williams, E. R. *J. Am. Chem. Soc.* **2007**, *129*, 1612-1622.
94. Wong, R. L.; Paech, K.; Williams, E. R. *Int. J. Mass Spectrom.* **2004**, *232*, 59-66.
95. Prell, J. S.; O'Brien, J. T.; Williams, E. R. *J. Am. Mass. Spectrom.* **2010**, *21*, 800-809.
96. Shao, Y.; et al. *Phys. Chem. Chem. Phys.* **2006**, *8*, 3172-3191.
97. Price, W. D.; Schnier, P. D.; Jockusch, R. A.; Strittmatter, E. F.; Williams, E. R. *J. Am. Chem. Soc.* **1996**, *118*, 10640-10644.
98. Donald, W. A.; Williams, E. R. *J. Phys. Chem. A* **2008**, *112*, 3515-3522.

99. Cheng, T. C.; Bandyopadhyay, B.; Mosley, J. D.; Duncan, M. A. *J. Am. Chem. Soc.* **2012**, *134*, 13046-13055.
100. Chang, H. C.; Wu, C. C.; Kuo, J. L. *Int. Rev. Phys. Chem.* **2005**, *24*, 553-578.
101. Nicely, A. L.; Miller, D. J.; Lisy, J. M. *J. Mol. Spectrosc.* **2009**, *257*, 157-163.
102. Chang, H. C.; Wang, Y. S.; Lee, Y. T. *Int. J. Mass Spectrom.* **1998**, *180*, 91-102.
103. Bush, M. F.; Saykally, R. J.; Williams, E. R. *J. Am. Chem. Soc.* **2008**, *130*, 15482-15489.
104. Nagornova, N. S.; Rizzo, T. R.; Boyarkin, O. V. *Science*. **2012**, *336*, 320-323.
105. Prell, J. S.; Chang, T. M.; O'Brien, J. T.; Williams, E. R. *J. Am. Chem. Soc.* **2010**, *132*, 7811-7819.
106. Prell, J. S.; Correra, T. C.; Chang, T. M.; Biles, J. A.; Williams, E. R. *J. Am. Chem. Soc.* **2010**, *132*, 14733-14735.
107. Conway, B. E. *Ionic Hydration in Chemistry and Biophysics*; Elsevier: New York, NY, 1981.
108. Atkins, C. G.; Rajabi, K.; Gillis, E. A. L.; Fridgen, T. D. *J. Phys. Chem. A* **2008**, *112*, 10220-10225.

4.7. Supplementary Figures

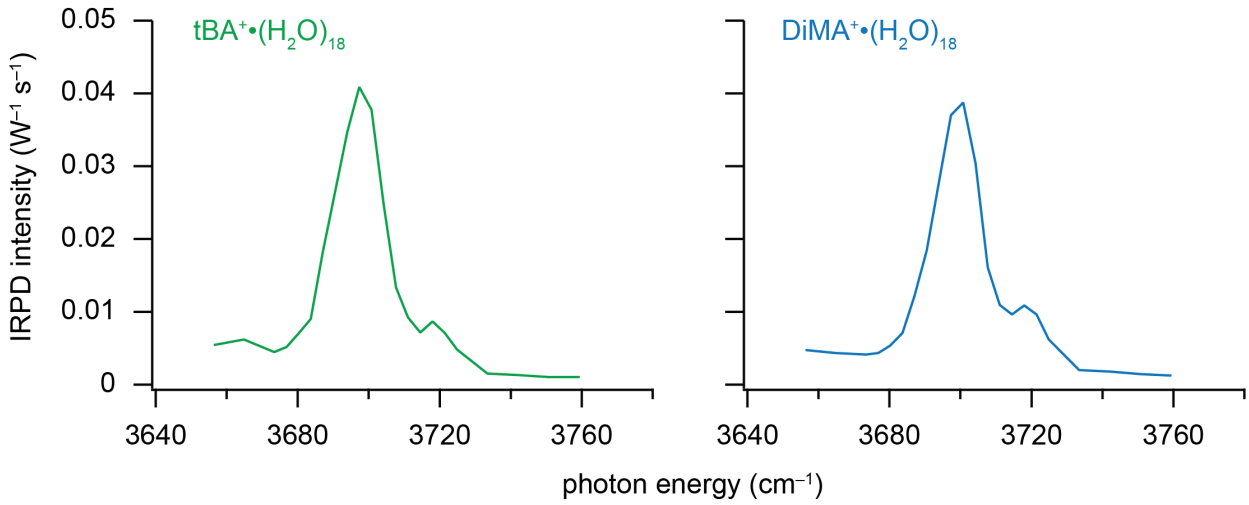

Figure S4.1. IRPD spectra in the free O–H region for $tBA^{+}\bullet(H_2O)_{18}$ and $DiMA^{+}\bullet(H_2O)_{18}$ measured at 133 K.

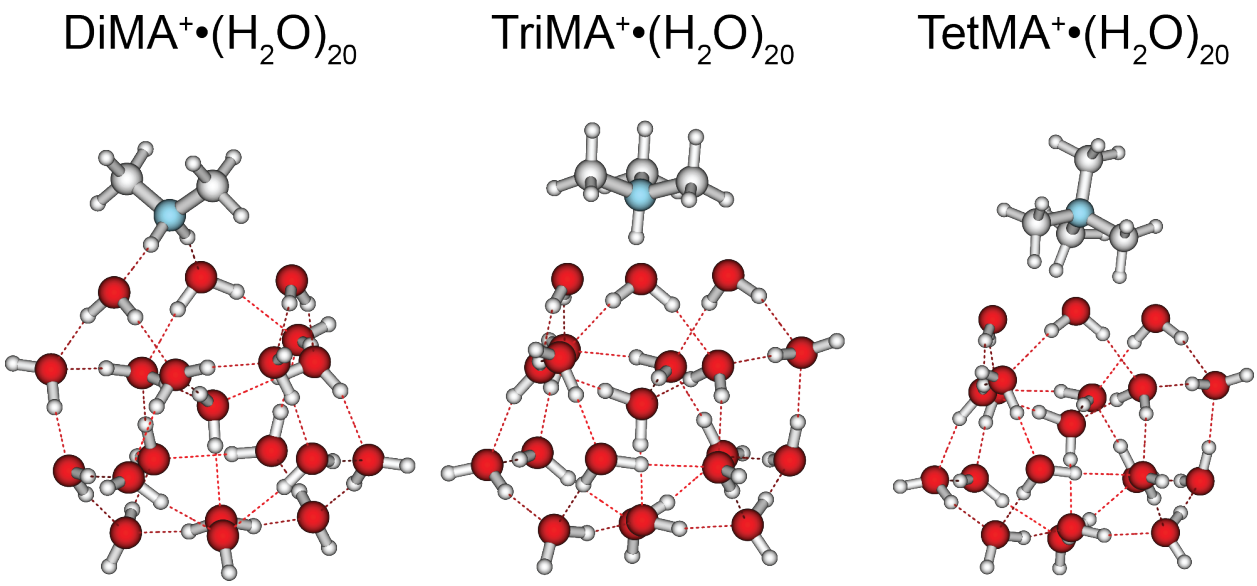

Figure S4.2. Dodecahedral clathrate structures calculated at the B3LYP/6-31+G** level of theory.

Chapter 5. Halide Anion Binding to Gly_3, Ala_3 and Leu_3

5.1. Abstract

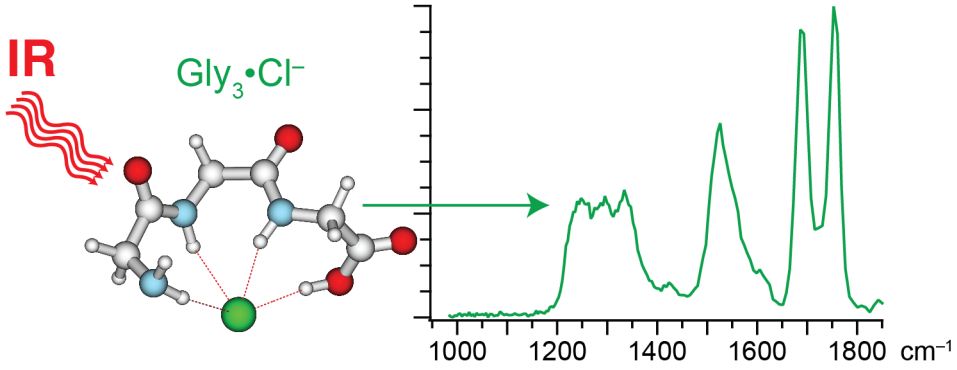

Originally published in the Journal of the American Chemical Society
http://dx.doi.org/10.1016/j.ijms.2014.02.019

The structures of $Gly_3•X^-$, $Ala_3•X^-$ and $Leu_3•X^-$ (X = Cl, Br and I) are investigated with computational chemistry and infrared multiple-photon dissociation (IRMPD) spectroscopy. Low-energy structures calculated at the B3LYP/6-31+G** level of theory (or the CRENBL basis and effective core potential implemented for Br and I) for these complexes have similar structural motifs in which the halide anion binds to the peptide via hydrogen bonds at amide, amine, and/or carboxylic acid H atoms. IRMPD results in the loss of HX, and the resulting spectra do not depend significantly on anion identity. Comparisons between measured spectra and those calculated for low-energy structures of each of the chloridated complexes indicate that structures with similar binding motifs are present for all three complexes. These results suggest that the size of the alkyl side chain does not significantly influence how halide anions bind to these peptides. The coordination geometries of $Gly_3•X^-$ and $Ala_3•X^-$ are "inverted" compared to those for the Na^+ cationized peptides, where the peptides coordinate to Na^+ via lone pair electrons of O and N atoms. The "inversion" in structures between $Ala_3•Na^+$ and $Ala_3•X^-$ results in greater steric hindrance for some geometries of the latter. There is a subtle blue shift in the C-terminal C=O stretch frequency with increasing halide anion size for each peptide, consistent with contributions from Stark and charge transfer effects. In contrast, the N–H bends red shift with increasing halide anion size, which can only be attributed to the charge transfer effect. This is the first report of IR spectra of peptides complexed with anions, and these results provide insights into anion-peptide binding interactions.

5.2. Introduction

Ions and their interactions with amino acids, peptides and proteins are important in many biological processes, such as pH regulation,[1,2] protein structure and complex assembly,[3,4] uptake of amino acids by bacteria[5] and neuron signaling.[6] For example, Ca^{2+}-gated Cl^- channels regulate the conductance of olfactory receptors.[7-10] Investigating how ions interact with biomolecules in solution can be difficult because of the complex environment consisting of the biomolecules and ions of interest as well as ubiquitous counter ions, solvent molecules and impurities. In the gas phase, specific ion-biomolecule complexes can be isolated by mass spectrometry and probed using a wide variety of structurally informative techniques.

Information about ion-biomolecule interactions can be obtained from fragmentation,[11-16] ion-mobility[17-20] and spectroscopy experiments.[21-43] Infrared multiple-photon dissociation (IRMPD) spectroscopy studies have provided detailed information about structures of many amino acids and peptides as well as their complexes with ion adducts.[22-43] The size of the cation adducts can influence how the amino acid coordinates to the ion as well as the relative stabilities between zwitterionic and nonzwitterionic forms of amino acids.[30-37] These types of studies provide a fundamental understanding of how ions interact with amino acids and affect their structures in the absence of competing effects from counterions or solvent molecules.

The interactions between anions and amino acids have been the subject of fewer studies,[42-47] in contrast to the more widely investigated interactions of cations with amino acids or peptides. A zwitterionic form of Arg can be stabilized by the attachment of an excess electron[45,46] or by complexation with halide anions.[42-44] The zwitterionic form of Gly was calculated to be metastable when the dianion of oxalic or malonic acid is adducted.[47] IRMPD studies of anion and amino acids have been reported,[42,43] but more complex interactions between anions and peptides have yet to be characterized spectroscopically.

Here, we report the first IRMPD spectra of $Gly_3 \bullet X^-$, $Ala_3 \bullet X^-$ and $Leu_3 \bullet X^-$, X = Cl, Br and I, in combination with calculated low-energy structures and their relative Gibbs free energies (298 K). The relative energies as well as comparisons between the IRMPD spectra and the simulated spectra of low-energy structures are used to determine the most stable conformers. These results provide useful insight into how the size of alkyl side-chains affect the structure of peptides with anions adducted and are the first reported spectra of anions bound to peptides.

5.3. Computational and Experimental Methods

5.3.1. Computational

Separate conformational searches for $Gly_3 \bullet Cl^-$ and $Ala_3 \bullet Cl^-$ were performed using Macromodel v. 9.8 with MMFFs to generate at least 6,000 low-energy structures. These initial geometries were grouped into families based on similar backbone and hydrogen-bonding motifs, and a representative structure from each family was selected for quantum mechanical optimization using Q-Chem v. 4.0[48] at the B3LYP/6-31+G** level of theory. Zero-point energies and 298 K enthalpies and entropies were computed using unscaled harmonic oscillator vibrational frequencies calculated at the same level of theory. Initial geometries for $Leu_3 \bullet Cl^-$

were generated by side chain substitution for the three lowest-energy structures of Ala_3•Cl^-. Quantum mechanical optimization for Leu_3•Cl^- was also done at the B3LYP/6-31+G** level of theory. Low-energy structures for Gly_3•Cl^-, Ala_3•Cl^- and Leu_3•Cl^- were used to generate starting structures for the brominated and iodated peptide complexes by replacing the Cl atom with Br or I, respectively. Quantum-chemical calculations for each peptide with Br^- and I^- adducted were performed with the B3LYP density functional and the 6-31+G** basis set for each atom except Br and I, for which the CRENBL basis set and effective core potential were used. Simulated spectra were generated using harmonic frequencies scaled by a factor of 0.975 and convolved with a full width half maximum (fwhm) Gaussian profile of 40 cm^{-1}.[40,42]

5.3.2. Experimental

All experimental spectra were measured using a 4.7 T Fourier-transform ion cyclotron resonance (FT/ICR) mass spectrometer coupled with a free electron laser (FELIX), which generates tunable infrared radiation between 900 and 1900 cm^{-1}.[49] A description of the instrument and experimental parameters is given elsewhere.[50] The halidated peptide complexes were generated by electrospray ionization with methanol/water (~85/15) solvent and flow rates of 5 – 10 μL min^{-1}. Solutions of peptides with sodium halide salts were prepared at 1 – 2 mM concentrations for both components. Ions are accumulated for ~5 s in a hexapole linear trap for collisional and radiative cooling prior to injection into the mass spectrometer. Ions that are trapped in the ion cell of the mass spectrometer are isolated with a stored waveform inverse Fourier-transform before they are irradiated by photons from FELIX (typically for ~3 s). First order rate constants are calculated from the precursor and product abundances and are corrected for frequency dependent variations in laser power.[51]

5.4. Results and Discussion

5.4.1 Calculated Structures and Relative Gibbs Free Energies (298 K)

Gly_3•Cl^-. The binding motifs of model aliphatic tripeptides to Cl^- were investigated at the B3LYP/6-31+G** level of theory. The three lowest-energy structures for Gly_3•Cl^- are shown at the top of Figure 5.1 (**Gly_3A – C**). The anion can coordinate to Gly_3 through hydrogen bonds (HBs) with the amides, carboxylic acid or the N-terminus. In the lowest-energy structure, **Gly_3C**, Cl^- hydrogen bonds to the two amide H atoms as well as the carboxylic acid, and the N-terminus forms a HB to the adjacent amide carbonyl O atom. In **Gly_3B** (+7 kJ mol^{-1} in Gibbs free energy at 298 K), a HB with an amide H atom is displaced by a HB with the N-terminus. A fourth HB to Cl^- (**Gly_3A**, +5 kJ mol^{-1}) does not result in additional stabilization. These results indicate that Gly_3 forms at least three HBs to Cl^-, and that any energy gained by forming a fourth HB to the anion is similar to that of forming an intramolecular HB.

The carboxylic acid groups in **Gly_3A – C** are in an exo conformation, where the acidic H atom is *trans* relative to the carbonyl O atom. The lowest-energy structure with an endo carboxylic acid, **Gly_3D**, in which the acidic H atom is *cis* relative to the carbonyl O atom, has only two HBs to Cl^- via the N- and C-termini. This structure is 23 kJ mol^{-1} higher in Gibbs free energy compared to the lowest-energy exo structure. Endo structures with a greater number of HBs to Cl^- were even higher in energy, and these results suggest that it is unfavorable for Gly_3•Cl^- to adopt a structure with an endo carboxylic acid.

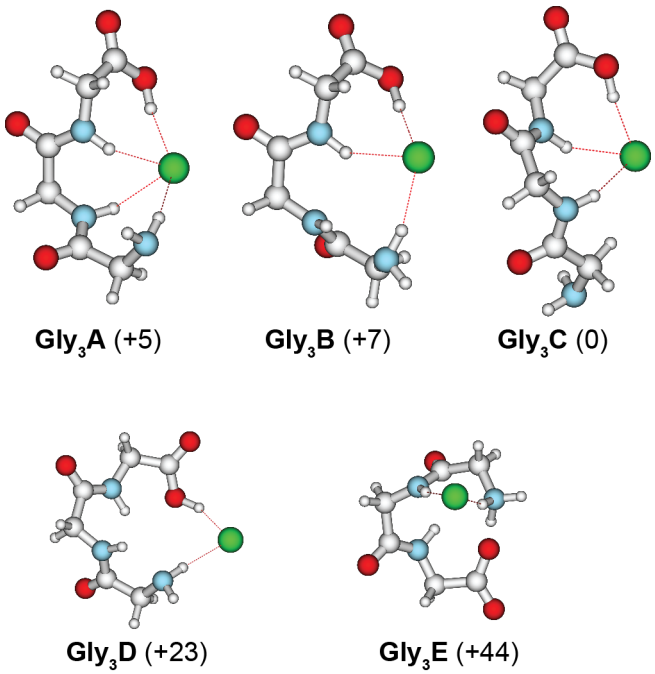

Figure 5.1. Low-energy structures for Gly_3•Cl^- (top) and lowest-energy structures of the endo carboxylic acid and zwitterionic forms (bottom) calculated at the B3LYP/6-31+G** level of theory (relative 298 K Gibbs free energy in kJ mol^{-1}).

Structures in which Gly_3 is zwitterionic were also investigated, and the lowest-energy zwitterionic structure (**Gly_3E**) is cyclic, where both Cl^- and the carboxylate interact with the protonated N-terminus. **Gly_3E** is 44 kJ mol^{-1} higher in Gibbs free energy than **Gly_3C**, indicating that zwitterionic structures are unfavorable compared to charge-solvated structures. Based on the calculated energies, Gly_3•Cl^- is likely to adopt a charge-solvated exo structure. The energy differences between **Gly_3A** – **C** are relatively small, indicating all three structures may exist at room temperature.

Low-energy structures reported for Gly_3•Na^+ are similar to those found for Gly_3•Cl^-, but the coordination of the peptide to the corresponding ion is "inverted."[39,40] The peptide coordinates to Cl^- via HBs, whereas Na^+ coordinates to the lone pairs of the carbonyl O atoms and the N-terminus. In this respect, **Gly_3A** and **Gly_3C** are "inversions" of low-energy structures GGG-Na^+*1* and GGG-Na^+*3*, respectively, previously reported by Balaj et al.[39] As is the case for Gly_3Cl^-, three-coordinate structures for Gly_3•Na^+ are lower in energy than those that are four-coordinate.

Ala_3•Cl^-. To determine the effect of side chain size on anion coordination, low-energy structures for Ala_3•Cl^- and their relative Gibbs free energies at 298 K (Figure 5.2, top) were calculated. The hydrogen-bonding motifs and relative energies for **Ala_3A** – **C** are similar to those for **Gly_3A** – **C**, respectively. **Ala_3C** is lowest in energy, but **Ala_3A** and **Ala_3B** are energetically competitive (within 4 kJ mol^{-1}). **Ala_3D**, the lowest-energy endo structure, and **Ala_3E**, the lowest-energy zwitterionic structure, (Figure 5.2, middle) are 20 and 40 kJ mol^{-1}, respectively, higher in Gibbs free energy than **Ala_3C**. Based on the calculated relative energies

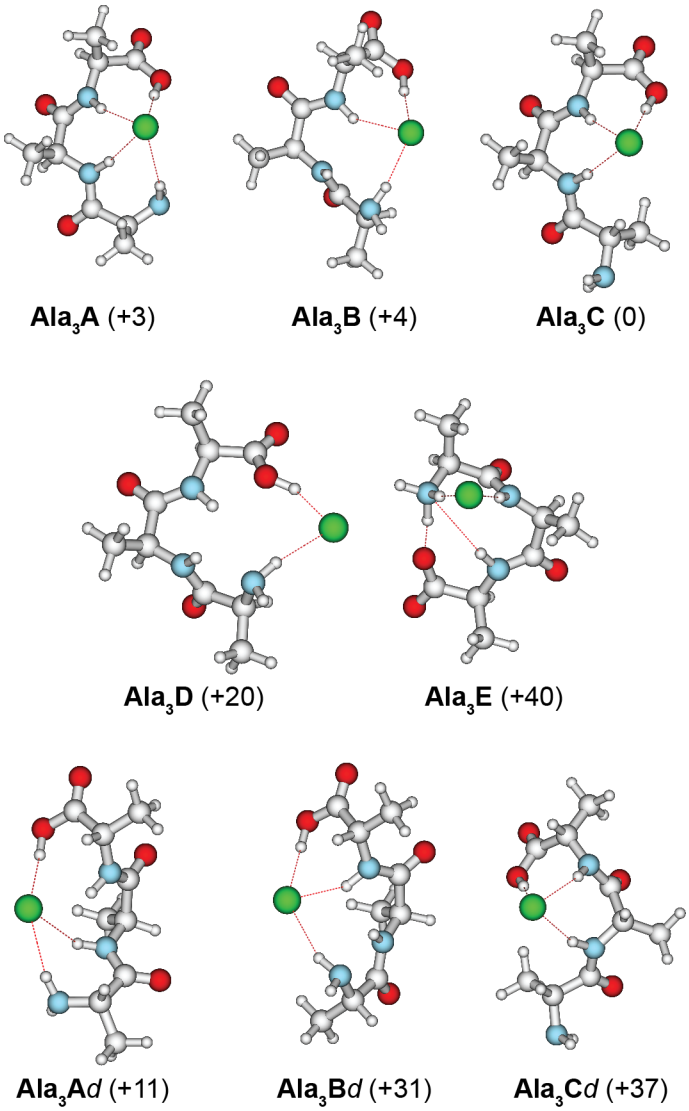

Figure 5.2. Low-energy structures for $Ala_3 \bullet Cl^-$ (top), lowest-energy structures of the endo carboxylic acid and zwitterionic forms (middle) as well as diastereoisomers of low-energy structures (bottom) calculated at the B3LYP/6-31+G** level of theory (relative 298 K Gibbs free energy in kJ mol^{-1}).

for $Ala_3 \bullet Cl^-$ and $Gly_3 \bullet Cl^-$, both complexes adopt similar structures, indicating that the larger side chain has little effect on anion coordination to Ala_3. As was the case for $Gly_3 \bullet Cl^-$, low-energy structures for $Ala_3 \bullet Cl^-$ are "inverted" compared to those for Ala_3 with Na^+ and other alkali ions adducts.[39,40]

The anion in $Ala_3 \bullet Cl^-$ is a stereocenter, where the HBs between Cl^- and the peptide are analogous to covalent bonds. Initial geometries for diastereoisomers of **Ala_3A – C** were formed by changing the chirality of the anion. Geometry optimizations were performed, resulting in structures **Ala_3A***d* – C*d*** (Figure 5.2, bottom). **Ala_3A***d* is only 11 kJ mol^{-1} higher in energy compared to the lowest-energy structure (**Ala_3C**), whereas **Ala_3B***d* and **Ala_3C***d* are >30 kJ mol^{-1} higher in energy compared to **Ala_3C**. Thus, it is unlikely that **Ala_3B***d* and **Ala_3C***d* have

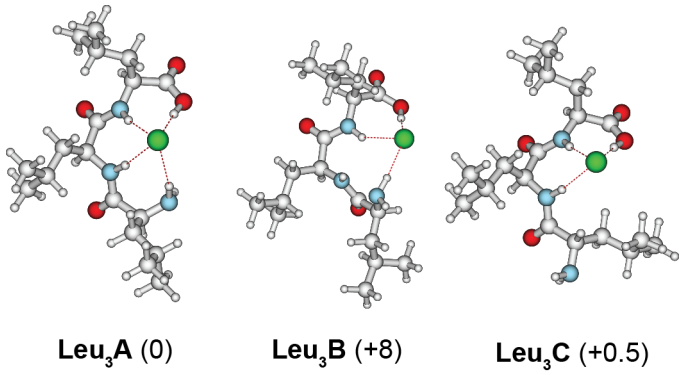

Figure 5.3. Structures for $Leu_3 \bullet Cl^-$ calculated at the B3LYP/6-31+G** level of theory (relative 298 K Gibbs free energy in kJ mol^{-1}). Initial geometries for $Leu_3 \bullet Cl^-$ were generated by side chain substitution for the three lowest-energy structures of $Ala_3 \bullet Cl^-$.

significant contributions to the ion population. The relative enthalpies of low-energy structures for $Ala_3 \bullet Na^+$ and their diastereoisomers are within ≤10 kJ mol^{-1} of each other.[39] The high relative Gibbs free energies for **Ala$_3$B***d* and **Ala$_3$C***d* are due to the steric interactions between the methyl side chains and the amide O atoms. In contrast, the analogous steric effect for $Ala_3 \bullet Na^+$ is between the methyl groups and the relatively small amide H atoms.

Leu$_3$•Cl$^-$. Low-energy structures for $Ala_3 \bullet Cl^-$ (**Ala$_3$A – C**) were modified to create initial geometries for $Leu_3 \bullet Cl^-$ by changing the side chain. The resulting structures for $Leu_3 \bullet Cl^-$ only change slightly upon geometry optimization (**Leu$_3$A – C**, Figure 5.3) and maintain the same structural motifs as $Gly_3 \bullet Cl^-$ and $Ala_3 \bullet Cl^-$. **Leu$_3$A** and **Leu$_3$C** are essentially isoenergetic, and **Leu$_3$B** is 8 kJ mol^{-1} higher in Gibbs free energy (298 K). In summary, these results indicate that increasing steric hindrance of the alkyl side chains does not significantly change the relative energies or hydrogen-bonding motifs of low-energy structures for these complexes.

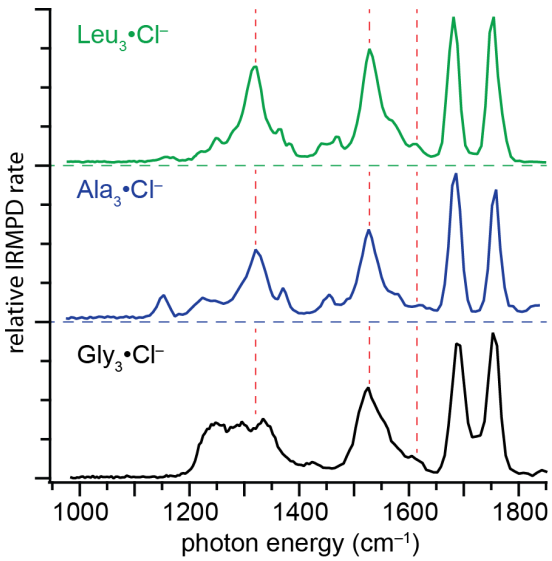

Figure 5.4. IRMPD spectra of $Gly_3 \bullet Cl^-$, $Ala_3 \bullet Cl^-$, and $Leu_3 \bullet Cl^-$ at 298 K. Horizontal dashed lines indicate a vertical offset. Vertical dashed lines serve as a guide for the eye.

5.4.2. Spectroscopy of Chloridated Tripeptides

IR photodissociation of $Gly_3•Cl^-$, $Ala_3•Cl^-$ and $Leu_3•Cl^-$ results in the loss of HCl and the formation of the deprotonated amino acid. The IRMPD spectrum of each complex was measured from 1000 – 1850 cm^{-1} (Figure 5.4). There are four bands in the region between 1500 and 1800 cm^{-1} with frequencies close to bands reported for Li^+, Na^+, K^+ and Cs^+ adducted to Gly_3 and Ala_3.[39-41] The band near 1760 cm^{-1} corresponds to the carbonyl stretch of the C-terminus.[28,31,32,37,39-42,52] The bands that occur near 1520 and 1690 cm^{-1} correspond to the amide II (N–H bends) and I (carbonyl C=O stretch) vibrational modes, respectively.[39-41] The absence of an asymmetric stretch of a carboxylate group near 1650 cm^{-1} indicates that there is not a significant zwitterionic population,[26-28,31-38,42] consistent with a ~40 kJ mol^{-1} higher Gibbs free energy calculated for the zwitterionic forms of $Gly_3•Cl^-$ and $Ala_3•Cl^-$. The amide I band as well as the NH_2 scissor mode at ~1625 cm^{-1} could overlap with the carboxylate asymmetric stretch and obscure contributions from a minor population of zwitterionic structures.

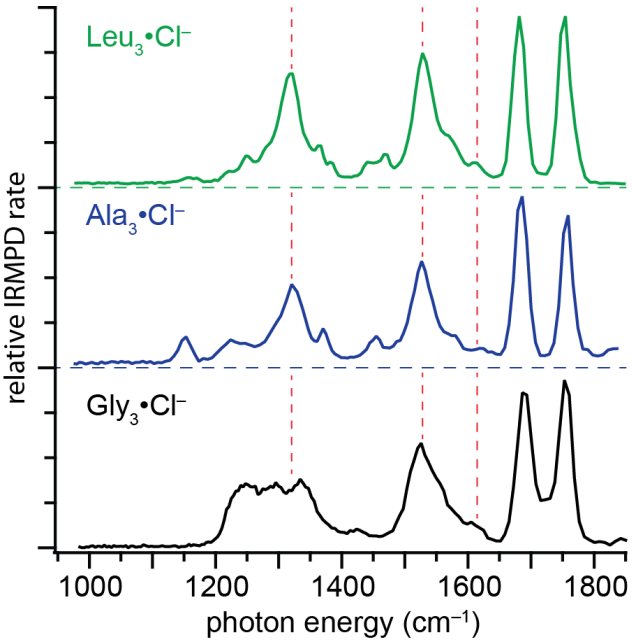

Figure 5.4. IRMPD spectra of $Gly_3•Cl^-$, $Ala_3•Cl^-$, and $Leu_3•Cl^-$ at 298 K. Horizontal dashed lines indicate a vertical offset. Vertical dashed lines serve as a guide for the eye.

Spectra of $Glu•X^-$ (X = Cl, Br, I) have relatively strong absorptions near 1375 cm^{-1} corresponding to the hydroxyl O–H bends of the carboxylic acid of the side chain and the C-terminus.[42] For $Ala_3•Cl^-$ and $Leu_3•Cl^-$, the only band of comparable intensity in this region of the spectrum is at ~1325 cm^{-1}, indicating that this feature corresponds to the hydroxyl O–H bend of the C-terminal carboxylic acid. Although there is a band at 1329 cm^{-1} in the spectrum of $Gly_3•Cl^-$, there are also bands of comparable intensity at 1243 and 1285 cm^{-1}. For $Gly_3•Na^+$, a broad feature was observed by Balaj et al. at 1160 cm^{-1} that corresponds to the C-terminal carboxylic acid O–H bend, whereas bands for N–H and CH_2 bends occur from 1210 – 1290 cm^{-1}.[39] A large shift in the hydroxyl O–H bend is expected between the spectra of $Gly_3•Cl^-$ and $Gly_3•Na^+$ due to the difference in frequency of this mode for an exo vs. endo carboxylic acid whereas the N–H and CH_2 bends are expected to shift only slightly. Thus, the band for $Gly_3•Cl^-$

at 1329 cm^{-1} is likely the hydroxyl in-plane O–H bend, and the bands at 1243 and 1285 cm^{-1} are attributed to N–H and CH_2 bending modes.

5.4.3. Comparisons Between Experimental and Calculated Spectra

Gly_3•Cl^-. The IRMPD spectrum and calculated spectra for low-energy structures of Gly_3•Cl^- are shown in Figure 5.5. The carbonyl C=O stretches of the C-terminus occur near 1750 cm^{-1} for Gly_3A – D, in good agreement with the band at 1754 cm^{-1} in the IRMPD spectrum. In contrast, the calculated spectrum of Gly_3E has a carboxylate asymmetric stretch that occurs near 1650 cm^{-1}. The hydroxyl O–H bend is calculated to occur at ~1325 cm^{-1} for structures with an exo carboxylic acid (Gly_3A – C), in good agreement with the band in the IRMPD spectrum at 1329 cm^{-1}. This vibrational mode for an endo carboxylic acid (Gly_3D) is at ~1160 cm^{-1}, a region where no significant dissociation occurs. Neither spectra for Gly_3D nor Gly_3E are a good match to the IRMPD spectrum.

The calculated spectra for **Gly_3A – C** are similar, having only subtle differences that reflect only slight changes in the coordination of Cl^- to the peptide. For **Gly_3A** and **Gly_3C**, the amide N–H bends couple, resulting in a relatively intense band near 1550 cm^{-1} and a weaker band near 1575 cm^{-1}. In contrast, the coupled N–H bends for **Gly_3B** are calculated to be between 1500 and 1550 cm^{-1} and have similar intensities. The relative intensities for **Gly_3A** and **Gly_3C** are more similar to the peak at 1523 cm^{-1} in the measured spectrum, which has a shoulder at ~1560 cm^{-1}, but the calculated bands are at slightly higher frequency compared to both **Gly_3B** and the measured spectrum. The calculated spectra for **Gly_3A – C** also have bands corresponding to backbone CH_2 twists and scissor modes near the same frequencies as the bands at 1243 and 1421 cm^{-1}, respectively, in the IRMPD spectrum. There are several coupled backbone vibrations with calculated frequencies near 1300 cm^{-1}, which overlap well with the feature at ~1285 cm^{-1} in the measured spectrum. The calculated spectra for **Gly_3A** and **Gly_3C** are most consistent with the IRMPD spectrum, but contributions from **Gly_3B** cannot be ruled out. These results indicate that it is likely that all three structures are present in the ion population.

Ala_3•Cl^-. As was the case with Gly_3•Cl^-, the C-terminal carbonyl C=O stretches of charge-solvated structures for Ala_3•Cl^- are calculated to occur near 1750 cm^{-1}, in good agreement with the band at 1759 cm^{-1} in the IRMPD spectrum (Figure 5.6). In contrast, there is no feature near 1650 cm^{-1} of comparable intensity to the carboxylate asymmetric stretch calculated for **Ala_3E**. The hydroxyl O–H bend of the C-terminus is calculated for **Ala_3A** and **Ala_3C** to be at 1315 and 1324 cm^{-1}, respectively, in good agreement with the band at 1322 cm^{-1} in the IRMPD spectrum. The corresponding band in **Ala_3B** (1344 cm^{-1}) is slightly higher in frequency. The observed band at 1153 cm^{-1} is assigned to the methyl rocking motions, which are calculated to occur near 1150 cm^{-1}. This feature potentially overlaps with the O–H bend of an endo carboxylic acid calculated to be at ~1170 cm^{-1} for **Ala_3D**, obscuring potential contributions from this structure. Methyl umbrella and scissor motions also occur near 1375 and 1425 cm^{-1}, respectively, for each structure, and are in good agreement with the bands that appear near these frequencies in the IRMPD spectrum. The spectra of **Ala_3A** and **Ala_3C** most closely match the measured spectrum, although contributions from **Ala_3B** cannot be ruled out. In contrast, **Ala_3D** and **Ala_3E** are unlikely to have significant populations based on both calculated energies and poor match to the IRMPD spectrum.

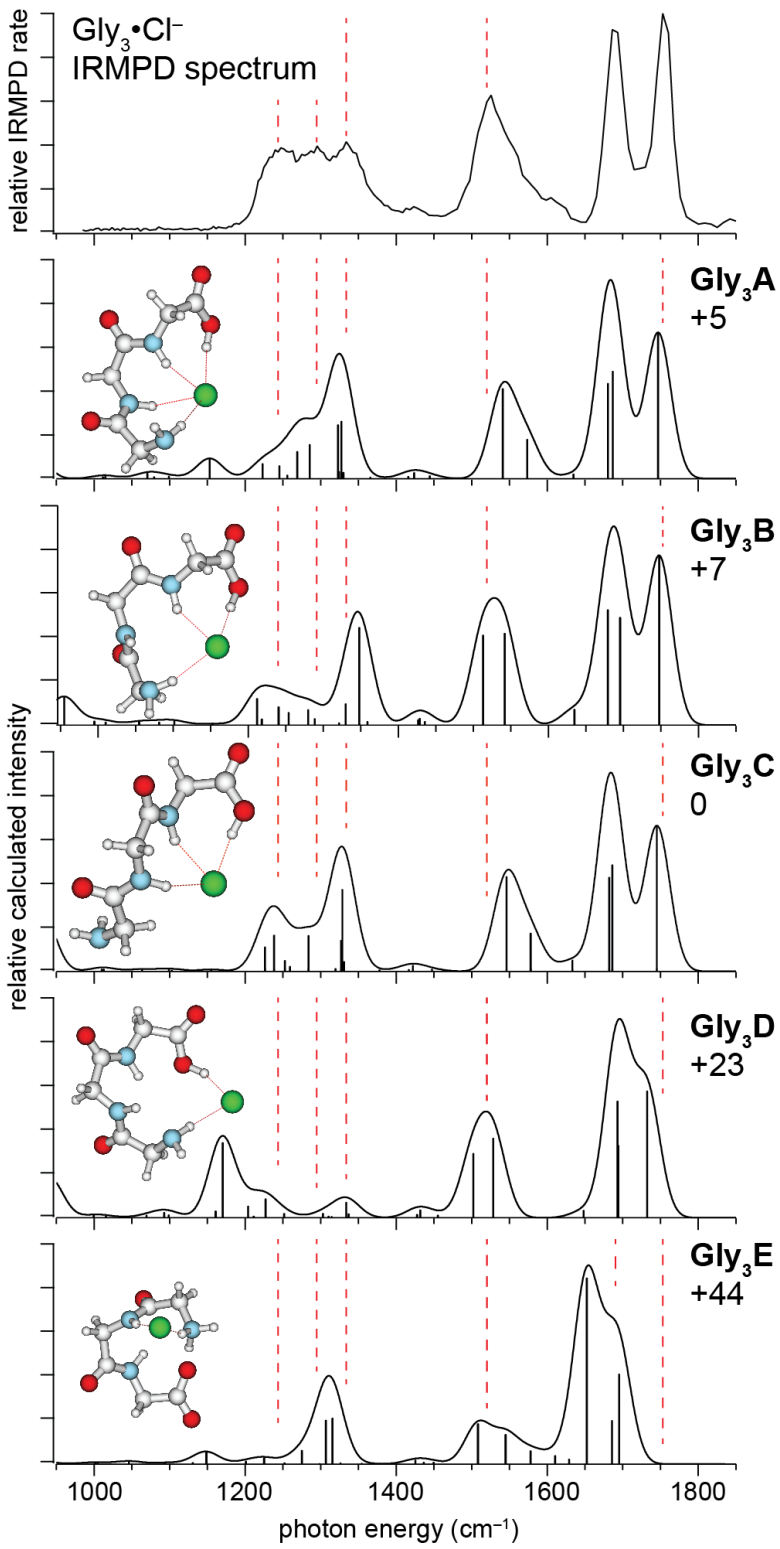

Figure 5.5. Comparison of the IRMPD and calculated spectra for $Gly_3•Cl^-$. All calculations were performed at the B3LYP/6-31+G** level of theory and differences in Gibbs free energies (at 298 K) are in kJ mol^{-1}.

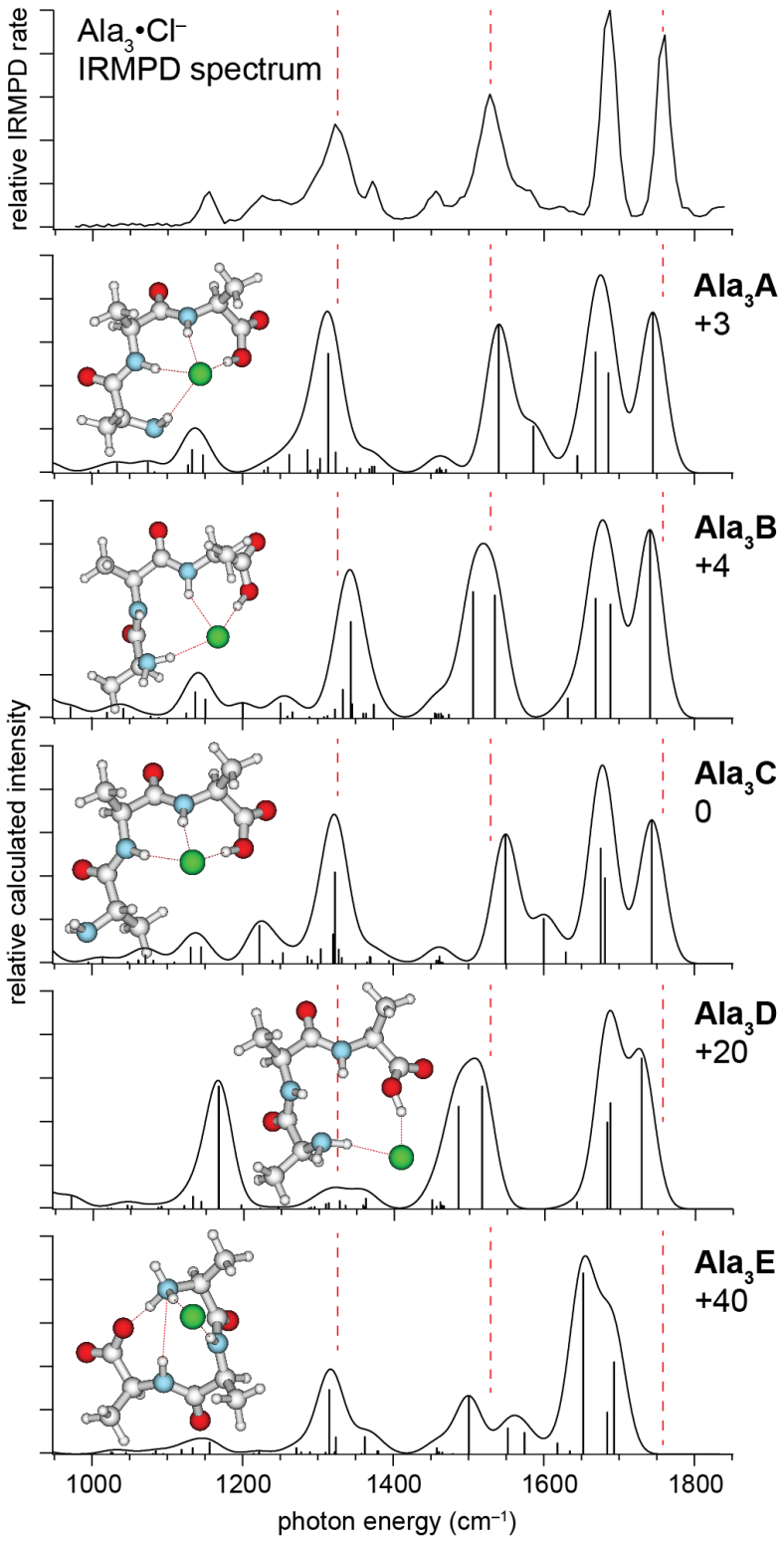

Figure 5.6. Comparison of the IRMPD and calculated spectra for Ala_3•Cl^-. All calculations were performed at the B3LYP/6-31+G** level of theory and differences in Gibbs free energies (at 298 K) are in kJ mol^{-1}.

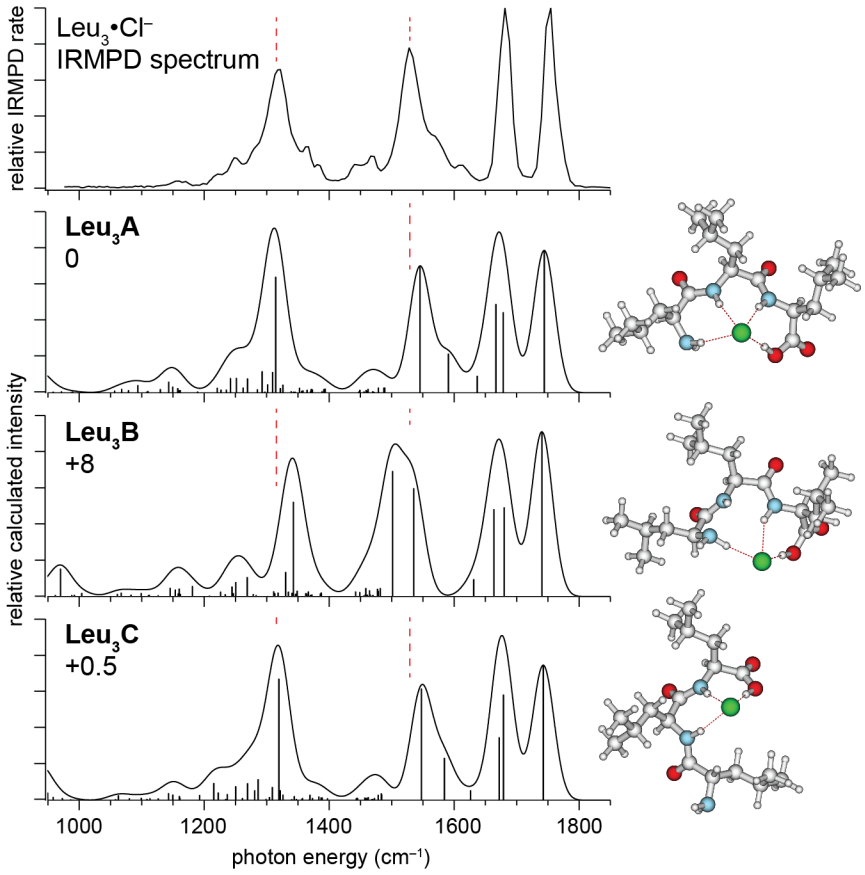

Figure 5.7. Comparison of the IRMPD and calculated spectra for $Leu_3•Cl^-$. All calculations were performed at the B3LYP/6-31+G** level of theory and differences in Gibbs free energies (at 298 K) are in kJ mol^{-1}.

$Leu_3•Cl^-$. Calculated spectra for **Leu_3A – C** (Figure 5.7) each contain relatively intense bands corresponding to the hydroxyl O–H bend, the amide N–H bends, amide C=O stretch, and the C-terminal C=O stretch near 1300, 1550, 1675 and 1750 cm^{-1}, respectively. These calculated frequencies are in good agreement with the bands in the IRMPD spectrum (Figure 5.7), but **Leu_3A** and **Leu_3C** are in better agreement than **Leu_3B**. The relative energies of **Leu_3A** and **Leu_3C** are nearly the same, indicating that both structures likely contribute to the ion population, but contributions from **Leu_3B** cannot be ruled out. The calculated vibrational modes of the side chain methyl groups are near 1375 and 1425 cm^{-1}. The IRMPD spectrum has two bands at ~1375 and another two centered at ~1425 cm^{-1}, and these are likely due to the coupling between the two methyl groups of each side chain.

5.4.4. IRMPD spectra and Calculations for $Gly_3•X^-$, $Ala_3•X^-$, and $Leu_3•X^-$ (X = Cl, Br, and I)

The coordination of an ion adduct to an amino acid[30-37] or peptide[22,23,38] can depend on ion size. IRMPD spectra for $Gly_3•X^-$, where X = Cl, Br, and I, are nearly identical in the region from 1200 – 1400 cm^{-1}, and each spectrum has analogous bands between 1400 and 1900 cm^{-1}, albeit with slight shifts in frequency with changing halide anion size (Figure 5.8, left). The NH_2 scissor and C-terminal carbonyl C=O bands appear at 1631 and 1768 cm^{-1}, respectively, for $Gly_3•I^-$ and

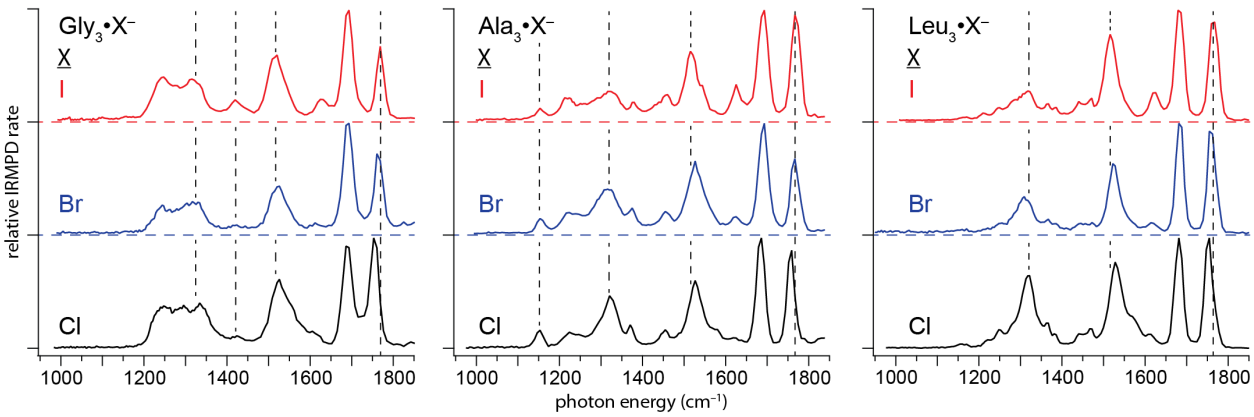

Figure 5.8. IRMPD spectra (298 K) of $Gly_3•X^-$, $Ala_3•X^-$, and $Leu_3•X^-$, where X = Cl, Br, and I. Horizontal dashed lines indicate a vertical offset.

are shifted to the blue by ~20 and ~15 cm^{-1}, respectively, compared to the corresponding band frequencies measured for $Gly_3•Cl^-$. In contrast, the amide N–H bends are red shifted by ~5 cm^{-1} from Gly_3Cl^- (1520 cm^{-1}) to $Gly_3•I^-$ (1515 cm^{-1}). This change in frequency is subtle, but it is also observed for $Ala_3•X^-$ and $Leu_3•X^-$ (Figure 5.8 middle and right). In addition, there is a red shift in the corresponding feature for $Ala_3•M^+$ with increasing ion adduct size,[40] though the change in frequency is greater for cationized vs. anionized Ala_3. The amide carbonyl C=O stretch (1691 cm^{-1}) and the backbone CH_2 bends (1421 cm^{-1}) for $Gly_3•X^-$ do not change with anion size.

There are subtle shifts in the N–H bends and the C-terminal carbonyl C=O stretch frequencies in the calculated spectra of **Gly_3A – C** with the different anions (Figure S5.1), in good agreement with the IRMPD spectra. In contrast, the NH_2 scissor mode is calculated to red shift with increasing halide anion size whereas this band blue shifts in the measured spectra, and this discrepancy is not clearly understood. The similarities between the IRMPD spectra for $Gly_3•X^-$ indicate that all three complexes adopt similar conformations, and that the anion size does not significantly affect the structure of the complex. **Gly_3A – C** have similar Gibbs free energies for each of the different anions (Table 5.1), and the calculated spectra of **Gly_3A** and **Gly_3C** are most consistent with the corresponding measured spectra, although all three structures could likely exist for $Gly_3•X^-$.

As was the case for $Gly_3•X^-$, the spectra for $Ala_3•X^-$ and $Leu_3•X^-$ for the same peptide are similar, indicating that conformations adopted by Ala_3 and Leu_3 do not change substantially with the size of the anion adduct. The calculated spectra of structures **A** and **C** for Ala_3 and Leu_3 with the different anions (Figure S5.2 and S5.3, respectively) are in best agreement with the corresponding IRMPD spectrum, although contributions from structure **B** cannot be ruled out. There are only minor shifts in band frequencies (< 30 cm^{-1}) with anion size in the measured spectra. The N-terminal NH_2 scissor motion and the C-terminal C=O stretch features shift to higher frequencies going from Cl^- to I^- whereas the amide N–H bends move to lower frequencies as the anion size increases. Similar shifts with increasing halide anion size occur in the calculated spectra for **Ala_3A – C** and **Leu_3A – C** for the amide N–H bends and the C-terminal C=O stretch, but the opposite trends occur for the NH_2 scissor modes between the calculated and the measured spectra.

Table 5.1. Calculated relative Gibbs free energies (298 K) in kJ mol^{-1} for low-energy structures of $Gly_3 \bullet X^-$, $Ala_3 \bullet X^-$, and $Leu_3 \bullet X^-$, where X = Cl, Br, and I. All calculations were performed with the B3LYP functional. The CRENBL effective core potential and basis set were used for Br and I, and the 6-31+G** basis was used for all other elements.

	Cl^-	Br^-	I^-
Gly_3A	+5	+3	0
Gly_3B	+7	+5	+3
Gly_3C	0	0	+2
Ala_3A	+3	+4	+3
Ala_3B	+4	+7	+3
Ala_3C	0	0	0
Leu_3A	0	+6	+6
Leu_3B	+8	+5	+5
Leu_3C	+0.5	0	0

Shifts in band frequencies with anion size can be attributed to either a charge transfer or Stark effect. Charge transfer can occur because the anion donates electron density to a nearby bond, which results in a change in bond strength. The vibrational frequencies of these bonds can either blue or red shift from an unperturbed oscillator depending on which orbital the electron density is donated,[53-55] and the extent of charge transfer depends on the anion size. The electric field of an ion can extend to long distances and can also change the vibrational frequencies of functional groups remote from the ion, i.e., a Stark shift. This effect has been observed for the O–H oscillators of water molecules at the surface of hydrated ion[56,57] as well as the carbonyl C=O stretch for halidated Glu.[42]

For Gly_3, Ala_3, and Leu_3 bound to Cl^-, the C-terminal C=O stretch frequency is red shifted from the corresponding band for neutral acetic acid (~1780 cm^{-1}).[58] Anions coordinated to amino acids and peptides are closer to the carbonyl C atom than the O atom, and this arrangement results in the favorable alignment of the dipole moment of the carbonyl C=O bond and the anion's electric field. This favorable alignment causes a Stark shift in the C=O stretch frequency, which results in a red shift compared to the frequency of an unperturbed oscillator.[42,56,57] As the size of the anion adduct increases, contributions from the Stark effect diminish and the frequency of the C=O stretch approaches that of neutral acetic acid, i.e., there is a blue shift with increasing anion size. The extent to which a charge transfer or Stark effect contribute to these shifts is unknown.

The N-terminus in structures **A** and **B** for Gly_3, Ala_3, and Leu_3 donates a HB to the anion adduct such that there is favorable alignment between the dipole of the amine N–H bonds and the anion's electric field. A Stark effect would result in a blue shift in the frequency of the NH_2 scissor mode with increasing ion size for these structures, consistent with experimental spectra. In contrast, the N-terminus in **Gly_3C**, **Ala_3C**, and **Leu_3C** is oriented such that the dipole of the amine N–H bonds and the anion's electric field are unfavorably aligned, which would result in a

red shift with increasing ion size. Because structures **A** and **C** are both likely to be present, the shift in the NH_2 scissor normal mode is likely due to a charge transfer effect.

The dipoles of the amide N–H bonds are favorably aligned with the anion's electric field for **Gly_3A – C**, **Ala_3A – C**, and **Leu_3A – C**. The features corresponding to the amide N–H bends shifts to lower frequencies with increasing ion size, but this trend opposite to what would be expected for a Stark shift. Thus, the change in frequency of these vibrational modes can only be attributed to the charge transfer effect.

5.5. Conclusion

IRMPD spectra were measured for $Gly_3 \bullet X^-$, $Ala_3 \bullet X^-$ and $Leu_3 \bullet X^-$ (where X = Cl, Br and I). For each peptide, spectra appear nearly identical, albeit with slight differences in frequency for some spectral features, indicating that each peptide adopts similar conformations that do not depend significantly on anion size. These results are also supported by theory. Comparisons between measured spectra and those calculated for low-energy structures of Cl^- adducted to Gly_3, Ala_3 and Leu_3 indicate that all three complexes adopt the same binding motifs and that the size of the alkyl size chain has little influence on coordination patterns. Low-energy structures for $Gly_3 \bullet X^-$ and $Ala_3 \bullet X^-$ are "inverted" compared to those for $Gly_3 \bullet Na^+$ and $Ala_3 \bullet M^+$ (M = Li, Na, K, Cs), respectively.[39,40] The "inversion" in coordination between $Ala_3 \bullet M^+$ and $Ala_3 \bullet X^-$ results in greater steric hindrance for some structures for the latter. The bands for the C-terminal C=O stretch blue shift with increasing size of the anion adduct whereas the amide

5.6. References

1. Chesler, M. *Physiol. Rev.* **2003**, *83*, 1183-1221.
2. Russell, J. M.; Boron, W. F. *Nature* **1976**, *264*, 73-74.
3. Loo, J. A. *Mass Spectrom. Rev.* **1997**, *16*, 1-23.
4. Pyle, A. M. *J. Biol. Inorg. Chem.* **2002**, *7*, 679-690.
5. Dashper, S. G.; Brownfield, L.; Slakeski, N.; Zilm, P. S.; Rogers, A. H.; Reynolds, E. C. *J. Bacteriology* **2001**, *183*, 4142-4148.
6. Frings, S.; Reuter, D.; Kleene, S. J. *Prog. Neurobiol.* **2000**, *60*, 247-289.
7. Kleene, S. J.; Gesteland, R. C. *J. Neurosci.* **1991**, *11*, 3624-3629.
8. Firestein, S.; Shepherd, G. M. *J. Neurophysiol.* **1995**, *73*, 562-567.
9. Delay, R. J.; Dubin, A. E.; Dionne, V. E. *J. Membrane Biol.* **1997**, *159*, 53-60.
10. Hallani, M.; Lynch, J. W.; Barry, P. H. *J. Membrane Biol.* **1998**, *161*, 163-171.
11. Jockusch, R. A.; Price, W. D.; Williams, E. R. *J. Phys. Chem. A.* **1999**, *103*, 9266-9274.
12. Cerda, B. A.; Cornett, L.; Wesdemiotis, C. *Int. J. Mass Spectrom.* **1999**, *193*, 205-226.
13. Cerda, B. A.; Wesdemiotis, C. *Analyst* **2000**, *125*, 657-660.
14. Rogalewicz, F.; Hoppilliard, Y.; Ohanessian, G. *Int. J. Mass Spectrom.* **2000**, *195*, 565-590.
15. Farrugia, J. M.; O'Hair, R. A. J. *Int. J. Mass Spectrom.* **2003**, *222*, 229-242.
16. Shek, P. Y. I.; Zhao, J. F.; Ke, Y.; Siu, K. W. M.; Hopkinson, A. C. *J. Phys. Chem. A* **2006**, *110*, 8282-8296.
17. Wyttenbach, T.; Bowers, M. T. "Gas-phase conformations: The ion mobility/ion chromatography method" in *Modern Mass Spectrometry*, Schalley, C. A., Ed.; Topics in Current Chemistry 225; Springer-Verlag: Berlin, 2003, 207-232.
18. Han, L. J.; Hyung, S. J.; Mayers, J. J. S.; Ruotolo, B. T. **2011**, *133*, 11358-11367.
19. Merenbloom, S. I.; Flick, T. G.; Daly, M. P.; Williams, E. R. *J. Am. Soc. Mass Spectrom.* **2011**, *22*, 1978-1990.
20. Glover, M. S.; Dilger, J. M.; Zhu, F.; Clemmer, D. E. *Int. J. Mass Spectrom.* **2013**, *354-355*, 318-325.
21. Kamariotis, A.; Boyarkin, O. V.; Mercier, S. R.; Beck, R. D.; Bush, M. F.; Williams, E. R.; Rizzo, T. R. *J. Am. Chem. Soc.* **2006**, *128*, 905-916.
22. Dunbar, R. C.; Polfer, N. C.; Berden, G.; Oomens, J. *Int. J. Mass Spectrom.* **2012**, *330*, 71-77.
23. Dunbar, R. C.; Oomens, J.; Berden, G.; Lau, J. K. C.; Verkerk, U. H.; Hopkinson, A. C.; Siu, K. W. M. *J. Phys. Chem. A* **2013**, *117*, 5335-5343.
24. Polfer, N. C.; Paizs, B.; Snoek, L. C.; Compagnon, I.; Suhai, S.; Meijer, G.; von Helden, G.; Oomens, J. *J. Am. Chem. Soc.* **2005**, *127*, 8571-8579.
25. Dunbar, R. C.; Polfer, N. C.; Oomens, J. *J. Am. Chem. Soc.* **2007**, *129*, 14562-14563.
26. Kapota, C.; Lemaire, J.; Maitre, P.; Ohanessian, G. *J. Am. Chem. Soc.* **2004**, *126*, 1836-1842.
27. Bush, M. F.; Oomens, J.; Williams, E. R. *J. Phys. Chem. A* **2009**, *113*, 431-438.
28. Prell, J. S.; O'Brien, J. T.; Steill, J. D.; Oomens, J.; Williams, E. R. *J. Am. Chem. Soc.* **2009**, *131*, 11442-11449.
29. Prell, J. S.; Flick, T. G.; Oomens, J.; Berden, G.; Williams, E. R. *J. Phys. Chem. A* **2010**, *114*, 854-860.

30. Heaton, A. L.; Bowman, V. N.; Oomens, J.; Steill, J. D.; Armentrout, P. B. *J. Phys. Chem. A* **2009**, *113*, 5519-5530.
31. Forbes, M. W.; Bush, M. F.; Polfer, N. C.; Oomens, J.; Dunbar, R. C.; Williams, E. R.; Jockusch, R. A. *J. Phys. Chem. A.* **2007**, *111*, 11759-11770.
32. Armentrout, P. B.; Rodgers, M. T.; Oomens, J.; Steill, J. D. *J. Phys. Chem. A.* **2008**, *112*, 2248-2257.
33. Bush, M. F.; Oomens, J.; Saykally, R. J.; Williams, E. R. *J. Am. Chem. Soc.* **2008**, *130*, 6463-6471.
34. Rodgers, M. T.; Armentrout, P. B.; Oomens, J.; Steill, J. D. *J. Phys. Chem. A* **2008**, *112*, 2258-2267.
35. O'Brien, J. T.; Prell, J. S.; Steill, J. D.; Oomens, J.; Williams, E. R. *J. Phys. Chem. A.* **2008**, *112*, 10823-10830.
36. Dunbar, R. C.; Hopkinson, A. C.; Oomens, J.; Siu, C. K.; Siu, K. W. M.; Steill, J. D.; Verkerk, U. H.; Zhao, J. F. *J. Phys. Chem. B* **2009**, *113*, 10403-10408.
37. Citir, M.; Stennett, E. M. S.; Oomens, J.; Steill, J. D.; Rodgers, M. T.; Armentrout, P. B. *Int. J. Mass Spectrom.* **2010**, *297*, 9-17.
38. Prell, J. S.; Demireva, M.; Oomens, J.; Williams, E. R. *J. Am. Chem. Soc.* **2009**, *131*, 1232-1242.
39. Balaj, O. P.; Kapota, C.; Lemaire, J.; Ohanessian, G. *Int. J. Mass Spectrom.* **2008**, *269*, 196-209.
40. Dunbar, R. C.; Steill, J. D.; Oomens, J. *Int. J. Mass Spectrom.* **2010**, *297*, 107-115.
41. Balaj, O. P.; Semrouni, D.; Steinmetz, V.; Nicol, E.; Clavaguera, C.; Ohanessian, G. *Chem. Eur. J.* **2012**, *18*, 4583-4592.
42. O'Brien, J. T.; Prell, J. S.; Berden, G.; Oomens, J.; Williams, E. R. *Int. J. Mass Spectrom.* **2010**, *297*, 116-123.
43. Schmidt, J.; Kass, S. R. *J. Phys. Chem. A* **2013**, *117*, 4863-4869.
44. Milner, E. M.; Nix, M. G. D.; Dessent, C. E. H. *J. Phys. Chem. A* **2012**, *116*, 801-809.
45. Skurski, P.; Rak, J.; Simons, J.; Gutowski, M. *J. Am. Chem. Soc.* **2001**, *123*, 11073-11074.
46. Xu, S. J.; Zheng, W. J.; Radisic, D.; Bowen, K. H. *J. Chem. Phys.* **2005**, *122*, 091103.
47. Kass, S. R. *J. Am. Chem. Soc.* **2005**, *127*, 13098-13099.
48. Shao, Y.; et al. *Phys. Chem. Chem. Phys.* **2006**, *8*, 3172-3191.
49. Valle, J. J.; Eyler, J. R.; Oomens, J.; Moore, D. T.; van der Meer, A. F. G.; von Helden, G.; Meijer, G.; Hendrickson, C. L.; Marshall, A. G.; Blakney, G. T. *Rev. Sci. Instrum.* **2005**, *76*, 023103.
50. Polfer, N. C.; Oomens, J.; Moore, D. T.; von Helden, G.; Meijer, G.; Dunbar, R. C. *J. Am. Chem. Soc.* **2006**, *128*, 517-525.
51. Prell, J. S.; O'Brien, J. T.; Williams, E. R. *J. Am. Mass. Spectrom.* **2010**, *21*, 800-809.
52. Steill, J. D.; Oomens, J. *J. Am. Chem. Soc.* **2009**, *131*, 13570-13571.
53. Scheiner, S. *Hydrogen Bonding*; Oxford University Press: New York, 1997.
54. Hobza, P.; Havlas, Z. *Theor. Chem. Acc.* **2002**, *108*, 325-334.
55. Wright, A. M.; Howard, A. A.; Howard, C.; Tschumper, G. S.; Hammer, N. I. *J. Phys. Chem. A* **2013**, *117*, 5435-5446.
56. Prell, J. S.; O'Brien, J. T.; Williams, E. R. *J. Am. Chem. Soc.* **2011**, *133*, 4810-4818.
57. O'Brien, J. T.; Williams, E. R. *J. Am. Chem. Soc.* **2012**, *134*, 10228-10236.

58. Coblentz Society, Inc., Evaluated infrared reference spectra, in: P.J. Linstrom, W.G. Mallard (Eds.), *NIST Chemistry WebBook, NIST Standard Reference Database Number 69*, 2009; National Institute of Standards and Technology, Gaithersburg, MD, p. 20899, http://webbook.nist.gov (retrieved 11.04.13)

5.7. Supplementary Figures

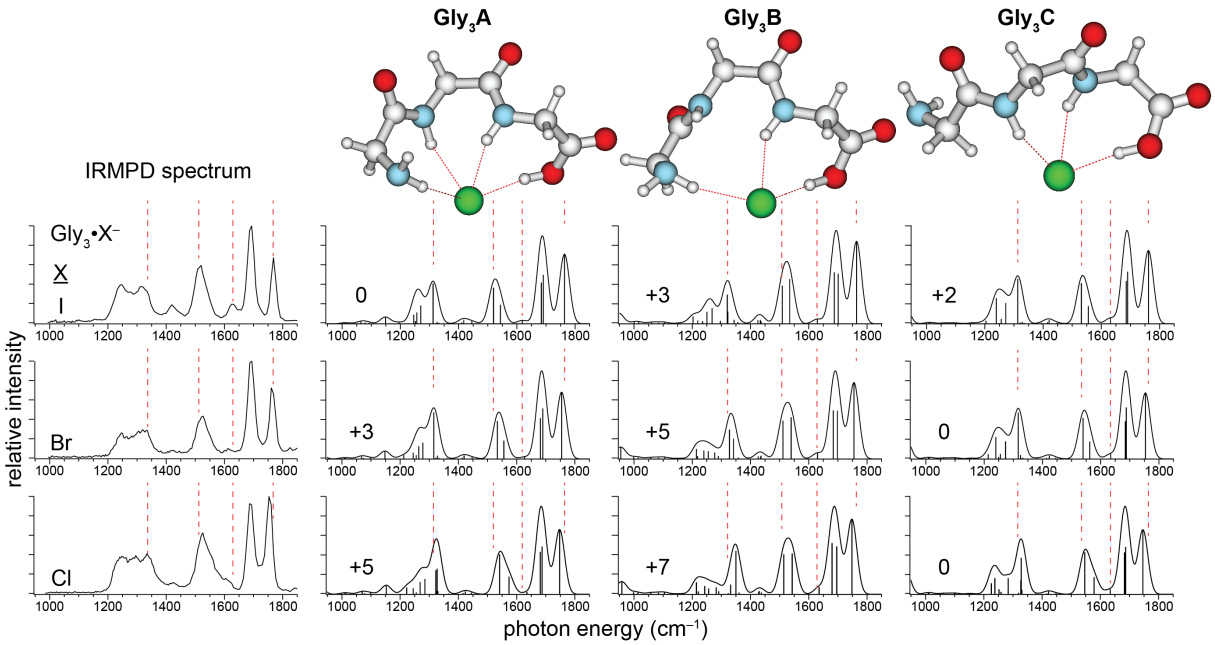

Figure S5.1. Comparisons between IRMPD and calculated spectra of $Gly_3 \bullet X^-$ (X = Cl, Br and I). Calculated structures ($Gly_3 \bullet Cl^-$) and 298 K Gibbs free energies (kJ mol^{-1}) are also included. All calculations were performed with the B3LYP functional. The CRENBL effective core potential and basis set were used for the Br and I atoms, whereas the 6-31+G** basis set was implemented for all other atoms.

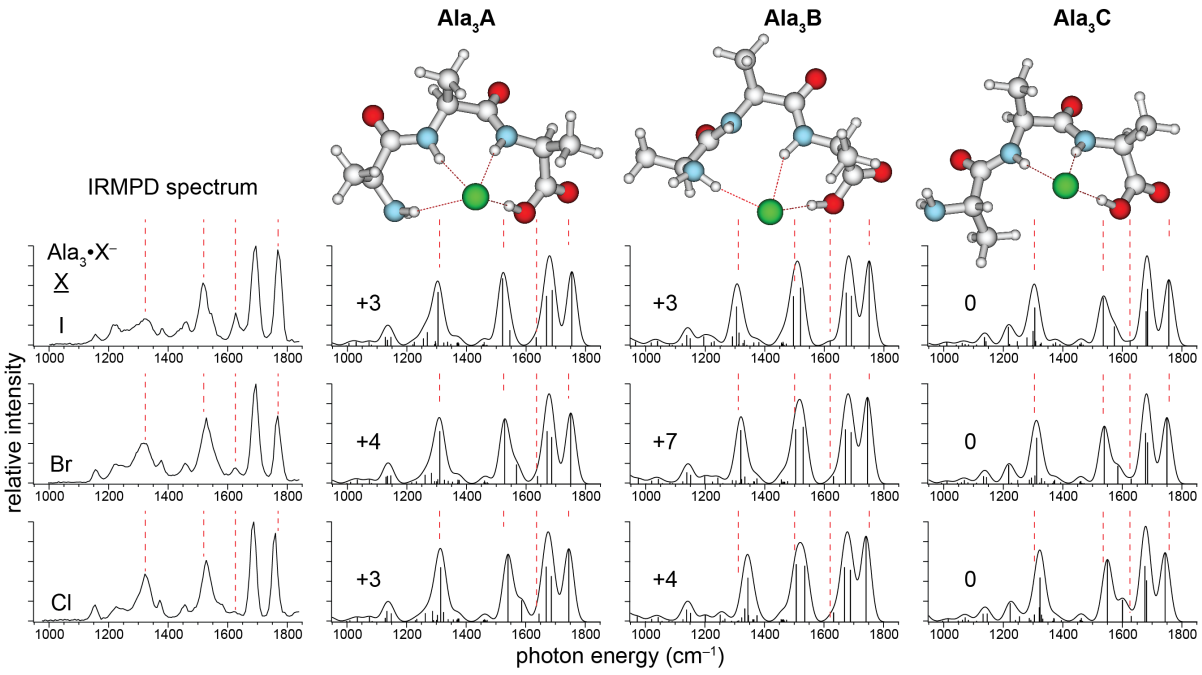

Figure S5.2. Comparisons between IRMPD and calculated spectra of $Ala_3 \bullet X^-$ (X = Cl, Br and I). Calculated structures ($Ala_3 \bullet Cl^-$) and 298 K Gibbs free energies (kJ mol^{-1}) are also included. All calculations were performed with the B3LYP functional. The CRENBL effective core potential and basis set were used for the Br and I atoms, whereas the 6-31+G** basis set was implemented for all other atoms.

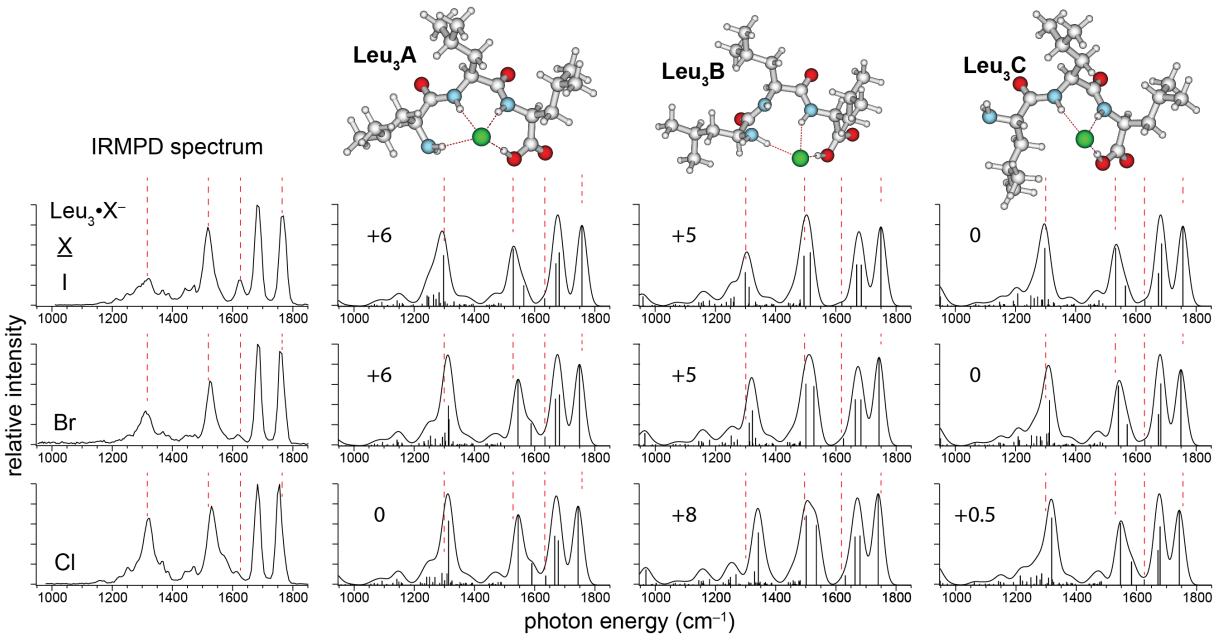

Figure S5.3. Comparisons between IRMPD and calculated spectra of $Leu_3 \bullet X^-$ (X = Cl, Br and I). Calculated structures ($Leu_3 \bullet Cl^-$) and 298 K Gibbs free energies (kJ mol^{-1}) are also included. All calculations were performed with the B3LYP functional. The CRENBL effective core potential and basis set were used for the Br and I atoms, whereas the 6-31+G** basis set was implemented for all other atoms.